第54卷 第1期
2016年1月

古 脊 椎 动 物 学 报
VERTEBRATA PALASIATICA

pp. 1−20
figs. 1−6

Morphology and taxonomy of *Gazella* (Bovidae, Artiodactyla) from the Late Miocene Bahe Formation, Lantian, Shaanxi Province, China

ZHANG Zhao-Qun[1] YANG Rui[1,2]

(1 *Key Laboratory of Vertebrate Evolution and Human Origins of Chinese Academy of Sciences*, *Institute of Vertebrate Paleontology and Paleoanthropology*, *Chinese Academy of Sciences* Beijing 100044 zhangzhaoqun@ivpp.ac.cn)
(2 *University of Chinese Academy of Sciences* Beijing 100049)

Abstract Fossil gazelles have been widely distributed in Eurasia and Africa during the late Neogene. They are key elements of "*Hipparion*" faunas with prominent biochronologic and ecological significance. However, no pre-Baodean age gazelle previously reported from China. We describe here in detail materials found from the Bahe Formation, Shaanxi Province, which include by far the most complete skulls and postcranials. The first fossil gazelle skeleton is mounted based on the new findings. Morphology and measurements show the similarity with *Gazella lydekkeri* from Dhok Pathan Formation of middle Siwaliks, different from the most common species *G. gaudryi*, *G. paotehensis*, and *G. dorcadoides* from Baodean age and other gazelles from Europe. Ecomorphology and measurements of long bones indicate the Lantian species, *Gazella* cf. *G. lydekkeri*, is possibly a fast runner, adapted to an open environment in Bahean age. The open environment was also suggested by faunal composition, sedimentological analysis and isotope data.

Key words Lantian, Shaanxi; Late Miocene; Bahe Formation; gazelles

Citation Zhang Z Q, Yang R, 2016. Morphology and taxonomy of *Gazella* (Bovidae, Artiodactyla) from the Late Miocene Bahe Formation, Lantian, Shaanxi Province, China. Vertebrata PalAsiatica, 54(1): 1−20

1 Introduction

The genus *Gazella* (Bovidae, Artiodactyla) is one of the most common taxa in the "*Hipparion*" faunas, widely distributed in Eurasia and Africa. The earliest gazelle fossils recovered are *Gazella* sp. from Fort Ternan of Middle Miocene (14 Ma) and *Gazella pregaudryi* from Bou Hanifia (10 Ma), Algeria (Arambourg, 1959; Gentry, 1970, 2010). Gentry (2010) also mentioned the occurrence of Middle Miocene *Gazella* from Siwaliks. The study of Chinese gazelles has a long history pioneered by Schlosser (1903) on specimens from drugstores without detailed provenances, followed by Bohlin (1935, 1939) on the

国家自然科学基金(批准号：40272009, 41072004, 41472003)、国家重点基础研究发展计划项目(编号：2012CB821904)和芬兰科学院资助。
收稿日期：2015-02-02

Lagrelius Collection kept in Uppsala, Sweden, and by Teilhard de Chardin and Young (1931) and Teilhard de Chardin and Trassaert (1938) on specimens from the Yushe Basin. Chen (1997) made a systematic revision on fossil gazelles from the Yushe Basin based on the Sino-American project collection and Licent's collection in Tianjin Natural History Museum. However, all the *Gazella* species from China previously described are recorded from the Baodean and younger ages (Chen and Zhang, 2009), leaving a long time gap for the evolution of gazelles in East Asia.

The ecological significance of gazelles was first noticed by Schlosser (1903), and greatly improved by Kurtén (1952) who emphasized the ecological significance of two species, e.g. *G. gaudryi* and *G. dorcadoides* for representatives of east wet forest and west dry steppe faunas in North China respectively. The paleodiets and habitats of these species were reinforced by stable carbon isotope evidences (Passey et al., 2007).

During 1997-2001, the Sino-Fennic joint project produced a large amount of fossil bovids, especially gazelles from the Bahe Formation, Lantian, Shaanxi Province (Zhang et al, 2002, 2013; Zhang and Liu, 2005). Of the totally 52 localities, Loc.31 yielded well preserved *Gazella* specimens, including 5 skulls and almost all postcranial elements which provide an unprecedented complete understanding of skeleton morphology and taxonomy of this taxa. This paper will describe in detail these specimens and discuss the taxonomy with brief discussion on the ecological environments.

Terminology of skull and teeth refers Chen (1997), Gentry (1966, 1970), Gray (1977). Measurement method follows Pilgrim (1937), Yang et al. (2005) and Xia et al. (2005). Comparison materials are from Natural History Museum, London, Evolution Museum of Uppsala University, Paleontological Museum of Athens University, and IVPP (Institute of Vertebrate Paleontology and Paleoanthropology, CAS).

2 Systematic paleontology

Artiodactyla Owen, 1848

Bovidae Gray, 1821

Antilopinae Baird, 1857

***Gazella* de Blainville, 1816**

***Gazella* cf. *G. lydekkeri* Pilgrim, 1937**

(Figs. 1-6)

Specimens Five almost complete skulls with lower jaws (IVPP V 15246-V 15250); together with skull V 15246 attached four cervicals (C1-C4, V 15246.1-4), and other postcranials tentatively associated for a complete skeleton (V 15246.5-76); 8 vertebrae (C5-T2, T3-T7, V 15251.1-8); 5 lumbar bones, 1 sacrum and 1 caudal (V 15252.1-7); 9 vertebrae (2 axes, 1 C5/C6, 6 lumbars, V 15253.1-9); 3 broken scapulae (V 15254.1-3); 4 pelves (V 15255.1-4); 1 partial sternum (V 15256); 7 humeri (3 complete, 2 proximal and 2 distal parts,

V 15257.1-7); 2 broken ulnae (V 15258.1-2); 1 complete and 4 partial radii (V 15259.1-5); 3 proximal and 1 distal fragments of femur (V 15260.1-4); 2 proximal and 2 distal parts of tibia (V 15261.1-4); 1 complete juvenile metacarpal, 4 proximal and 3 distal partial metacarpals (V 15262.1-8); 3 complete adult and 1 juvenile metatarsals, 2 proximal parts (one articulated with naviculo-cuboid and cuneiform) (V 15263.1-6); 4 complete articulated tarsals (V 15264.1-4); 8 carpal bones (one with the scaphoid, lunar, cuneiform, and pisiform articulated, 1 scaphoid, 2 magnums, and 1 unciform) (V 15265.1-5); 4 1st phalanges, 3 2rd phalanges (V 15425.1-7).

Locality and stratigraphic horizon Loc.31 (N34°11′04″; E109°15′04″), named as Snake Locality, found by our colleagues, Dr. Liu Liping and Prof. Mikael Fortelius, after encountering a poisonous snake and fell upon the fossils. Stratigraphically this locality locates in the middle part of the Bahe Formation. Magnetostratigraphic data indicate its age of 8.9 Ma, Bahean age (Zhang et al., 2013).

Measurements See Tables 1-3.

Description There found totally five skulls from the locality, all well preserved with lower jaws. The skull IVPP V 15246 was the least distorted, only slightly compressed on the right side, with the right parietal, right zygomatic arch, and right lower jaw lost. V 15247 was more distorted laterally, with the upper part of horn-cores and the left zygomatic arch lost, the lower jaws are well preserved. V 15248 was also compressed without the right zygomatic arch, and pterygoid preserved, lower jaws are in good conditions. The anterior part of V 15249 was compressed laterally, with the pterygoid lost, lower jaws are well preserved. V 15250 was strongly distorted, with the zygomatic arch, pterygoid lost, and the lower jaws are well preserved. V 15246 and V 15247 have horn-cores, should be males. V 15248, 15249, and 15250 have no horn-cores, are female individuals. All five skulls are adult, and V 15248 is the oldest by tooth wear.

V 15246 has almost complete horn-cores. The horn-cores are long and slender, long oval shape in cross section, with the maximum thickness leveled posteriorly to the midpoint. No keel developed. The horn-cores inserted on frontals above orbits at an angle more than 60°. The divergence is moderate at the base (on V 15247, the long axes of horn-cores form an angle about 40° measured from the base), and getting less angled upwards. The curvature is moderate. The horn-cores taper gradually towards the tip. The inner side is relatively convex than the outside. No torsion is observable. There exist moderate deep postcornual fossae.

All five skulls are similar in size without sexual differentiations (Tables 1-2), and also similar to each other in morphology but the presence of horns on males.

The skulls are medium sized, long and slender in general view. The facial part is narrow and long though with taphonomic distortion. The maximum width of skull locates at the posterior ridge of orbits. The cranial part behind the orbit is long and narrow as well, shaping the skull longer and slender. The braincase is bent downwards, with cranial axis about 30° angled to the facial axis.

Dorsal view The nasals are narrow and doomed with paralleled sides at the anterior

Table 1 Skull measurements of *Gazella* cf. *G. lydekkeri* from Lantian (mm)

	V 15246	V 15247	V 15248	V 15249	V 15250
Anteroposterior diameter/transverse diameter at base	26.5/20	32/21.5e			
Distance from anterior orbital rim to akrokranion	100		<105	96.7	
Distance from infra-orbital foramen to anterior orbital rim	43	39	39.5	<44	
Minimum length of frontal	55e		59e	55.5	
Maximum width across orbits			68	70e	
Orbital length	<37			36	
Orbital height	32.5			32.4	
Post orbital width	49e			49.6	
Braincase length: fronto-parietal suture to akrokranion	56		<58	52.3	55e
Braincase width across mastoid	48e			51	51.5
Maximum width across the occipital condyles	39		35	38	38.5
Length of tympanic bulla	24.5	25	23.9	26.8	23.6
Width of tympanic bulla	13.7	14.3	12.6	15.7	13.5
Maximum width of basioccipital across posterior tuberosities	21.7	20.6	20.5	20	
P2-M3	54	55.5	53.7	52.8	54.2
P2-P4	21.7		23	22.2	22.5
M1-M3	33.4	32.6	33.8	32.2	33
Maximum length of mandible				148	
Length of diastema				37	
Mental foramen to p2	25.5		24	24.7	22.5
Height of vertical ramus	68.5	>68			
p2-p4	19.7	21.2	20.8	19	22.2
m1-m3	35.7	37.4	36.2	34.9	37.2
p2-m3	55.4	58.2	56.2	54	58.3

Note: e. estimated value.

Table 2 Tooth measurements of *Gazella* cf. *G. lydekkeri* from Lantian (mm)

	V 15246	V 15247	V 15248	V 15249	V 15250	*G. lydekkeri*
p2	5.2	6.0	6.6	4.7	6.1	6
p3	7.4	7.1	6.0	7.0	7.4	8.5
p4	8.4	8.4	8.9	8.2	8.5	9.5
m1	9.2	9.7	8.9	9.4	8.8	10
m2	10.8	11.7	10.8	10.3	11.7	13
m3	16.6	15.4	16.6	15	16.0	17.5
P2	7.2	7.9	7.0	6.7	7.4	10
P3	6.6	8.2	6.9	6.8	7.0	8
P4	7.2	7.1	7.2	7.2	6.9	7
M1	10	10	8.8	9.4	8.7	11
M2	12.6	12.2	10.5	12.2	13	13.5
M3	12.1	11.7	13.2	12.0	13.3	15

Note: measurements of *Gazella lydekkeri* (AMNH 19663) cited from Pilgrim (1937).

part, widened at the middle way, then tapered in between the developed nasal processes of frontals (Fig. 1A). The posterior end of nasal extends to the level of the frontal edge of orbit. The anterior part of frontal depressed slightly and the posterior part elevated along the suture. The supraorbital foramina locate at the base of horn-core on males, above the orbital roof on females with anteroposteriorly extended surrounding pits. Dorsal orbit rim is wide (Fig. 2A). The parietal-frontal suture is straight and wide. The parietal gets to narrower posteriorly

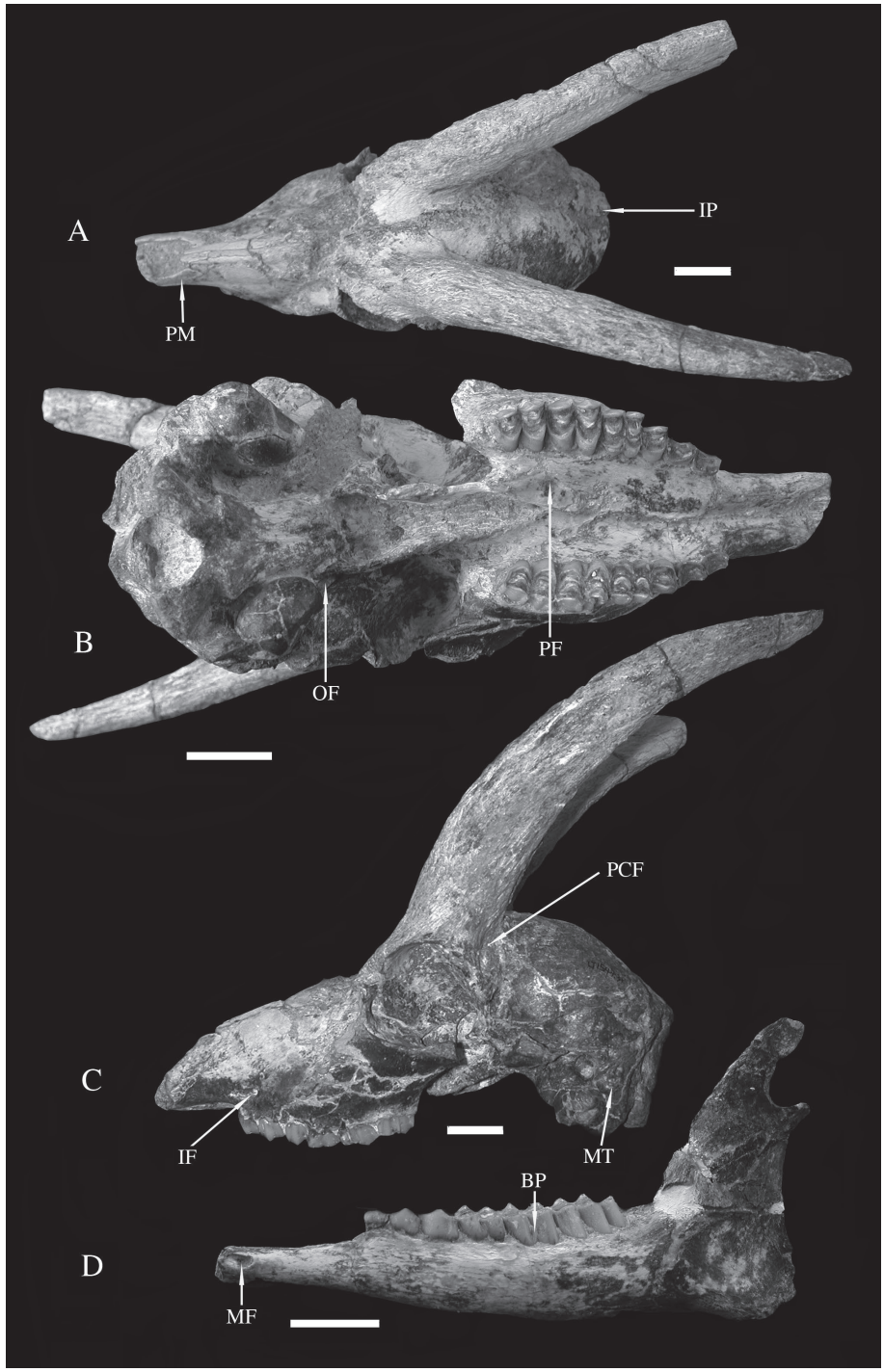

Fig. 1 Skull and mandible of *Gazella* cf. *G. lydekkeri* (IVPP V 15246) from Lantian
A-C. skull: A. dorsal view, B. ventral view, C. left side view; D. labial view of the left mandible. Scale bars=2 cm
Abbreviations: BP. basal pillar; IF. infraorbital foramen; IP. interparietal; MF. mental foramen;
MT. mastoid; OF. oval foramen; PCF. postcornual fossa; PF. palatine foramen; PM. premaxilla

with observable temporal ridges on both sides leading to the minimum distance at the parietal-interparietal suture. The interparietal is narrow anteriorly and contacts with mastoid posterolaterally by the posterior extension. The occipital face has a prominent median crest, which makes each side of occipital surface facing lateroposteriorly.

Lateral view The premaxilla is thin and narrow plate like, strongly inclined and contacts the nasal at the vertical level slightly anterior to P2 (Fig. 1A). The maxillae get to narrower anteriorly in front of tooth rows and widen posteriorly to the maximum width at the level of maxillary tuberosities. The preorbital fossa is moderately deep with developed lachrymal bone. There exists an ethmoidal fissure between the lachrymal and the nasal. The infraorbital foramen opens anteriorly, situates above P2 at a low position (Fig. 1C). The maxillary tuberosity, above M1, is moderate in size. The orbit fossa is round shaped, with well developed upper and lower ridges. The upper orbit ridge is lower than the highest point of the skull, which is positioned at the posterior part of the frontals. The anterior ridge of orbit levels with the M3 paracone. The zygomatic arch posterior to the orbit is short. The zygomatic process of squamosal is long and wide with a saddle like morphology for articulation with the coronoid process dorsally and condylar process ventrally. There exists a large postglenoid foramen. The tympanic bulla is large, round in lateral view with short acoustic meatus. The oval foramen is large, round and open laterally at the posterior end of lateral plate of pterygoid (Fig. 1B). The jugular process extends downwards, tightly encloses the posterior surface of tympanic bulla (Fig. 2C), and anterodorsally contacts the mastoid, which is visible in lateral view.

Ventral view No incisive foramen preserved on all five skulls. The palatal ridges in front of tooth rows approach but do not touch. The palatine foramen locates at the level of posterior lobe of M2 (Fig. 1B). The maxilla width gets to maximum at the level of M2 and greatly diminishes forwards from P4. The median palatine indentation (choana) is anterior to the lateral ones and especially on female individuals (Fig. 2B). The basioccipital is long quadrate in shape with weakly developed and laterally extended posterior tuberosites on male individuals, the anterior tuberosities are even weaker, and the groove between them is extremely shallow. On the female individual, the basioccipital is slightly narrower and with slightly larger anterior tuberosites. The tympanic bulla length does not exceed that of the basioccipital.

The mandible ramus is also long and slender (Fig. 2D). The inner side is flat, and the outer side is outbowed, and thickness of the horizontal ramus increases posteriorly. The symphysis is short, extends to the level of the mental foramen. The mental foramen is long oval shaped, posterior to the canine. The diastema is longer than the molar row. The coronoid process is high and curved posteriorly, with a slightly concave inner side and flat outer side. The condyle is below the highest point of coronoid process, separated by a deep notch (Fig. 2D). The angular process extends slight away to the posterior edge of the vertical ramus.

The premolar row is relatively short (Fig. 3; Table 1). P2 is very small in size; the paracone is large with a rib. P3 is very similar to P2, but shorter. P4 has a triangle shaped

Fig. 2 Skull and mandible of *Gazella* cf. *G. lydekkeri* (IVPP V 15249) from Lantian
A–C. skull: A. dorsal view, B. ventral view, C. left side view; D. labial view of the right mandible. Scale bars=2 cm
Abbreviations: AM. acoustic meatus; CN. choana; CP. condyle process; CRP. coronoid process;
JP. jugular process; PCF. postcornual fossa; PTB. posterior tuberosity of basioccipital;
SOF. supraorbital foramen; TB. tympanic bulla; TR. temporal ridge; ZM. zygomatic plate

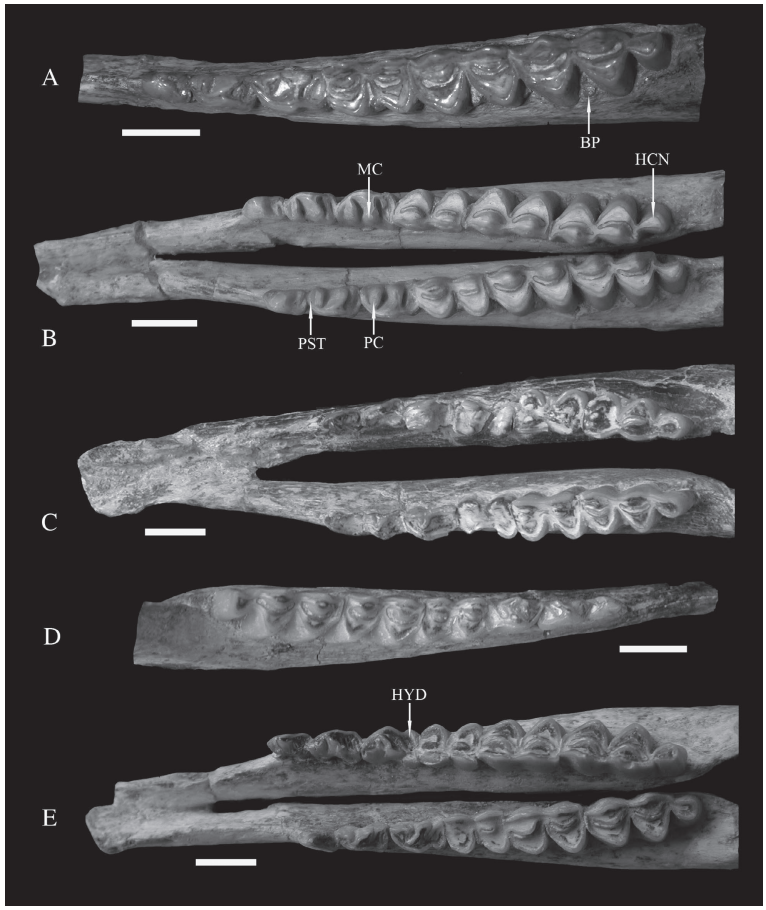

Fig. 3 Occlusal view of mandibles of *Gazella* cf. *G. lydekkeri* from Lantian
A. IVPP V 15246, B. V 15247, C. V 15248, D. V 15249, E. V 15250. Scale bars=1 cm
Abbreviations: BP. basal pillar; HCN. hypoconulid; HYD. hypoconid; MC. metaconid; PC. paraconid; PST. parastyle

occlusal surface. The paracone is large. There is parastyle, however, the metastyle is weak. The protocone is located in the middle line, with the anterior and posterior ridges to form the triangle shape together with the labial cusps. The molars are basically quadrate in shape. The size increases from M1 to M3. On M1-2, there are small lingual basal pillars. Labial styles are developed, of them the mesostyle is the largest. The rib between the parastyle and mesostyle is more developed than the posterior rib.

The i1 is shovel shaped, with a straight medial side, and flanged distal side. The i2 is long rectangular in shape, and much smaller than i1. There preserved only the root of i3 on V 15249. The canine exists by preservation of its root, and extends anteriorly by the direction of root, possible having the shape of incisors. The p2 is small with a simple occlusal structure. The protoconid is the main cusp, and the paraconid is much lower and not well separated from the protoconid. The p3 is significantly larger than p2. Its paraconid is well separated

from protoconid, and not connected with parastyle and metaconid. The metaconid extends posterolingually, but does not contact with entoconid. The protoconid is slightly more anterior than the metaconid, and the hypoconid is not enlarged. The p4 has rather derived looking characters, e.g. the metaconid extends anteriorly and connects with the paraconid in later wear, and posteriorly connected with the entoconid. The hypoconid is prominent, with a furrow separating with the protoconid on labial side. There exists hypoconulid, which connects with the entoconid. The paraconid extends posterolingually and well separated from the parastyle. Lower molars have basal pillars on buccal sides, which are more developed on males than on female individuals. The basal pillar decreases from m1 to m3. The goat folds are almost indistinguishable. The m3 has a large and labially offset third lobe, and developed anterior cingulum.

With skull V 15246, four cervical bones attached in situ. The other four skulls attached with atlases respectively. The atlas is trapezoid in outline with narrower proximal and wider distal side (Fig. 4A). The articulate fossae with the occipital condyles are deep and laterally bounded, separated by a shallow and wide notch dorsally, and wider and deeper U shaped notch ventrally. There developed two separate depressions by a central ridge at the anterior one third of dorsal arch. The ventral arch presents a median tubercle. The transverse processes are thin plate like, extending posterolaterally to form a sharp spike. The alar foramen is round without groove in dorsal view.

The axis (Fig. 4B) is longer than wide, with high and plate like spinous process dorsally, while the body is not developed, about half length of the axis. The odontoid process is C shaped surrounded by well developed saddle like articular facet. The transverse process flanges posterolaterally. The ventral ridge extends cranially but does not reach the level of the collar. The vertebral artery foramen opens obliquely, posteroventrally to it a smaller foramen opens anteriorly.

The third cervical (C3) is slightly shorter but stronger than the axis. The transverse processes are think plate shape, with longer length than the body, and lateral flange posterolaterally protruding. The ventral ridge in the middle of the surface is complete across the body. The dorsal arch is rectangular shape with four equally sized articular processes. The fourth cervical (C4) is similar to the third in morphology and size except the dorsal arch wider with stronger articular surfaces, and the transverse processes not confluent anteroposteriorly.

C6 has a more slender spinous process, and anteriorly pointed, more constrained lateral side of dorsal arch, and rod like transverse process which is more anteriorly positioned.

Different from the previous cervical bones, C7 has well developed spinous process which has same basal length with the dorsal arch and getting triangle shape from the mid height. The caudal width across the posterior articular processes is narrower and shorter than on the previous cervical.

The first thoracic (T1) is characterized by a saber shaped dorsal spine, and the presence

of anterior articular processes which are smaller than on the cervicals. Inferior to the transverse process there developed a saddle like articular facet for the tubercle of rib. The transverse processes and facets are getting smaller in the posterior thoracic bone. The last thoracic (T13) is more like a lumbar except having anterior costal pits and triangle shaped transverse processes.

Lumbars are similar in structure, tightly articulated each other with hook like articular processes, having flat wing like transverse processes. From the first to the last lumbar (L7), the body and dorsal arch get to shorter and wider from rectangular towards more square shape. The posterior articular surface of the body becomes wide oval shape to fit the anterior articular surface of the sacrum body.

The sacrum consists of four sacral elements (Fig. 4D). It has larger and more anteroposteriorly elongated hook like articular surfaces with the lumbars. The wing is roughly round shape, facing posterolaterally. The width of sacrum gets to narrow sharply posterior to the wing and minimum at the third sacral bone. The medial ridge is well united and forms a wall like plate with slightly enlarged dorsal roof.

Ribs are not well preserved because of the slenderness. The first rib is slightly curved. It has large tubercle articulated tightly with the saddle like facet of the first thoracic. The head is almost horizontally orientated with a long neck. The rib body gets to flatter and wider downwards.

There also preserved a partial sternum, which is flat plate like with a long rod shape xiphoid process (Fig. 4F).

The scapula (Fig. 4C) is triangle in shape. The spine is prominent, located anteriorly, with the central part curved. The glenoid fossa is round without obvious notch. The articular surface is at the same level with acromion.

In lateral view the humerus shaft is moderately curved, with the proximal posteriorly and distal anteriorly (Fig. 5A). The deltoid tuberosity is low and ridge like. The humerus head is large and round in shape. The greater tubercle is prominent and much higher than the lesser tubercle, and the intertubercular sulcus in between them is wide and shallow. The distal end of humerus extends laterally, with developed trochlea. The lateral epicondyle is larger than the medial epicondyle. The olecranon fossa is deep bounded by developed epicondylar ridges.

The ulna is almost fused with the radius in proximal end and leaves space downwards in the middle of the shaft. The proximal part above the trochlear notch is a thin and rectangular plate in lateral view with slightly curved posterior edge.

The radius is also moderately curved in lateral view as the ulna. The posterior surface of the shaft gets to flat or slightly concave in the middle part. The proximal head is short and wide, extending laterally with the medial part slightly longer than the lateral end. At the distal part, there exist two dorsal low ridges which are parallel each other.

The carpal bones are tightly in situ and not separated (Fig. 4I). The scaphoid is rectangular in medial view, anteroposteriorly longer than high, articulated proximally with the

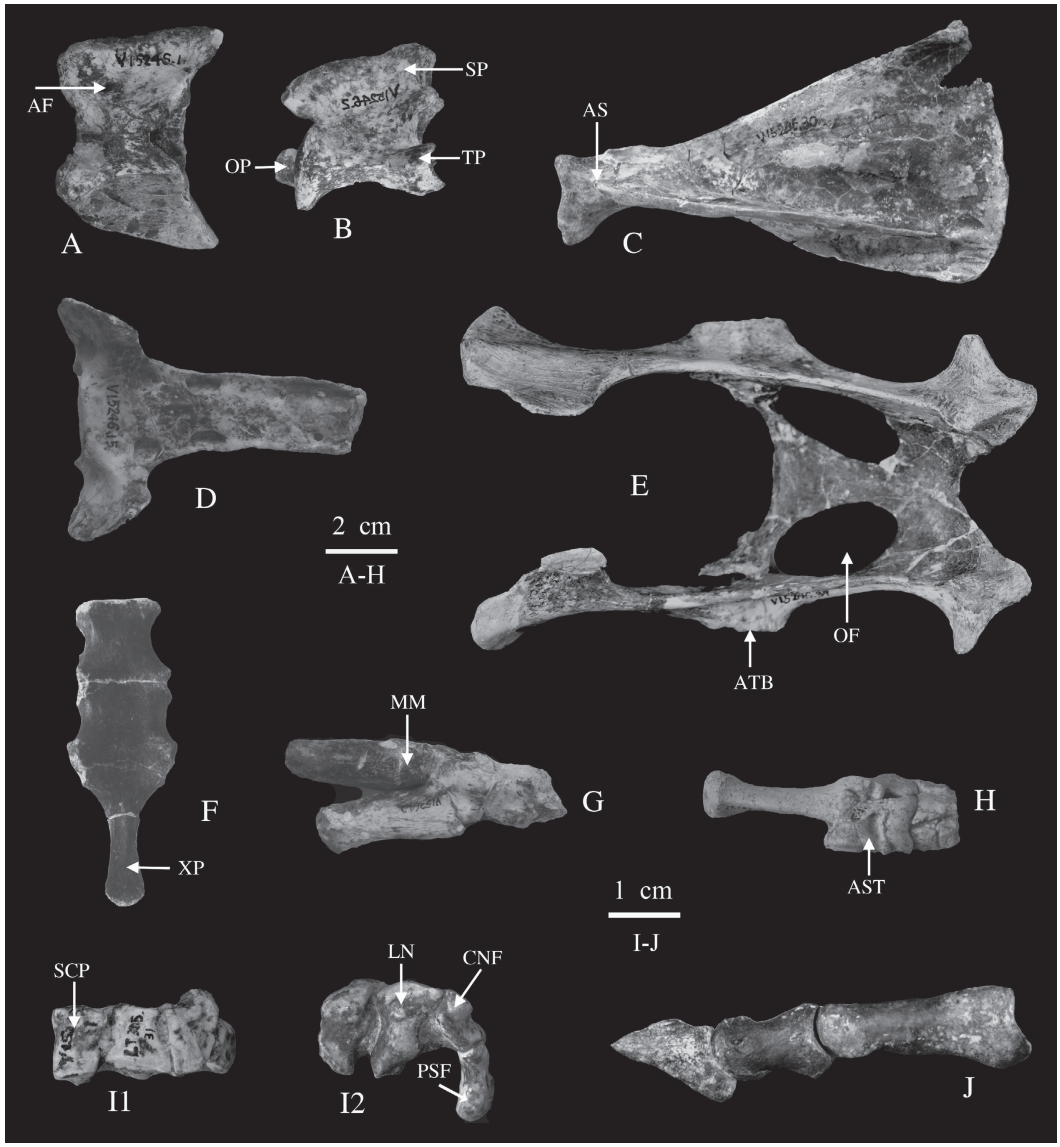

Fig. 4 Postcranials of *Gazella* cf. *G. lydekkeri* from Lantian
A. dorsal view of atlas (IVPP V 15246.1); B. lateral view of axis (reverse, V 15246.2); C. dorsal view of right scapula (V 15246.30); D. ventral view of the sacrum (V 15246.15); E. dorsal view of pelvic (V 15246.39); F. ventral view of sterum (V 15256); G. lateral view of tarsal with distal part of tibia (V 15264.2); H. dorsal view of the tarsal (V 15264.1); I. carpal (V 15265.1): I1. anterior view, I2. distal view; J. lateral view of left phalanges (V 15246.76)
Abbreviations: AF. alar foramen; AS. acromion of scapula; AST. astragalus; ATB. acetabulum; CNF. cuneiform; LN. lunar; MM. median malleolus; OF. obturator foramen; OP. odontoid process; PSF. pisiform; SCP. scaphoid; SP. spinous process; TP. transverse process; XP. xiphoid process

medial end of radius. The lunar locates in between the scaphoid and cuneiform, and articulates with the lateral end of radius, and both the magnum and unciform distally.

The metacarpal is about the length of the radius (Table 3), and the shaft is slightly curved

in lateral view. There exists a developed and wide groove on the plantar surface. On the dorsal surface at the distal part there is a slight vascular groove. The proximal articular surface is triangle shape, with developed metacarpal tuberosity. Two articular surfaces with sagittal ridge are separated by a deep intertrochlear notch.

Table 3 Length of long bones of *Gazella* cf. *G. lydekkeri* from Lantian (mm)

	femur	tibia	metatarsal	humerus	radius	metacarpal
V 15246	164	204		124	142	141
V 15257.1				122		
V 15257.2				122		
V 15259.1					155	
V 15263.1			167			
V 15263.2			168			
V 15263.3			169.5			

The pelvic is almost complete with only slightly loss at the iliar wing (Fig. 4E). The articular surface with the sacrum is flat. The ventral side of the ilium body is straight and end with a deep fossa anterior to the acetabulum, which located in the middle of the ilium and ischium. The greater sciatic notch is obtuse incised. The lesser sciatic notch is very shallow. There developed three tubercles at the posterior end of ischium, of them the lateral one is the largest. The obturator foramen is long oval shaped. The pubis is L shaped with a ridge developed along the pelvic symphysis.

The femur (Fig. 5B) head is round and bulky in the medial part and the articular surface gets to narrower and constrained laterally toward the level of middle line of the femur shaft. The greater trochanter is rectangular plate like in lateroposterior view, and the proximal end higher than the femur head. The notch in between them is narrow. The lesser trochanter is moderately developed and connected with the greater trochanter by a crest, which enclose the deep trochanteric fossa. The femur shaft is slightly curved in lateral view. The medial trochlear ridge is thicker and higher than the lateral ridge and extends more proximately. The trochlear ridges extend obliquely with the long axis of the shaft, with an angle about 20°. The lateral condyle is more robust than the medial one, and both are obliquely elongated, however, with reversed direction with the trochlear ridges.

The tibia is the longest limb bone (Fig. 5C). The proximal part is stronger with developed tibial tuberosity and high crest extending downward to the one third of the shaft. The medial side of the crest is flat and lateral side concave. The cross section of the shaft near the proximal part is triangle in shape and turns to be rectangular shape distally. With the developed tuberosity, the proximal articular surface is a sharp triangle, incised laterally by the extensor groove. The intercondylar tubercles are prominent. The lateral articular surface with femur condyle is slightly larger than the medial one by extension of the posterolabial corner of the triangle. Below this protrusion, there fused the proximal part of vestige fibula. At the distal end, two deep sagittal orientated trochlear grooves separated by a central ridge. The medial groove is narrow and longer than the lateral one and bounded medially by the medial malleolus, which

Fig. 5 Long bones of *Gazella* cf. *G. lydekkeri* from Lantian
A. right humerus (IVPP V 15246.32); B. right femur (V 15246.40); C. right tibia (V 15246.42); D. right radius (V 15246.22); E. right metacarpal (V 15246.38); F. right metatarsal (V 15263.1)
A1-F1. anterior view; A2-F2. posterior view. Scale bar=2 cm

is spike like and protrudes downwards and articulates with the medial surface of astragalus.

The calcaneum is robust built with medial-laterally compressed body. The calcaneal tuberosity is prominent dorsally and triangle shape, while ventrally there developed a trochlear shape groove. The anteroposterior length of the calcaneum body gets to longer and reaches the maximum below the sustentaculum. The articulate surface with the medium malleolus has similar size proximal convexity and distal concavity (Fig. 4G, H).

The metatarsal is about 20% longer than the metacarpal. The cross section of the shaft is

subrectangular, with width slightly shorter than the length (Fig. 5F). There is a wide and deep groove on the dorsal surface of the shaft. The proximal articulate surface is pentagonal shape. The distal end consists of two similar sized articulate trochleae.

The phalanges of hand and foot in bovids are very similar in shape and size (Sisson, 1914). Before further analysis, we describe them together as phalanges. The first phalanx is the longest one with slightly convex lateral surface and flat medial side. The proximal articulate surface is divided into two parts by a deep central groove. The lateral part is larger than the medial part. The first and second phalanxes have similar distal morphology, centrally separated into two articulate surfaces. The second phalanx is about two thirds of the first phalanx in length. The third phalanx is triangle shape diminishing distally (Fig. 4J).

Based on the materials described, we mounted a complete skeleton using casts of the specimens (Fig. 6) with only some ribs and tails reconstructed referring living goats.

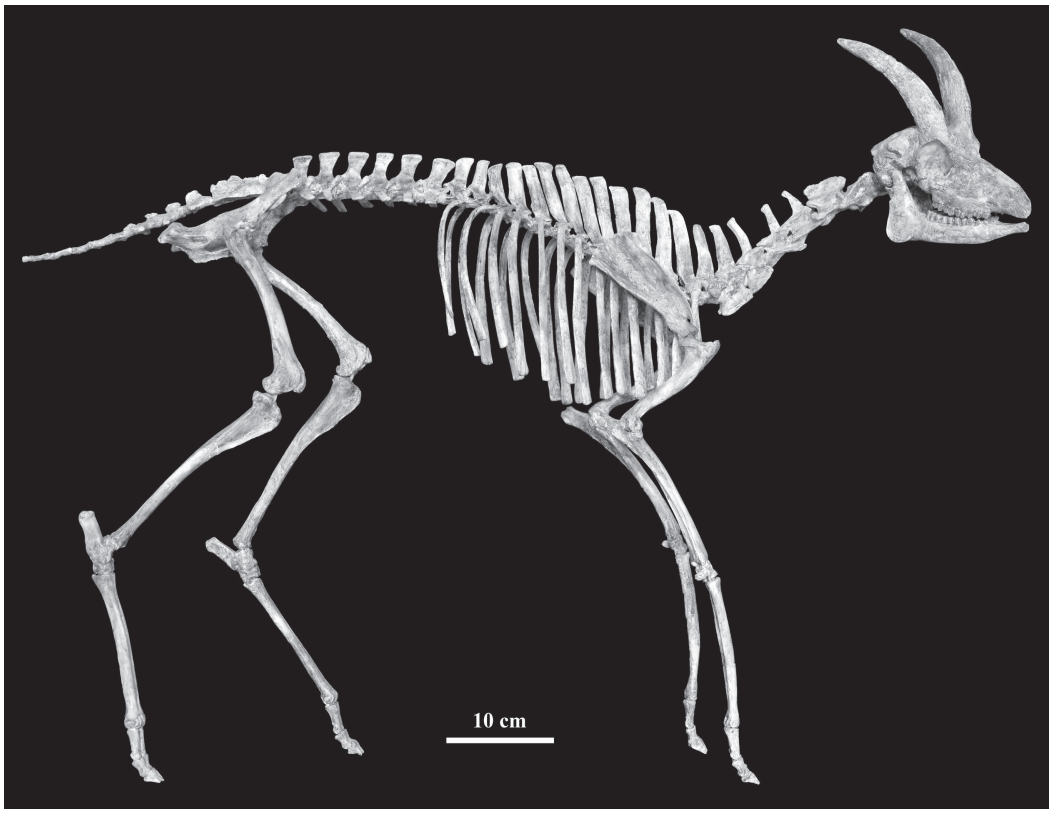

Fig. 6 Mounted skeleton (cast) of *Gazella* cf. *G. lydekkeri* from Lantian mainly based on IVPP V 15246 and reconstructions on other referred specimens
Courtesy of Mr. Cao Qiang and his colleagues for the reconstruction and mounting

3 Comparison

All the five skulls with jaws have similar size (Table 1-2) and morphology except the males having horns. One way ANOVA analysis of the tooth measurements confirms no significant differentiations. Hence, they can readily be attributed into one species.

The specimens here described have similar size with the female skull of *Dorcadoryx orientalis* (IVPP V 14423) from the same formation (Chen, 2005: fig. 1B), however their cheek teeth are proportionally smaller than the latter species. Although dorsal-ventrally distorted, V 14423 shows shallow preorbital fossae and wider snout by less forward diminishing at the premolar rows. The horn-cores from the frontlets of *Dorcadoryx orientalis* are also larger and tapering faster upwards.

The morphology of the Lantian species has characters of the most common bovid genus *Gazella* as listed by Gentry (2010), e.g. size small with moderate long horn-cores, the level of mediolateral width lying slightly behind the anteroposterior midpoint, without keels or torsion, of oval shaped cross section, the lateral surface flatter than the medial, moderately upright insertions, backward curved, placed the back of the orbits. There developed postcornual fossa, no sinuses within the frontals, braincase not shortened, occipital surface with each half facing partly laterally as well as backward, large tympanic bullae, m3 with large third lobe.

Fossil gazelles are rich in the "*Hipparion*" faunas. There have recorded more than a dozen species.

From Chinese Late Miocene, three species (*Gazella gaudryi*, *G. dorcadoides* and *G. paotehensis*) are the most common taxa, and in detail studied (Bohlin, 1935; Teilhard de Chardin and Young, 1931). Table 4 shows comparison with them based on observation of the specimens in the Lagrelius collection. Though with many similarities, the differences between the Lantian species and these three species are obvious.

The Lantian specimens are, however, more similar to *Gazella lydekkeri*, described by Pilgrim (1937), from the Dhok Pathan Formation of middle Siwaliks. They share many characters as following: females have no horn-cores; long and slender skull, with deep preorbital fossa and narrow face, the premaxilla extends back to the level of P2, the braincase longer than the width, face bent down on cranial axis at about 35°; The occipital surface is not flat, with a prominent median crest, terminating above in a knob-like swelling with flattened depressions on either side of it; tympanic bulla laterally flattened. The horn-cores have relatively flat lateral side and convex median side. The cross-section is basically oval or subtriangular. Molars have basal pillars, and p4 has hypoconulid separated with entoconid in early wear stage. The third lobe of m3 offsets labially. However, the Lantian specimens have some different characters: braincase more heavily bent down, horn-cores more compressed laterally, more divergent and less inclined, and relatively less closely set, lower mandible more slender, molars having goat folds less developed, ribs on upper and lower molars less developed, especially on P4 and last molars, the premolar row shorter relatively, and less

Table 4 Morphological comparisons with three species of *Gazella* from Chinese Late Miocene

Characters	*Gazella* cf. *G. lydekkeri*	*G. paotehensis*	*G. gaudryi*	*G. dorcadoides*
Female with horns or not	no	no	no	no
Cross section of horn-core	oval	oval	oval to round	round
Maximum transverse width	posterior	middle	middle	middle
Horn-cores compressed laterally	yes	moderate	no	no
Horn-cores inclination	moderate	moderate	moderate	strong
Horn-cores divergence	moderate	moderate	slightly	slightly
Horn-cores with longitudinal grooves	shallow	moderate	shallow	shallow
Postcornual fossa	deep	deep	deep	deep
Dorsal orbital rim	wide	wide	wide and horizontal	wide and horizontal
Frontal sinuses	no	no	no	no
Cranial roof inclined or curved posteriorly	inclined	hind part curved	curved	hind part inclined
Inter-frontal suture complicated	hind part complicated	complicated	hind part complicated	hind part complicated
Supraorbital foramina with surrounding pits	yes	yes	yes	yes
Length of braincase	long	short	long	short
Braincase sides widening	no	yes	no	yes
Temporal ridges approach	strongly posteriorly	strongly posteriorly	less	less
Lachrymal size	large	large	large	large
Maxillary tuberosity prominent	yes	yes	yes	yes
Ethmoidal fissure	yes	yes	yes	yes
Preorbital fossa	deep and wide	shallow and wide	deep and wide	deep and wide
Posterior tip of nasals surpass the level of orbital anterior rim	no	no	just reach the line	just reach the line
Infra-orbital foramen	P2	P2	P2	P2
Premaxilla contacting nasals or not	yes	yes	yes	yes?
Palatine foramina at the level of	M2	M2/M3	M2	M2
Auditory bulla	large	long and narrow	long and narrow	small and round
Basioccipital, shape	subrectagular	rectangular	rectangular	rectangular
Anterior tuberosities of basioccipital, size	large	small	large	varies
Foramina ovalia size, open	large, lateral	large	–	–
Occipital surface faces laterally or posteriorly	laterally	slightly posteriorly	slightly laterally	slightly laterally
Mastoid exposure wide or narrow	wide	wide	wide	narrow
Mastoid contacts parietal	no	no	yes on female, no on male	no
Cheek teeth hypsodonty	mesodont	mesodont	mesodont	hypsodont
Length of premolar row less than 60% molar row	less		more	less
p3 metaconid ridge, oblique or transverse	oblique	oblique	oblique	oblique
Paraconid of p3+p4 indistinct or well separated from parastylid	distinct	distinct	distinct	indistinct
p4 with labial origin of metaconid situated posterior to protoconid	yes	yes	yes	yes
p4 with shallow or deep valley anterior to hypoconid	shallow	deep	shallow	deep

Continued

Characters	*Gazella* cf. *G. lydekkeri*	*G. paotehensis*	*G. gaudryi*	*G. dorcadoides*
Metaconid-entoconid fused or not on p4	no	yes in later wear	no	yes for young
Paraconid-metaconid fused or not on p4	variable	yes in early wear	no	no
m3 with extension of lingual wall posteriorly	yes	no	no	slightly
Upper molar mesostyles strong and with concave labial wall of metacone behind	no	yes	no	yes
M3 metastyle as a flange	no	no	no	slightly
Labial ribs between the styles on upper molars	week	week	week	no
Ectostylids on lower molars (basal pillar)	m1-m3	m1	m1-m3	no, even on very worn teeth
Lower molars with outbowed or flat lingual walls	outbowed	outbowed	slightly outbowed	flat
Lower molars with or without goat folds	no	no	no	no

prominent basioccipital tuberosities and no groove between them. Considering of the unknown individual variation of *Gazella lydekkeri*, we tentatively assign the Lantian specimens as *Gazella* cf. *G. lydekkeri* herein.

The Lantian species is distinct from *Gazella capricornis* form Pikermi, Greece in having less robust and more median-laterally flattened horn-cores, and relatively larger teeth. Compared with *G. deperdita* from Cucuron, France, the Lantian species has longer horn-cores, with the anteroposterior length decreasing gradually from the base to tip, and more straight insertion above the orbit, and also differs from *G. deperdita* which has strong posteriorly narrow horn-cores. The Lantian species differs from the Samos species *G. mytilini* in the latter having hinder half of the orbit situated beneath the horn-core, horn-cores parallel each other, more hypsodont teeth, basal pillars on molars wholly lacking etc. Different from *G. pilgrimi*, the Lantian species has more curved horn-cores, premolar row relatively shorter and basal pillars more developed on molars.

4 Discussion and conclusion

Bovid fossils from Chinese Middle Miocene are relatively rare and less diversified than from the Late Miocene. Only three genera, *Eotragus* of Bovinae, *Kubanotragus* of Hippotraginae and *Turcocerus* of Urmiatheriinae were documented previously (Chen and Zhang, 2009). The gazelle fossils found from Bahe Formation are the earliest records of Antelopinae in China.

Systematic study on all species of *Gazella* is still pending and out of the scope of this paper. Nonetheless, it is hardly to relate the Lantian species with all the later occurred species from China with some seemingly derived characters, e.g. short premolar row, enlargement of metaconid on p4, compressed oval shaped cross section of horn-core, long and bent downward

braincase etc.

Kurtén (1952) analyzed the "*Hipparion*" faunas found from Chinese Late Miocene, indicating the ecological significance of the high crowned *Gazella dorcadoides* and low crowned *Gazella gaudryi*, representing west dry and east humid realm in North China respectively. By tooth crown height, the Lantian species is intermediate between these two species, showing no strong diet preferences.

However, the Lantian species with slim and elegant body plan may indicate its good running ability. The femur has long and horizontal neck of femur head, deep notch between the head and greater trochanter, wide distal articulation and anteriorly projected median ridge. The tibia has prominent tubercles on the proximal articulation surface and two sagittally orientated deep trochlear grooves separated by a central ridge at the distal end. The metatarsal and metacarpal both have same size and paralleled articulate trochleae. The proximal articulate surface of first phalanx is divided into two parts by a deep central groove. All these but least characters indicate the adaptation of running forward fast without much flexibility of turning around (Gentry, 1970). The length ratios of radius/humerus and tibia/femur are roughly 120%, also suggest their fast running ability (Osborn, 1929). The fast running lifestyle possibly suggests an open environments during their living time period, consistent with the ecological pattern of Bahean Fauna (Zhang et al., 2002; Zhang, 2006), based on sedimentological study (Kaakinen and Lunkka, 2003) and isotope data (Kaakinen et al., 2006).

The bovid assemblage from the Bahe Formation, together with *Shaanxispira baheensis*, *Dorcadoryx orientalis*, *Lantiantragus longirostralis* (Zhang, 2003; Chen, 2005; Chen and Zhang, 2004) is in sharp contrast with the much more diversified assemblage of Baodean age (Chen and Zhang, 2009). The turnover of the bovid assemblage across the Bahean/Baodean fit the climatic and ecological change scenario suggested by Kaakinen et al. (2006) and Zhang et al. (2013).

Acknowledgements The authors sincerely thank all participants in the Lantian project for the discovery and excavation of the fossils described in this paper. Professor Chen Guanfang from IVPP provides critical comments and suggestions which highly improve the draft. ZZQ appreciates help from his senior colleague and mentor, Dr. Alan Gentry, when he visited Natural History Museum, London in 2002 as a newcomer. He also indebts to Dr. Solweig Stunes, recently deceased curator of Evolution Museum of Uppsala University for hosting his visits and study on the Lagrelius collection.

陕西蓝田灞河组晚中新世*Gazella*羚羊的形态特征与分类

张兆群[1] 杨 睿[1,2]

(1 中国科学院脊椎动物演化与人类起源重点实验室，中国科学院古脊椎动物与古人类研究所 北京 100044)

(2 中国科学院大学 北京 100049)

摘要：*Gazella*羚羊是“三趾马动物群”中常见成员，在晚中新世至更新世地层中广泛分布，演化速率相对较快，具有重要的生物地层学及生态指示意义，但在我国尚未有保德期之前的化石报道。本文研究的化石发现于陕西蓝田灞河组中部，磁性地层学资料显示其年代为晚中新世灞河期。化石标本包括了5个近乎完整的头骨、下颌以及颅后骨骼。根据发现的标本装架起第一个完整的*Gazella*羚羊骨架。形态对比与测量数据表明，蓝田标本与巴基斯坦西瓦里克发现的*Gazella lydekkeri*非常相近，而不同于欧洲晚中新世常见的*Gazella*各种以及我国发现的种类。从肢骨的形态分析与测量比例数据来看，*Gazella* cf. *G. lydekkeri*适合快速奔跑运动，可能生活在相对开阔的环境中，与灞河期动物群的生态类型以及与灞河组沉积学、同位素地球化学等研究所指示的相对干旱、半干旱的开阔草原环境相一致。

关键词：陕西蓝田，晚中新世，灞河组，羚羊

中图法分类号：Q915.876 **文献标识码**：A **文章编号**：1000−3118(2016)01−0001−20

References

Arambourg C, 1959. Vertébrés continentaux du Miocène supérieur de l’Afrique du Nord. Publ Serv Carte Géol Algérie, n s, Paléont, Mém, 4: 1–159

Bohlin B, 1935. Cavicornier der *Hipparion*-Fauna Nord China. Palaeont Sin, Ser C, 9(4): 1−166

Bohlin B, 1939. *Gazella* (*Protetraceros*) *gaudryi* (Schlosser) and *Gazella dorcadoides* Schlosser. Bull Geol Inst Uppsala, 28: 79−122

Chen G F, 1997. The genus *Gazella* Blainville, 1816 (Bovidae, Artiodactyla) from the late Neogene of Yushe Basin, Shanxi Province, China. Vert PalAsiat, 35(4): 233−249

Chen G F, 2005. *Dorcadoryx* Teilhard et Trassaert, 1938 (Bovidae, Artiodactyla) from the Bahe Formation of Lantian, Shaanxi Province, China. Vert PalAsiat, 43(4): 272−282

Chen G F, Zhang Z Q, 2004. *Lantiantragus* gen. nov. (Urmiatheriinae, Bovidae, Artiodactyla) from the Bahe Formation, Lantian, China. Vert PalAsiat, 42(3): 205−215

Chen G F, Zhang Z Q, 2009. Taxonomy and evolutionary process of Neogene Bovidae from China. Vert PalAsiat, 47(4): 265−281

Gentry A W, 1966. Fossil Antilopini of East Africa. Bull Br Mus (Nat Hist) Geol, 12: 43−106

Gentry A W, 1970. The Bovidae (Mammalia) of the Fort Ternan fossil fauna. In: Leakey L S B, Savage R J G eds. Fossil Vertebrates of Africa. London and New York: Academic Press. 243−323

Gentry A W, 2010. Bovidae. In: Werdelin L, Sanders W J eds. Cenozoic Mammals of Africa. Berkeley and Los Angeles: University of California Press. 741−796

Gray H, 1977. Anatomy, Descriptive and Surgical. New York: Gramercy Books. 1−1257

Kaakinen A, Lunkka J P, 2003. Sedimentation of the Late Miocene Bahe Formation and its implications for stable environments adjacent to Qinling Mountain in Shaanxi, China. J Asian Earth Sci, 22: 67−78

Kaakinen A, Sonninen E, Lunkka J P, 2006. Stable isotope record in paleosol carbonates from the Chinese Loess Plateau: implications for late Neogene paleoclimate and paleovegetation. Palaeogeogr, Palaeoclimatol, Palaeoecol, 237: 359−369

Kurtén B, 1952. The Chinese *Hipparion* fauna – a quantitative survey with comments on the ecology of the machairodonts and hyaenids and the taxonomy of the gazelles. Soc Sci Fenn Comment Biol, 13: 1−82

Osborn H F, 1929. The titanotheres of ancient Wyoming, Dakota and Nebraska. US Geol Surv Monogr, 55: 1−953

Passey B H, Eronen J T, Fortelius M et al., 2007. Paleodiets and paleoenvironments of Late Miocene gazelles from North China: evidence from stable carbon isotopes. Vert PalAsiat, 45(2): 118−127

Pilgrim G E, 1937. Siwalik antelopes and oxen in the American Museum of Natural History. Bull Am Mus Nat Hist, 72: 729−847

Schlosser M, 1903. Die fossilen Säugethiere Chinas nebst einer Odontographie der recenten Antilopen. Abh Bayer Akad Wiss, 22: 1−221

Sisson S, 1914. The Anatomy of the Domestic Animals. Philadelphia: W.B. Saunders Company. 1−930

Teilhard de Chardin P, Trassaert M, 1938. Cavicornier of South-Eastern Shansi. Palaeont Sin, New Ser C, 6: 1−99

Teilhard de Chardin P, Young C C, 1931. Fossil mammals from northern China. Palaeont Sin, Ser C, 9(1): 1−66

Xia L, Yang Q S, Feng Z J et al., 2005. A guide to the measurement of mammal skull II: Perissodactyla, Artiodactyla and Carnivora. Chinese J Zool, 40(6): 67−73

Yang Q S, Xia L, Ma Y et al., 2005. A guide to the measurement of mammal skull I: basic measurement. Chinese J Zool, 40(3): 50−56

Zhang Z Q, 2003. A new species of *Shaanxispira* (Bovidae, Artiodactyla, Mammalia) from the Bahe Formation, Lantian, China. Vert PalAsiat, 41(3): 230−239

Zhang Z Q, 2006. Chinese late Neogene land mammal community and the environmental changes of east Asia. Vert PalAsiat, 44(2): 133−142

Zhang Z Q, Liu L P, 2005. The late Neogene mammal biochronology in the Loess Plateau, China. Ann Paléont, 91: 257−266

Zhang Z Q, Gentry A W, Kaakinen A et al., 2002. Land mammal faunal sequence of the Late Miocene of China: new evidence from Lantian, Shaanxi Province. Vert PalAsiat, 40(2): 165−177

Zhang Z Q, Kaakinen A, Liu L P et al., 2013. Mammalian biochronology of the Late Miocene Bahe Formation. In: Wang X M, Flynn L J, Fortelius M eds. Fossil Mammals of Asia − Neogene Biostratigraphy and Chronology. New York: Columbia University Press. 187−202

第54卷 第1期
2016年1月

古 脊 椎 动 物 学 报
VERTEBRATA PALASIATICA

pp. 21−35
figs. 1−5

New record of a haplocyonine amphicyonid in Early Miocene of Nei Mongol fills a long-suspected geographic hiatus

WANG Xiao-Ming[1,2*] WANG Hong-Jiang[3] JIANGZUO Qi-Gao[2,4]

(1 *Department of Vertebrate Paleontology*, *Natural History Museum of Los Angeles County* Los Angeles, California 90007, USA * Corresponding author: xwang@nhm.org)
(2 *Key Laboratory of Vertebrate Evolution and Human Origins of Chinese Academy of Sciences*, *Institute of Vertebrate Paleontology and Paleoanthropology*, *Chinese Academy of Sciences* Beijing 100044, China)
(3 *Administration Station of Cultural Relics of Xilinguole League* Xilinhaote 026000, Nei Mongol, China)
(4 *University of Chinese Academy of Sciences* Beijing 100049)

Abstract We place on the record a newly discovered amphicyonid (beardogs) upper molar from the Early Miocene Lower Red Mudstone Member of Aoerban Formation in central Nei Mongol. This molar is highly diagnostic of European haplocyonine or North American temnocyonine, two subfamilies of beardogs that have long been known in those continents but notably absent in Asia. The new molar is strikingly similar to *Haplocyonoides mordax* and *Temnocyon percussor* with its dumbbell-shaped M1 outline, reduced parastyle, isolated protocone by a surrounding cingulum, and extreme reduction of pre- and postprotocristae. Given the limited material at hand, we tentatively refer the new Chinese fossil to the European *Haplocyonoides* cf. *H. mordax* because of their similar size and age relationship. If this identification is correct, our new record thus fills a large gap in the geographic distribution of the haplocyonines and represents an excursion of this rare subfamily from Europe.

Key words Aoerban, Nei Mongol; Early Miocene; Amphicyonidae; zoogeography

Citation Wang X M, Wang H J, Jiangzuo Q G, 2016. New record of a haplocyonine amphicyonid in Early Miocene of Nei Mongol fills a long-suspected geographic hiatus. Vertebrata PalAsiatica, 54(1): 21−35

1 Introduction

Straddling between Europe to the west and North America to the east, Asia has long been suspected to be either a source of certain Cenozoic mammals that, thus far, are only found in Europe and/or North America, or at the very least, must have been a “jumping board” to and from the continents of destination as they disperse. When taxa are found in both Europe and North America, their absence in Asia thus fuels speculation of a Holarctic continuity,

国家自然科学基金重点项目(批准号：41430102)资助。
收稿日期：2015-10-26

and the expectation that filling in the Asian gap may be a matter of time. Temnocyonine and haplocyonine amphicyonids are such an example of a long-suspected geographic hiatus waiting to be filled.

Temnocyoninae and Haplocyoninae are peculiar lineages of amphicyonids, or beardogs, with hypercarnivorous dentitions and in some species, digitigrade posture (Hunt, 2011). Members of these groups typically have a very trenchant lower molar battery that align their main cusps in a single row to facilitate shearing function and associated narrow, high-crowned premolar series (e.g., Bonis, 1973; Hunt, 2011; Peigné and Heizmann, 2003). Asian records of amphicyonids have generally lagged behind those of Europe and North America, partly because of a shorter history of field explorations associated with a late start of scientific enterprise in almost all Asian countries. Occasionally, field records in Asia do catch up, and we have the satisfaction of reporting a new fossil record of the haplocyonines from the Early Miocene of Nei Mongol (Inner Mongolia) that confirms, once again, Asia has much to offer in our understanding of Holarctic zoogeography.

Abbreviations ACM, Amherst College Museum of Natural History, Amherst, Massachusetts; AMNH, Division of Paleontology, American Museum of Natural History, New York; F:AM, Frick Collection, American Museum of Natural History, New York; IVPP, Institute of Vertebrate Paleontology and Paleoanthropology, Chinese Academy of Sciences, Beijing; IM, IVPP fossil localities from Nei Mongol; LACM, Natural History Museum of Los Angeles County, Los Angeles; NM, Northwest Museum, Portland State University, Portland, Oregon; SMF, Senckenberg Forschungsinstitut und Naturmuseum, Frankfurt; TRO, Timberlane Research Organization, Lake Wales, Florida; UCMP, Museum of Paleontology, University of California, Berkeley; UNSM, Vertebrate Paleontology, University of Nebraska State Museum, Lincoln; USNM, Department of Paleobiology, Smithsonian Institution, Washington, D.C.; YPM-PU, Princeton Collection, Peabody Museum, Yale University, New Haven.

2 Systematic paleontology

Class Mammalia Linnaeus, 1758
Order Carnivora Bowdich, 1821
Family Amphicyonidae Haeckel, 1866
Subfamily Haplocyoninae Bonis, 1966
Genus *Haplocyonoides* Hürzeler, 1940
***Haplocyonoides* cf. *H. mordax* Hürzeler, 1940**

Referred specimen IVPP V 22639, an isolated left M1. Collected by X. Wang on August 8, 2015.

Locality, stratigraphy, and age IVPP IM1530 locality (XWIM04), N43°20'34", E113°54'30", elevation 1050 m, Sonid Zuoqi, Xilinhot League, central Nei Mongol (Fig. 1).

Locality IM1530 is stratigraphically straddling the boundary of the Lower Red Mudstone and Middle Green Mudstone members of Aoerban Formation (Fig. 2). Locally the two members transition into each other, possibly due to diagenetic effects of the green coloration. IVPP

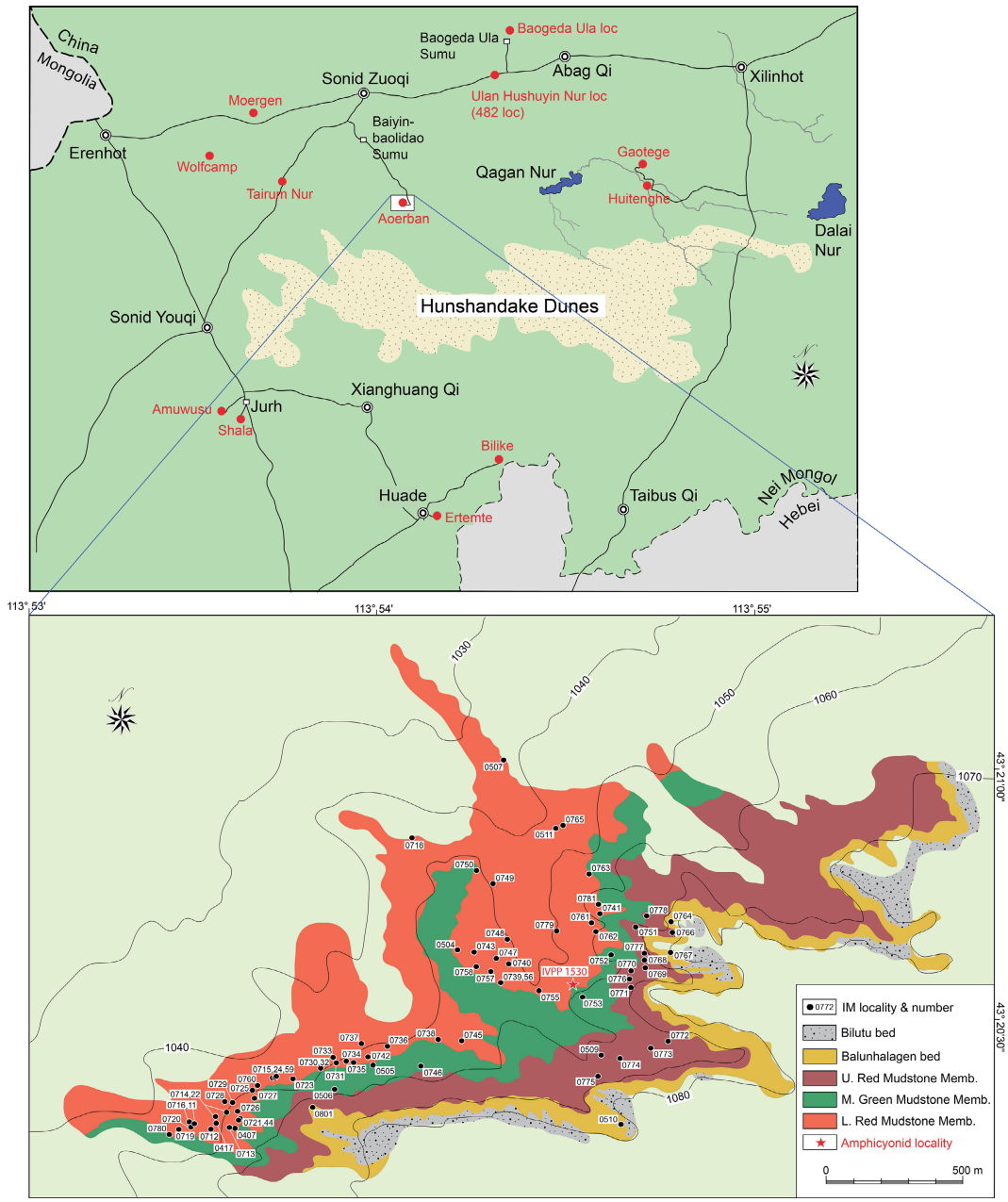

Fig. 1 Location of Aoerban area in central Nei Mongol (upper) and IVPP IM1530 locality (red star) and updated geologic map of Aoerban strata (lower)

Modified from Wang et al. (2009). Note that distribution of the Bilutu bed (light grey) differs substantially from that of Wang et al. (2009:fig. 1).

V 22639 thus belongs to the upper-most Lower Aoerban Fauna (Wang et al., 2009). Based on biochronology of small mammals, Qiu et al. (2013a) estimated that the upper part of the Lower Aoerban Fauna was approximately 19 Ma in the late Xiejian or possibly early Shanwangian Chinese land mammal ages (see Qiu et al., 2013b).

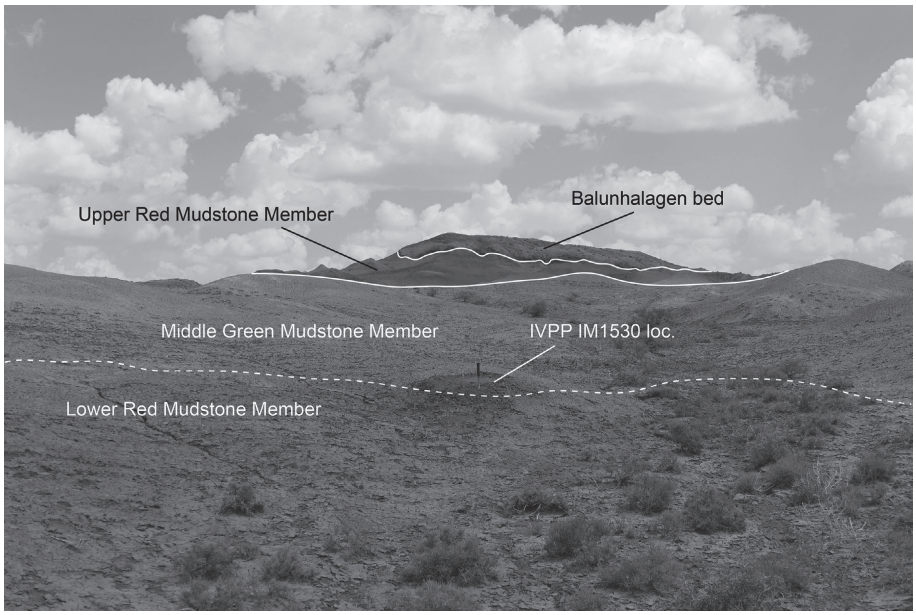

Fig. 2 Photograph of the IVPP IM1530 locality (marked by geologic hammer) at a transitional zone between the Lower Red Mudstone and Middle Green Mudstone members of Aoerban Formation
Stratigraphic scheme follows that of Wang et al. (2009:fig. 3). Photo looking south

Description With the exception of the missing roots, IVPP V 22639 is almost perfectly preserved, missing only the anterior rim of the enamels at the waist. Fresh breakage at the base of the roots indicates that the roots were broken after re-emergence from sediment encasement during the erosion. V 22639 shows signs of only minor wear at the apex of the metacone and thus represents that of a young adult.

V 22639 is almost twice as transversely wide as anteroposteriorly long (see measurements in Table 1). Overall it is dumbbell-shaped with a distinctly constricted waist at the junction of the protocone on the lingual side and paracone-metacone on the labial side. In occlusal view, paracone and metacone are about the same size, although the paracone is taller; this is especially true when viewed from the lingual side, but less so from the labial side. A parastyle is poorly developed, indicated by a slightly thickened and higher cingulum surrounding the parastyle. A distinct notch separates the paracone and metacone. Both paracone and metacone have an anterior and posterior ridge, which are aligned in a single line, and are completely encircled by a thin cingulum.

The protocone has a rounded base and located slightly anterior to the paracone-metacone notch. The low-crowned protocone is about half as tall as the metacone and about 1/3 of paracone. An extremely faint preprotocrista is present on its anterolabial face and is

Table 1 Measurements of upper first molars of Temnocyoninae and Haplocyoninae (mm)

Taxa	Specimen	n	L1	L2	L3	L4	L5
M1 of Aoerban	IVPP V 22639		15.1	15.0	20.7	21.8	10.8
Temnocyon altigenis	UCMP 9999			13.8	19.5		8.3
Temnocyon altigenis	AMNH 6857			14.0	21.5		9.3
Temnocyon altigenis	USNM 7940			13.8	20.5		9.0
Temnocyon altigenis	UCMP 1549			13.5	18.7		8.8
Temnocyon subferox	YPM 10065			14.7	20.6		10.2
Temnocyon fingeruti	NM 280/61			17.1	22.4		10.5
Temnocyon ferox	YPM-PU 10787			18.2	23.9		12.1
Temnocyon percussor	AMNH 81047			20.9	27.9		12.9
Mammacyon obtusidens	ACM 34-41			20.4	28.2		15.5
Mammacyon obtusidens	LACM 5386			17.8	24.8		13.1
Mammacyon ferocior	F:AM 54134			21.4	29.8		17.4
Delotrochanter oryktes	ACM 4804			17.7	25.4		14.7
Delotrochanter oryktes	UNSM 47800			17.5	23.9		14.1
cf. *Delotrochanter*	TRO 390			17.6	23.5		15.7
Haplocyon crucians		2	15.2	15.1e		21.8	10.5
Haplocyon elegans		5	12.2	12.2e		16.6	8.2
Haplocyon dombrowski		1	15.5	15.4e		21.5	9.5
Haplocyonoides suevicus		4	14.0	13.9e		20.9	9.8
Haplocyonoides morda		2	15.4	15.2e		20.2	10.4
Haplocyonopsis crassidens		1	18.4	18.3e		26.0	11.7

Note: Those for Temnocyoninae are adopted from Hunt (2011:tables 3, 5) and those for Haplocyoninae are means (when numbers of specimens are greater than one) from Peigné and Heizmann (2003:table 11). Since the lengths of M1s are defined somewhat differently between those in Hunt (2011:fig. 46) and those in Peigné and Heizmann (2003:8, fig. 3), we used the ratio of these two measurements (see Fig. 3 for definition of measurements) in IVPP V 22639 to estimate those of the haplocyonines (designated with an "e" after each measurement).

pointed to the narrowest point (anterior waist) of the tooth. A postprotocrista is slightly more distinct than the preprotocrista. It is anteroposteriorly oriented and ends posteriorly at the posterior cingulum. Both paraconule (protoconule) and metaconule are absent and this gives the protocone an isolated appearance. The protocone is nearly completely encircled by a cingulum of various thickness. Lingually this cingulum forms an almost perfect half circle and has similar crown-heights throughout the protocone. The cingulum, however, thickens toward the posterolingual aspect of the protocone, more than twice as thick as its anterior segment, and along the medial and

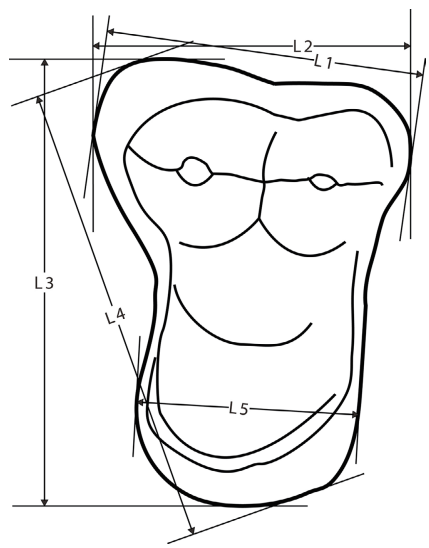

Fig. 3 Definitions of measurements for IVPP V 22639
L1. labial length; L2. anteroposterior length; L3. mediolateral width; L4. maximum transverse width; L5. length at protocone area

posterior sides of the protocone the cingulum has some minor wrinkles on its crest.

In anterior and posterior views, V 22639 has a distinctly concave appearance (Fig. 4A,

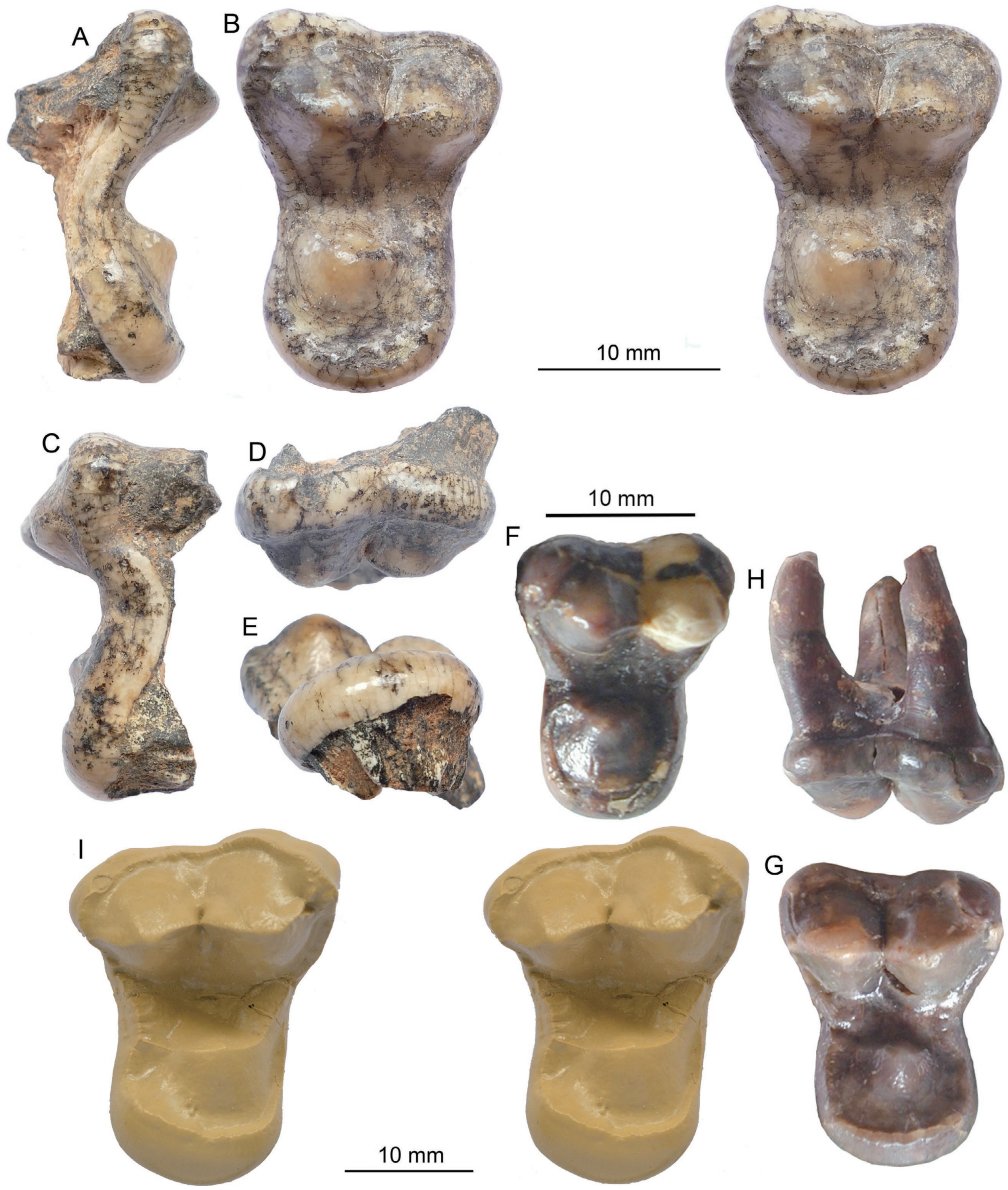

Fig. 4 *Haplocyonoides* cf. *H. mordax* Hürzeler, 1940 (A−E), IVPP V 22639, left M1 from Aoerban, Nei Mongol, *Haplocyonoides mordax* Hürzeler, 1940 (F−H), and *Temnocyon percussor* Cook, 1909 (I), AMNH 81047, right M1 from Cook Quarry, Sioux County, Nebraska

A. anterior view; B. stereo occlusal view; C. posterior view; D. labial view; E. lingual view; F. occlusal view of SMF-M1653e, left M1, paralectotype (sensu Peigné and Heizmann, 2003) from Hessler, Mainz Basin, Germany; G. occlusal and H. labial views of SMF-M6000, right M1, referred specimen from Budenheim, Rhineland-Palatinate, Germany (photograph courtesy of Stéphane Peigné of Muséum national d'Histoire naturelle, Paris); I. stereo occlusal view (photograph of a cast). Top scale bar is for A−E, middle one is for F−H, and lower one is for I

C) due to a deep trigon basin that occludes with a high-crowned m1 hypoconid. The high-crowned paracone-metacone crest shears with the labial face of the m1 hypoconid.

3 Comparisons

Despite the meager material from Aoerban, there is no doubt that V 22639 belongs to Amphicyonidae, although a dumbbell-shaped M1 is found in other similar-sized carnivorans, such as *Enhydrocyon* and *Paraenhydrocyon* of hesperocyonine canids (Wang, 1994), *Megalictis* of basal musteloids (Matthew, 1907), and *Eomellivora* of mellivorine mustelids (e.g., Valenciano et al., 2015). However, in all of the latter three cases, a prominently developed M1 parastyle dominates the labial half of the tooth with a much larger paracone and very reduced metacone, in sharp contrast to a more evenly developed paracone and metacone (with a more quadrate outline for the labial half of the tooth) in most amphicyonids.

The Aoerban tooth is easily distinguished from all known amphicyonids in Asia. Excluding small, primitive forms in the Late Eocene through Early Miocene, such as *Guangxicyon sinoamericanus* from the Late Eocene of Guangxi Province (Zhai et al., 2003), unnamed species from Late Eocene of Mongolia (Egi et al., 2009), *Cynodictis elegans* from Middle Oligocene of Nei Mongol (Huang, 1982), and the questionable *Ictiocyon* cf. *I. socialis* from Early Miocene of Gansu (Wang et al., 2005), almost all Asian Miocene forms are large amphicyonine amphicyonids. Well known examples include the Early Miocene *Amphicyon confucianus* and *Ysengrinia* sp. from Shanwang, Shandong Province (Qiu and Qiu, 2013; Qiu et al., 1986; Young, 1937), Middle Miocene *Ysengrinia* sp. of Japan (Kohno, 1997; Kohno et al., 1997), Middle Miocene *A. tairumensis* of Nei Mongol (Colbert, 1939) and Gansu (Deng et al., 2013), Middle Miocene *A. ulungurensis* of Xinjiang (Qi, 1989), and Late Miocene *A. palaeoindicus* and *Vishnucyon* cf. *V. chinjiensis* from Yunnan Province (Qi, 2006), although caution must be exercised in some of these generic assignments because many Asian taxa of large size, often based on fragmentary materials, tend to be placed in *Amphicyon* as tentative assignments (Hunt, 2003). From Southeast and South Asia, several taxa are assignable to amphicyonines, such as Middle Miocene *Maemohcyon potisati* of Thailand (Peigné et al., 2006), Late Miocene *Amphicyon* of Myanmar (Egi et al., 2010; Sein and Thein, 2011), *A. sindiensis*, *A. palaeoindicus*, *A. pithecophilus*, *Arctamphicyon lydekkeri*, and *Vishnucyon chinjiensis* from Early to Late Miocene Siwalik strata of India and Pakistan (Colbert, 1935; Lydekker, 1884; Pilgrim, 1932). M1 in *V. chinjiensis* has a markedly narrowed lingual half with a constricted appearance, but its protocone retains distinct pre- and postprotocristae (Pilgrim, 1932:plate II, fig. 9). When present, the M1s in these Asian forms have triangular outlines with distinct pre- and postprotocristae typical of amphicyonines, and are easily distinguishable from the dumbbell-shaped Aoerban M1. Even without an upper molar, these taxa have the reduced, low-crowned lower premolars or basined lower molars in contrast to the high-crowned premolars and trenchant molars in haplocyonines and temnocyonines.

Aktaucyon brevifacialis from the Early Miocene of Kazakhstan shows a hint of waist

constriction in M1 (Kordikova et al., 2000). However, its pre- and postprotocristae are still distinct and it has a large M2 relative to M1, features that suggest that its M1 constriction may be a result of convergence. The Middle Miocene *Gobicyon macrognathus* from Nei Mongol (Colbert, 1939; Zhai, 1964), and possibly also from Xinjiang (Wang et al., 1998) and Gansu (Deng et al., 2013), may be an aberrant form of haplocyonines because of its high-crowned, piercing premolars, although its fragmentary m1 talonid appears to be not quite as trenchant as its European relatives (Hunt, 1998:208). Unpublished upper M1s from Hezheng area, Gansu Province, also exhibit a dumbbell shape (Qiu Zhanxiang pers. comm.). A Serbian (formerly Yugoslavian) partial mandible previously referred to *G. macrognathus* by Pavlovic and Thenius (1959) has since become the basis of a new species *Haplocyonoides serbiae* (Ginsburg, 1999a), although its diagnostic characters are still in dispute (Peigné and Heizmann, 2003).

The distinctly constricted waist with a dumbbell outline in V 22639 is the most salient feature of this specimen, seen only in European haplocyonines and North American temnocyonines. Haplocyoninae is a lineage of hypercarnivorous amphicyonids from Late Oligocene to Middle Miocene of Europe, commonly including genera such as *Haplocyon*, *Haplocyonoides*, and *Haplocyonopsis* (Ginsburg, 1999a; Peigné and Heizmann, 2003). Dentally, it is characterized by high-crowned premolars and highly trenchant lower molars that may lose metaconids and entoconids (Bonis, 1966, 1973; Helbing, 1928; Peigné and Heizmann, 2003; Rothausen, 1988). Most haplocyonine species with a known M1 (including *Haplocyon crucians*, *Haplocyon elegans*, *Haplocyon dombrowskii*, *Haplocyonopsis crassidens*, *Haplocyonoides mordax*, *Haplocyonoides suevicus*) tend to be somewhat more primitive than V 22639 in their stronger parastyle, larger paracone relative to metacone with more acute angle of labial border of M1 with that of P4, M1 protocone with at least a remnant pre- and postprotocristae, and not very constricted waist area.

Advanced haplocyonines may have a dumbbell-shaped upper M1s, such as in *Haplocyonoides mordax* (Hürzeler, 1940). However, published figures of the only M1 of *H. mordax* (SMF-M1653e; Hürzeler, 1940:figs. 3-5) from the type locality in Hessler, Mainz Basin show several differences from that of V 22639: a relatively larger protocone, narrow cingulum surrounding the protocone, and a stronger preprotocrista with a distinct paraconule at the end (see Fig. 4F). Peigné and Heizmann (2003), however, referred a second M1 (SMF-M6000) from Budenheim, Rhineland-Palatinate, Germany, which has never been figured thus far. S. Peigné has graciously provided a photograph of this specimen to us that permits a much needed sense of variation (Fig. 4G, H). This referred specimen is strikingly similar to V 22639 in its much reduced protocone as a result of a widened surrounding cingulum, greatly reduced pre- and postprotocristae, and a nearly complete loss of a paraconule. As a result, lingual half of SMF-M6000 assumes a distinct appearance of an isolated protocone, not only because of its smaller protocone footprint relative to the broad surrounding cingulum but also its isolation from the trigon basin due to the reduction of pre- and postprotocristae. Details on the labial half of this tooth are also remarkably consistent with

that of V 22639. The labial side of SMF-M6000 is almost symmetrical with nearly identical size of paracone and metacone to the point that it is difficult to ascertain which side this tooth belongs without associated P4 or M2. Nevertheless judging by the slightly higher-crowned paracone and parastyle (Fig. 4H), we interpret this tooth to be a right M1, which, if correct, would be slightly more derived than V 22639 because of the general morphocline among European haplocyonines toward decreased parastyle and symmetrical paracone and metacone. Minor differences between the European and Chinese forms include a more anteriorly located protocone, a slightly more bulging parastyle, and a less distinct (not very ridge-like) lingual cingulum in V 22639.

Haplocyonoides mordax was initially established from Hessler near Wiesbaden in Mainz Basin, Germany in the Early Miocene (MN2) based on isolated upper and lower teeth (Hürzeler, 1940) that may or may not belong to a single individual (Rothausen, 1988). Bonis (1973:pl. 4, fig. 5) referred an additional right maxillary fragment with P4-M1 from Laugnac (MN2, Lot-et-Garonne) as ?*H. mordax*, although he noted that its M1 lacks a median constriction. More recently Ginsburg (1999b:119) also listed *H.* cf. *H. mordax* from "faluns of Anjou (MN3 or 5)" in addition to recognizing a new species, *H. serbiae* (formerly *Gobicyon macrognathus* by Pavlovic and Thenius, 1959), plus the previously described *H. ponticus* (Kuss, 1960). While describing a new German species, *H. suevicus*, Peigné and Heizmann (2003:appendix) provided a complete list of hypodigm for *H. mordax*. In addition to materials from the type locality and Laugnac mentioned above, they included one specimen from Weisenau (MN1) and three specimens from Budenheim (MN2), both from Mainz Basin in Rhineland-Palatinate, Germany. Furthermore, they (Peigné and Heizmann, 2003:68) listed several sites from the MN3 of France and M2 of Spain, but preferred to treat *H. mordax huerzeleri* (Rothausen, 1988) as *nomen dubium* as well as casting doubt over generic assignments of *H. serbia*e and *H. ponticus*.

V 22639 is also quite comparable to some North American temnocyonines, which share considerable similarities with European haplocyonines, interpreted to be convergences by Hunt (2011). In several respects temnocyonines have become even more hypercarnivorous than haplocyonines with short and robust crushing P4 in advanced forms, M1 protocone isolated by a flat platform of surrounding cingulum, substantial reduction of M2 and loss of M3, and digitigrade posture (Hunt, 2011). The M1 morphology is particularly diagnostic for the temnocyonines and clear trends can be observed to help delineate lineages. The smallest and most basal species, *Temnocyon altigenis*, has an enlarged parastyle, a protocone at the beginning stage of isolation but still with a preprotocrista connecting to a small paraconule, and a lingual cingulum slightly widened. Successively larger and more derived species, such as *T. subferox* and *T. ferox*, have a more isolated protocone, lost preprotocrista (in *T. subferox* but not in *T. ferox*) and paraconule, and more expanded lingual cingulum. *T. fingeruti*, apparently a side branch from the main chronospecies series (*T. altigenis-subferox-ferox*) (Hunt, 2011:fig. 70), does not quite follow this same trend, such as its retaining a strong

pre- and postprotocristae and a lack of middle constriction. Large, bone-crushing genera, *Mammacyon* and *Delotrochanter*, further elaborate this theme by widening the cingulum surrounding protocone, among other specializations.

In light of above trends within the main *Temnocyon* chronospecies series (Hunt, 2011:fig. 70), V 22639 falls somewhere close to *T. subferox* and *T. ferox* both in metric plot (Fig. 5) and some qualitative characters. The Chinese form has extremely reduced pre- and postprotocristae, not quite the complete loss in *T. subferox* (Hunt, 2011:fig. 10A) but certainly exceeded that condition in *T. ferox* (Hunt, 2011:fig. 12B). However, neither of the two North American species has reduced their parastyles quite to the extent as in V 22639. The degree of protocone area enlargement in V 22639 is also somewhat more pronounced than the above two American species. We also note that some characters are not strictly in a linear sequence, such as the precocious reduction of pre- and postprotocristae in *T. subferox*, although current knowledge about intraspecific variations is too limited to permit evaluation of morphological outliers.

A poorly known large species, *Temnocyon percussor* Cook, 1909, is also intriguingly close to V 22639. An isolated M1 (AMNH 81047) from the type locality (Cook Quarry,

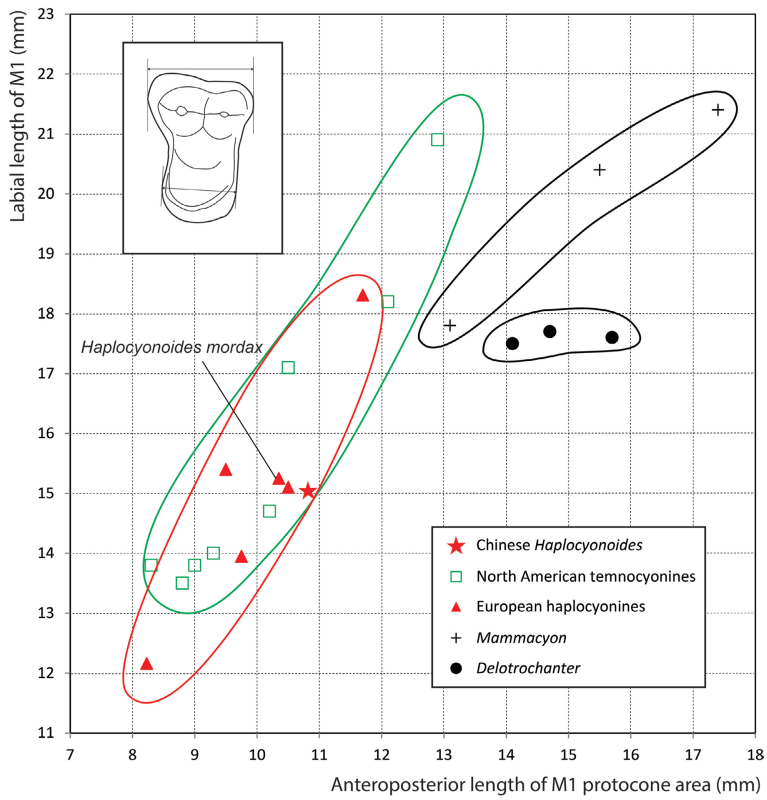

Fig. 5 Two dimensional plots of M1 anteroposterior length vs. M1 protocone length (see Fig. 3 for definitions) of Haplocyoninae and Temnocyoninae, as originally devised by Hunt (2011:fig. 46) to illustrate relative enlargement of the protocone area (Data from Table 1)

Anderson Ranch Formation, Sioux County, Nebraska, late Arikareean) was referred to this species (Fig. 4I). As described by Hunt (2011), this tooth is remarkably similar to V 22639. Its large size aside, AMNH 81047 has almost identical morphology of V 22639 in its protocone area enlargement: widening of lingual cingulum, reduction of pre- and postprotocristae, and reduction of parastyle. The only subtle difference is a slightly more convex labial border, compared to a very faint concave border in V 22639.

Although we cannot completely rule out the new Aoerban material being related to the North American temnocyonine, the balance of evidence, as shown in a single M1, seems to tip toward something close to *Haplocyonoides mordax*. In favor of such an assignment is the relatively closer age relationship of the Chinese and European forms (see Zoogeographic remarks below). If such a taxonomic assessment is correct, future discoveries of more complete materials of this Nei Mongol species should bear additional haplocyonine characters.

4 Zoogeographic remarks

In his study of Aquitanian mammals, Bonis (1973) commented the striking morphological similarities between European haplocyonines and North American temnocyonines, as was also noted earlier by Viret (1929). Bonis regarded these similarities as parallel developments by groups that are confined to their respective continents, a conclusion also maintained by Hunt (1996, 1998, 2011), who further explicitly derived his Temnocyoninae from within an early stock of Haplocyoninae (Hunt, 1998:fig. 11.3). Additionally, European haplocyonines and North American temnocyonines seem to have their independent evolutionary trajectory and chronological sequences, at least in the case of more derived temnocyonines (Fig. 5). If that is the case, it implies a single immigration event during the Early Oligocene that brought a primitive haplocyonine to North America to give rise to the temnocyonines, as has been postulated by Hunt (1998). However, *Haplocyonoides mordax* is much too late and too derived to be ancestral to temnocyonine.

If Peigné and Heizmann's (2003) concept of *Haplocyonoides mordax* is to be followed, the age range for *H. mordax* extends to European Neogene mammal zones 1-3. If we take this at its face value, i.e., a species range of as long as ~5 million years (23-18 Ma), the later part of the European records would be equivalent in age to the new Nei Mongol record. However, based on actual M1s from MN2 of Germany that we can compare, the Chinese form is likely an eastward expansion of this lineage. If so, the Aoerban form would be the first occurrence of this lineage in Asia, possibly followed by later *Gobicyon* in the Middle Miocene.

Acknowledgments We have profited greatly from discussions with Robert M. Hunt, Jr., who has been unstinting in sharing his vast knowledge of European and North American amphicyonids. We also greatly appreciate exchanges with Stéphane Peigné, who generously provided unpublished photos that are critical in the formulation of ideas in this paper.

Discussion with Louis de Bonis is also helpful in fossil identification. We thank Naoki Kohno for providing relevant reprints and a cast, and Naoko Egi for furnishing photos of Myanmar amphicyonid materials. We appreciate careful reviews by Qiu Zhanxiang and Zhang Zhaoqun; their comments and suggestions greatly improved this paper. We gratefully acknowledge the hard works by our 2015 field crew: Deng Tao, Yuri Kimura, Li Yikun, Sun Danhui, as well as our drivers Feng Wenqing and Gao Wei. Funding for field works during the past 20 years was provided by: Chinese National Natural Science Foundation (No. 41430102), Strategic Priority Research Program of the Chinese Academy of Science (XDB03020104), Chinese Academy of Science Outstanding Overseas Scholar Fund (KL205208), National Science Foundation (US) (EAR-0446699, 0444073, 0958704, 1227212 to XW), and National Geographic Society (NGS 5527-95 to XW).

内蒙古敖尔班地区早中新世犬熊类的新记录

王晓鸣[1,2*] 王洪江[3] 江左其杲[2,4]

(1 美国洛杉矶自然历史博物馆 洛杉矶 CA 90007 * 通讯作者)

(2 中国科学院脊椎动物演化与人类起源重点实验室，中国科学院古脊椎动物与古人类研究所 北京 100044)

(3 内蒙古锡林郭勒盟文物站 锡林浩特 026000)

(4 中国科学院大学 北京 100049)

摘要：犬熊科(Amphicyonidae)的4个亚科(Amphicyoninae, Daphoeninae, Haplocyoninae和Temnocyoninae)中，Haplocyoninae (简齿犬熊亚科)和Temnocyoninae (剪切犬熊亚科)是两类比较特殊的、高度食肉化的姊妹群。Haplocyoninae仅出现在欧洲的晚渐新世到早中新世，而Temnocyoninae则局限在北美的早渐新世到早中新世。目前亚洲虽还没有记录，但新近纪的亚洲无疑是欧洲与北美之间迁徙途中的必经之路。因此本文记录的新材料既是意外发现又是意料之中。2015年我们在内蒙古中部早中新世敖尔班组下红层中首次发现一枚犬熊类的左上第一臼齿。这颗臼齿虽然零星，但非常特征，属Haplocyoninae或Temnocyoninae无疑，值得记述。该牙齿由于中间的收缩及原尖周边齿带的变宽而具有明显的哑铃型轮廓。另外其原尖上的前、后脊也几乎消失，形成一种原尖缩小而且孤立的形态。上述特征与欧洲早中新世的*Haplocyonoides mordax* (咬合似简齿犬熊)似乎最接近，但由于材料稀少敖尔班犬熊类与北美的*Temnocyon percussor*更为接近的可能也不能完全排除。如果上述判断正确的话，新发现的*Haplocyonoides*则是目前发现的少数几例早中新世从欧洲迁移到亚洲的种类之一。这一支系在亚洲有可能延续到中中新世的*Gobicyon* (戈壁犬熊)。

关键词：内蒙古敖尔班，早中新世，犬熊亚科，地理分布

中图法分类号：Q915.874 **文献标识码**：A **文章编号**：1000–3118(2016)01–0021–15

References

Bonis L d, 1966. Sur l'évolution du genre *Haplocyon* Schlosser (Carnivora). Bull Soc Géol Fr, 8: 114−117

Bonis L d, 1973. Contribution à l'Étude des Mammifères de l'Aquitanien de l'Agenais, rongeurs-carnivores-perissodactyles. Mém Mus Natl Hist Nat, 28: 1−192

Bowdich T E, 1821. An analysis of the natural classifications of Mammalia, for the use of students and travellers. Paris: J. Smith. 1−115

Colbert E H, 1935. Siwalik mammals in the American Museum of Natural History. Trans Am Philos Soc, Philadelphia, New Ser, 26: 1−401

Colbert E H, 1939. Carnivora of the Tung Gur Formation of Mongolia. Bull Am Mus Nat Hist, 76: 47−81

Cook H J, 1909. Some new Carnivora from the Lower Miocene beds of western Nebraska. Bull Nebraska Geol Surv, 3(9): 261−272

Deng T, Qiu Z X, Wang B Y et al., 2013. Late Cenozoic biostratigraphy of the Linxia Basin, northwestern China. In: Wang X, Flynn L J, Fortelius M eds. Fossil Mammals of Asia: Neogene Biostratigraphy and Chronology. New York: Columbia University Press. 243−273

Egi N, Tsubamoto T, Tsogtbaatar K, 2009. New amphicyonid (Mammalia: Carnivora) from the Upper Eocene Ergilin Dzo Formation, Mongolia. Paleont Res, 13(3): 245−249

Egi N, Sein C, Maung-Thein Z-M et al., 2010. A new amphicyonid (Mammalia: Carnivora) from the lower Irrawaddy sediments (Myanmar) with comments on *Amphicyon* species from the Miocene of Asia. J Vert Paleont, 30(Suppl 3): 84A

Ginsburg L, 1999a. Order Carnivora. In: Rössner G E, Heissig K eds. The Miocene Land Mammals of Europe. München: Verlag Dr. Friedrich Pfeil. 109−148

Ginsburg L, 1999b. Order Creodonta. In: Rössner G E, Heissig K eds. The Miocene Land Mammals of Europe. München: Verlag Dr. Friedrich Pfeil. 105−108

Haeckel E, 1866. Generelle Morphologie der Organismen. Allgemeine Grundzüge der organischen Formen-Wissenschaft, mechanisch begründet durch die von Charles Darwin reformirte Deszendenz-Theorie. Band I: Allgemeine Anatomie der Organismen. Berlin: Georg Reimer. 1−462

Helbing H, 1928. Carnivoren des oberen Stampien. Abh Schweiz Palaeont Ges, 47: 1−82

Huang X S, 1982. Preliminary observation on the Oligocene stratigraphic section and on the fauna of the Wulantata'er area, Alxa Left Banner, Inner Mongolian Autonomous Region. Vert PalAsiat, 20(4): 337−345

Hunt R M Jr., 1996. Amphicyonidae. In: Prothero D R, Emry R J eds. The Terrestrial Eocene-Oligocene Transition in North America. Cambridge: Cambridge University Press. 476−485

Hunt R M Jr., 1998. Amphicyonidae. In: Janis C M, Scott K M, Jacobs L L eds. Evolution of Tertiary Mammals of North America, Volume 1: Terrestrial Carnivores, Ungulates, and Ungulatelike Mammals. Cambridge: Cambridge University Press. 196−227

Hunt R M Jr., 2003. Intercontinental migration of large mammalian carnivores: earliest occurrence of the Old World beardog *Amphicyon* (Carnivora, Amphicyonidae) in North America. In: Flynn L J ed. Vertebrate Fossils and Their Context: Contributions in Honor of Richard H. Tedford. Bull Am Mus Nat Hist, 279: 77−115

Hunt R M Jr., 2011. Evolution of large carnivores during the Mid-Cenozoic of North America, the temnocyonine radiation (Mammalia, Amphicyonidae). Bull Am Mus Nat Hist, 358: 1−153

Hürzeler J, 1940. *Haplocyonoides* nov. gen., ein aberranter Canide aus dem Aquitanien des Hesslers (Mainzer Becken). Eclogae Geol Helv, 33(2): 224−229

Kohno N, 1997. The first record of an amphicyonid (Mammalia: Carnivora) from Japan, and its implication for amphicyonid paleobiogeography. Paleont Res, 1(4): 311−315

Kohno N, Yamaoka T, Sugihara M, 1997. A Miocene amphicyonid (Mammalia: Carnivora) from Shobara City, Hiroshima Prefecture, southwestern Japan. J Hiba Soc Nat Hist, 182: 1−9

Kordikova E G, Heizmann E P J, Mavrin A V, 2000. Early Miocene Carnivora of Aktau Mountains, south eastern Kazakhstan. Paläont Z, 74(1/2): 195−204

Kuss S E, 1960. *Haplocyonoides ponticus* n. sp., ein neuer aberranter Canide aus dem Unterpliocän von Melchingen. Ber Naturf Ges Freiburg, 50(2): 247−250

Linnaeus C, 1758. Systema naturae per regna tria naturae, secundum classes, ordines, genera, species, cum characteribus, differentiis, synonymis, locis. Vol. 1: Regnum animale. Editio decima, 1758 (12th ed of Linaeus 1758). Stockholm: Societatis Zoologicae Germanicae. 1−824

Lydekker R, 1884. Indian Tertiary and post-Tertiary vertebrata. Vol. II, Part 6, Siwalik and Narbada Carnivora. Mem Geol Surv India Palaeont Indica, 2: 178−355

Matthew W D, 1907. A Lower Miocene fauna from South Dakota. Bull Am Mus Nat Hist, 23: 169−219

Pavlovic M, Thenius E, 1959. *Gobicyon macrognathus* (Canidae, Mammalia) aus dem Miozän Jugoslawiens. Anz Akad Wiss Wien, 11: 214−222

Peigné S, Heizmann E P J, 2003. The Amphicyonidae (Mammalia: Carnivora) from Ulm-Westtangente (MN2, Early Miocene), Baden-Württemberg, Germany − systematics and ecomorphology. Stuttg Beitr Naturkd Ser B, 343: 1−133

Peigné S, Chaimanee Y, Yamee C et al., 2006. A new amphicyonid (Mammalia, Carnivora, Amphicyonidae) from the late Middle Miocene of northern Thailand and a review of the amphicyonine record in Asia. J Asian Earth Sci, 26: 519−532

Pilgrim G E, 1932. The fossil Carnivora of India. Mem Geol Surv India Palaeont Indica New Ser, 18: 1−232

Qi G Q, 2006. Order Carnivora. In: Qi G Q, Dong W eds. *Lufengpithecus hudienensis* Site. Beijing: Science Press. 148−177

Qi T, 1989. Miocene carnivores from Altai region, Xinjiang. Vert PalAsiat, 27(2): 133−139

Qiu Z D, Qiu Z X, 2013. Early Miocene Xiejiahe and Sihong fossil localities and their faunas, eastern China. In: Wang X, Flynn L J, Fortelius M eds. Fossil Mammals of Asia: Neogene Biostratigraphy and Chronology. New York: Columbia University Press. 142−154

Qiu Z D, Wang X, Li Q, 2013a. Neogene faunal succession and biochronology of central Nei Mongol (Inner Mongolia). In: Wang X, Flynn L J, Fortelius M eds. Fossil Mammals of Asia: Neogene Biostratigraphy and Chronology. New York: Columbia University Press. 155−186

Qiu Z X, Qiu Z D, Deng T et al., 2013b. Neogene land mammal stages/ages of China − toward the goal to establish an Asian land mammal stage/age scheme. In: Wang X, Flynn L J, Fortelius M eds. Fossil Mammals of Asia: Neogene Biostratigraphy and Chronology. New York: Columbia University Press. 29−90

Qiu Z X, Yan D F, Jia H et al., 1986. The large-sized ursid fossils from Shanwang, Shandong. Vert PalAsiat, 24(3): 182−194

Rothausen K, 1988. Carnivoren im Kalktertiär (Oberoligozän-Untermiozän) des Mainzer Beckens (1. Amphicyonidae). Geol Jahrb, 110: 241−260

Sein C, Thein T, 2011. A new amphicyonid (Mammalia, Carnivora) from the Ayeyarwady Formation of central Myanmar. Univ Res J, 4(5): 45−57

Valenciano A, Abella J, Sanisidro O et al., 2015. Complete description of the skull and mandible of the giant mustelid *Eomellivora piveteaui* Ozansoy, 1965 (Mammalia, Carnivora, Mustelidae), from Batallones (MN10), Late Miocene (Madrid, Spain). J Vert Paleont, e934570

Viret J, 1929. Les faunes de mammifères l'Oligocène supérieur de la Limagne Bourbonnaise. Ann Univ Lyon N S, 47: 1−328

Wang X, 1994. Phylogenetic systematics of the Hesperocyoninae (Carnivora: Canidae). Bull Am Mus Nat Hist, 221: 1−207

Wang X, Ye J, Meng J et al., 1998. Carnivora from Middle Miocene of northern Junggar Basin, Xinjiang Autonomous Region, China. Vert PalAsiat, 36(3): 218−243

Wang X, Qiu Z X, Wang B Y, 2005. Hyaenodonts and carnivorans from the Early Oligocene to Early Miocene of Xianshuihe Formation, Lanzhou Basin, Gansu Province, China. Palaeont Electr, 8(1.6A): 1−14

Wang X, Qiu Z D, Li Q et al., 2009. A new Early to Late Miocene fossiliferous region in central Nei Mongol: lithostratigraphy and biostratigraphy in Aoerban strata. Vert PalAsiat, 47(2): 111−134

Young C C, 1937. On a Miocene mammalian fauna from Shantung. Bull Geol Soc China, 17: 209−245

Zhai R J, 1964. *Leptarctus* and other Carnivora from the Tung Gur Formation, Inner Mongolia. Vert PalAsiat, 8(1): 18−32

Zhai R J, Ciochon R L, Tong Y S et al., 2003. An aberrant amphicyonid mammal from the latest Eocene of the Bose Basin, Guangxi, China. Acta Palaeont Pol, 48(2): 293−300

第54卷 第1期
2016年1月

古 脊 椎 动 物 学 报
VERTEBRATA PALASIATICA

pp. 36−50
figs. 1−4

Restudy of the Late Oligocene dormice from northern Junggar Basin

WU Wen-Yu[1] MENG Jin[1,2] YE Jie[1] NI Xi-Jun[1] BI Shun-Dong[1,3]

(1 *Key Laboratory of Vertebrate Evolution and Human Origins of Chinese Academy of Sciences*, *Institute of Vertebrate Paleontology and Paleoanthropology*, *Chinese Academy of Sciences* Beijing 100044, China wuwenyu@ivpp.ac.cn)
(2 *Division of Paleontology*, *American Museum of Natural History* New York NY 10024, USA)
(3 *Department of Biology*, *Indiana University of Pennsylvania* Indiana PA 15705, USA)

Abstract A new glirid genus and species, *Gliruloides zhoui*, is named based on specimens from the Late Oligocene Tieersihabahe Mammal Assemblage Zone I (Tie-I zone) of the northern Junggar Basin, Xinjiang. The new genus is diagnosed by the following features: middle-sized dormouse; occlusal surface of cheek teeth concave; upper and lower cheek teeth dominantly with nine transverse ridges; the anterotrope(id) and posterotrope(id) well developed and extending almost full length of corresponding valleys; transverse ridges of upper cheek teeth usually free-ended labially; M1/2 with V- or narrow U-shaped trigon; the precentroloph not connected to the endoloph that is incomplete or nearly complete; the endolophid in lower cheek teeth discontinuous or continuous; labial end of the anterolophid curving slightly distally but not connected with the protoconid; root number of p4, m1-3, P4 and M1-3 being 2, 2, 3 and 3 respectively. We discuss the differences of *Gliruloides* from *Glirulus* and *Vasseuromys* and assign the Anatolian *Vasseuromys duplex* and *Vasseuromys* aff. *V. duplex* from the Early Miocene of Turkey to *Gliruloides*. It is posited that *Gliruloides* and *Glirulus* may share a common ancestor similar to *Glis guerbuezi* from the Lower Oligocene of Thrace, Turkey. *Gliruloides* might live in a relative wet and warm biotope.

Key words northern Junggar Basin, Late Oligocene, Tieersihabahe Mammal Assemblage Zone I, dormouse

Citation Wu W Y, Meng J, Ye J et al., 2016. Restudy of the Late Oligocene dormice from northern Junggar Basin. Vertebrata PalAsiatica, 54(1): 36−50

Our study on earliest Chinese dormice (Wu et al., 2000) was based on specimens collected in 1998 from the Late Oligocene Tieersihabahe Formation in northern Junggar Basin of Xinjiang. Only four teeth, among which three were assigned to *Glirulus* sp., were available at the time. Additional 11 teeth were collected by screenwashing at the same level of the

中国科学院战略性先导科技专项(编号：XDB03020501)和国家重点基础研究发展计划项目(编号：2012CB821904)资助。
收稿日期：2015-07-22

same locality (XJ 98024) and other nearby localities (XJ 98035, XJ 200209 and XJ 20004) in four field seasons from 1999 to 2002. All teeth but one right M3 (IVPP V 18113) are almost identical to the specimens described by Wu et al. (2000). Undoubtedly, they belong to the same taxon. Since the work of Wu et al. (2000), we have realized that these teeth show high similarities to *Vasseuromys duplex* from the Early Miocene of Anatolia (Ünay, 1994), and therefore cited *Vasseuromys* sp., instead of *Glirulus* sp., in fauna lists of our successive papers (Meng et al., 2001, 2006; Ye et al., 2001a,b; 2003a,b) but without further explanation. The present paper restudies the Late Oligocene Junggar dormouse based on all material available to us and reinterprets its taxonomic position.

Our study reveals that the specimens of the Late Oligocene Junggar dormouse are more similar to *Vasseuromys duplex* than to any other dormouse and that *V. duplex* differs considerably from other European *Vasseuromys* species and *Glirulus*. Thus, we name a new genus, *Gliruloides*, for the Junggar dormouse and assign the Anatolian species, *Vasseuromys duplex* and *Vasseuromys* aff. *V. duplex*, to this genus.

In describing the tooth morphology, we use a modified terminology derived from de Bruijn (1966) and Freudenthal (2004), which is convenient and unambiguous for description of the extra ridges of the dormice cheek teeth (Fig. 1). The SEM photographs were taken by Meng Jin, using the Hitach S-4700 scanning electron microscope at the American Museum of Natural History in 2005.

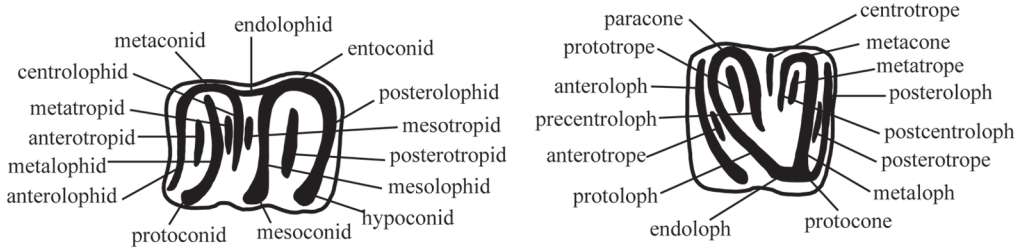

Fig. 1 Dental terminology of Gliridae
Modified from de Bruijn (1966) and Freudenthal (2004)

Family Gliridae Thomas, 1897
Subfamily Dryomyinae de Bruijn, 1967
Genus *Gliruloides* gen. nov.

Etymology *glirulus* + *oides,* indicates that the dormouse is morphologically similar to genus *Glirulus* but should not be *Glirulus*.

Type species *Gliruloides zhoui* gen. et sp. nov.

Diagnosis Medium-sized dormouse with concave occlusal surface of the cheek teeth. The upper and lower cheek teeth possess dominantly nine transversal ridges. The anterotrope(id) and posterotrope(id) of the upper and lower cheek teeth are well developed and extend almost full length of the corresponding positioned valleys. The trigon of M1-2 is V-

or narrow U-shaped, and the endoloph of upper cheek teeth is incomplete or nearly complete. The main ridges of the upper cheek teeth are labially free-ended. The endolophid of the lower cheek teeth is discontinous or continuous. The labial end of the anterolophid of the lower molars slightly curves distally, but not connected to the protoconid. Lower cheek teeth are two-rooted.

Differentiate diagnoses 1) *Gliruloides* differs from *Glirulus* in having a V-shaped or narrow U-shaped trigon on M1-2, the endoloph incomplete or nearly complete on upper cheek teeth, the lingual end of the precentroloph not connected to the endoloph, and main ridges in the upper cheek teeth free-ended labially. In contrast, the upper molars of *Glirulus* have wide U-shaped trigon, complete endoloph, and the precentroloph that connects lingually to the endoloph (except for geologically older representatives in which the endoloph may be incomplete and the precentroloph unconnected to the endoloph, refer Ünay, 1994). In *Glirulus* the main tooth ridges usually connect with each other labially and form the anterior and posterior loops (see Fig. 4D).

2) *Gliruloides* differs from *Vasseuromys* mainly in having nine ridges on most upper and lower molars, in having the developed anterotrope and posterotrope on the upper cheek teeth, and the usually regular and continuous extra ridges. In *Vasseuromys*, however, the anterotrope and posterotrope outside the trigon of the upper cheek teeth are absent or weak, and the extra ridges of the cheek teeth are usually irregular and interrupted (see Fig. 4B).

Included species *Gliruloides duplex* (Ünay, 1994) from Early Miocene (MN2) of Anatolia, localities Harami 1-3, Turkey. *Gliruloides* aff. *G. duplex* (Ünay, 1994) from Early Miocene (MN1) of Anatolia, localities Kilçak 0, Kilçak 0" and Kilçak 3A-3B.

***Gliruloides zhoui* gen. et sp. nov.**

Glirulus sp., Wu et al., 2000
Vasseuromys sp., Ye et al., 2001a, b, 2003a, b; Meng et al., 2001, 2006

Etymology In honor of the late Dr. Zhou Mingzhen (Minchen Chow), an academician of the Chinese Academy of Sciences and the pioneer paleomammalogist in China.

Holotype Left M2, IVPP V 18110.1 (Fig. 2C).

Paratype One left M3 (IVPP V 18110.2), one right m1 and one left m1 (V 18110.3-4), and one right m3 (V 18110.5) (Fig. 2D, H, J, K).

Type locality and horizon Locality XJ 98035, Tieersihabahe of northern Junggar Basin, Xinjiang; Tieersihabahe Mammal Assemblage Zone I; Late Oligocene.

Referred specimens One left P4 (IVPP V 18111.1, Fig. 2A), two right p4 (V 18111.2-3, Fig. 2F-G), one right m1 (V 18111.4, Fig. 2I) from XJ 98024. One left M1/2 (V 18112, Fig.2B) from XJ 200209.

The specimens described in 2000 include one right M2 (IVPP V 11812.1), one left M3 (V 11812.2) and one left m1 (V 11812.3) from XJ 98024 (Wu et al. 2000: pl. 1, figs. 1-3, 5).

All specimens listed above were from Tieersihabahe of northern Junggar Basin;

Tieersihabahe Mammal Assemblage Zone I; Late Oligocene.

One right M3 (V 18113, Fig. 2E), collected from XJ 20004 at Saerduoyila of northern Junggar Basin. The stratum producing the specimen is correlative to that of Tieersihabahe.

Diagnoses The p4 possesses eight transverse ridges. The anterotropid on the lower cheek teeth is usually single. The endoloph on upper cheek teeth is nearly complete, whereas the endolophid of lower cheek teeth is interrupted. The protoconid and mesoconid of the lower molars are hook-like. The metalophid extends slightly distally to the labial side and then turns abruptly mesiolabially.

Differentiate diagnoses *Gliruloides zhoui* differs from the Anatolian species *G. duplex* and *Gliruloides* aff. *G. duplex* in having 1) nearly complete endoloph on M1/2, 2) hook-like protoconid and mesoconid of the lower molars, 3) the metalophid almost always extends slightly distolabially and then turns abruptly mesiolabially and 4) possibly the rare presence of doubled-anterotropid on the lower molars. In contrast, *G. duplex* and *Gliruloides* aff. *G. duplex* normally have incomplete endoloph on M1/2 and rarely have hook-like protoconid and mesoconid. In both forms, the metalophid usually extends mesiolabially and a doubled-anterotropid is common on the lower molars.

Measurements (length × width in mm) P4 (V 18111.1) 0.87 × 1.05; M2 (V 18110.1) 1.05 × 1.25; M1/2 (V 18112) 1.03 × 1.09; M3 (V 18110.2) 0.92 × 1.05; M3 (V 18113) 0.77 × 0.98; p4 (V 18111.2) 0.86 × 0.68; p4 (V 18111.3) 0.84 × 0.67; m1 (V 18110.3) 1.17 × 1.05; m1 (V 18111.4) 1.16 × 1.09; m1 (V 18110.4) 1.13 × 1.06; m3 (V 18110.5) 1.11 × 1.00 (Except P4 is larger and m3 is slightly longer than in *G. duplex*, the other teeth are approximate to those of *G. duplex* in size.

Description The occlusal surface of all cheek teeth is concave. All the upper cheek teeth have usually nine transverse ridges, including the six main ridges (anteroloph, protoloph, metaloph, posteroloph, precentroloph and postcentroloph) and three extra ones (anterotrope, prototrope and posterotrope). Both the anterotrope and posterotrope extend almost the full length of the valleys where they locate. The labial ends of the main ridges are free or lightly connected. The lingual wall of the endoloph on upper cheek teeth is well decorated. All upper cheek teeth have three roots (one major lingual and two minor labial ones).

P4 The left P4 (V 18111.1; Fig. 2A) is suboval-shaped in occlusal view. Its occlusal surface is strongly concave. The anteroloph has its labial end separated from the protoloph and the lingual end touched the protoloph but not the endoloph. The lingual end of the posteroloph is weakly in contact with the endoloph and labially connects to the metaloph. The protoloph is labially free and lingually connects to the endoloph; it is interrupted midway by the U-shaped anterotrope-prototrope connection. The anterotrope extends to the labial border and stays free, whereas the prototrope is half long the anterotrope. The precentroloph ends free labially, but lingually it bifurcates to join the protoloph and metaloph, respectively. The postcentroloph is short and situated in the middle of the valley, with both ends being free. The metaloph is convex distally and interrupted near its lingual end. The posterotrope is long, filling nearly the

whole length of the corresponding valley. The trigon is V-shaped.

M1/2 Two M2 and one M1/2 are in the collection. The identification of specimen V 18112 (Fig. 2B) as M1 or M2 cannot be certain so that we denote it as M1/2 (but is probably M1 because of its V-shaped trigon). The holotype M2 (V 18110.1) is moderately worn and almost identical to the specimen V 11812.1 reported by Wu et al. (2000: pl. 1, fig. 1). The occlusal surface is wider than long. The paracone and metacone are prominent. The anteroloph is labially weakly connects to the paracone with a shallow furrow in between and lingually joins the endoloph. The paracone connects the labial end of the precentroloph loosely. The metacone is separated anteriorly from the postcentroloph and posteriorly from

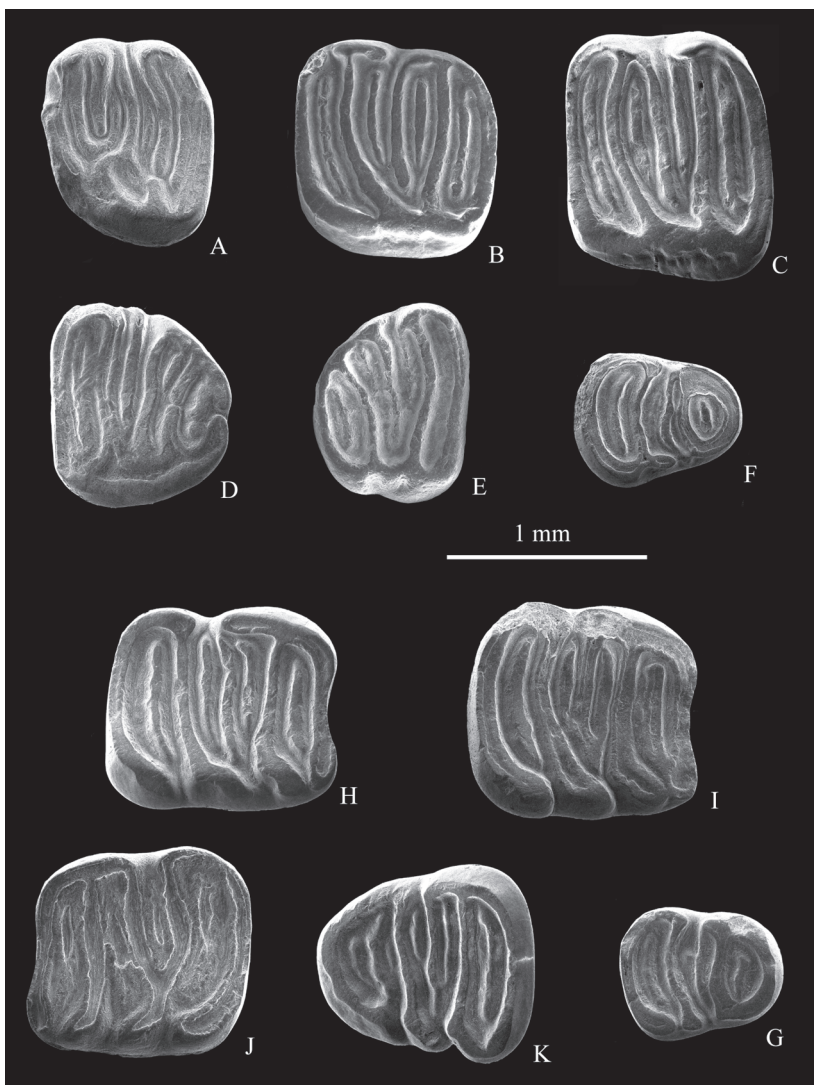

Fig. 2 *Gliruloides zhoui* gen. et sp. nov.
A. P4 sin. IVPP V 18111.1; B. M1/2 sin. V 18112; C. M2 sin. V 18110.1, holotype; D. M3 sin. V 18110.2, paratype; E. M3 dex V 18113; F. p4 dex, V 18111.2; G. p4 dex, V 18111.3; H. m1 dex, V 18110.3, paratype; I. m1 dex, V 18111.4; J. m1 sin., V 18110.4, paratype; K. m3 dex., V 18110.5, paratype

the posteroloph by a narrow and very shallow furrow, respectively. The precentroloph is long, extending to the point near the endoloph. The trigon is narrowly U-shaped and contains the long prototrope, precentroloph and postcentroloph. The lingual wall of the endoloph is well decorated. Specimen V 18112, a left M1/2 is slightly worn and closely similar to the holotype, but differs from the latter in being wider anteriorly than posteriorly, the V-shaped trigon, precentroloph being labially far separated from the paracone and curving backwards to the metacone, the anteroloph being labially free from the paracone, and loosely contacting with the protocone lingually to form a nearly complete endoloph. The anterotrope and posterotrope on all three specimens extend the whole length of the corresponding occupied valley.

M3 There are three M3 specimens (V 11812.2, V 18110.2 and V 18113), which are characterized by a trapezoid-shape, being much wider anteriorly than posteriorly. M3 has usually the same number of ridges as M1/2 but the precentroloph is much shorter than the postcentroloph. Specimen V 18110.2 is well worn. The labial side of the paracone was slightly damaged but it seems in connection with the anteroloph and protoloph. The precentroloph is much shorter than the postcentroloph and extends labially to the labial margin of the tooth and has no contact with both the paracone and metacone. The postcentroloph extends lingually and almost reaches the endoloph; its labial end is weakly connected with the metacone. The prototrope is absent, instead is a metatrope present inside the trigon. The metatrope is short, only a half width of the valley, and locates labially. Both metaloph and posteroloph are interrupted by a narrow gap at the midway. It seems that the endoloph is separated from the lingual end of the anteroloph before the tooth was worn. The specimen V 11812.2 (Wu et al., 2000: pl. 1, fig. 2) is highly similar to V 18110.2. There is, in addition to the anterotrope, an extra ridge between the anterotrope and protoloph. Both prototrope and metatrope are present. The specimen V 18113 (Fig. 2E) from XJ 20004 is similar to specimen V 11812.2, but its ridges are more slender and the anterotrope is weaker and shorter. We tentatively assign this tooth to this species.

The p4 Both p4 are round trapezoid in shape, wider posteriorly than anteriorly (Fig. 2F, G). The anterolophid is convex mesially and connected distally to the metalophid to form a closed loop. The centrolophid is thin and long, connected lingually to the metaconid weakly, and extends to the labial border. The labial end of the mesolophid turns abruptly mesially along the labial border on one specimen (V 18111.2) but becomes well-swollen labially on the other (V 18111.3); the mesolophid connects lingually to the posterolophid at the entoconid, and labially connected to or separated from the posterolophid. The anterotropid and posterotropid are well developed, and the mesotropid is short or long. The metatropid is absent in both teeth so that p4 is eight-ridged.

The m1 Four specimens are in the collection, including the one described by Wu et al. (2000: pl. 1, fig. 3). They are quite monotonous morphologically and generally trapezoid-shaped with the anterior end being slightly narrower than the posterior end. The m1 usually has nine transverse ridges, including five main ridges (anterolophid, metalophid, centrolophid,

mesolophid and posterolophid) and four extra ridges (anterotropid, metatropid, mesotropid and posterotropid). All four extra ridges are well developed, of which the anterotropid and posterotropid extend nearly the entire length of the located valleys. However, specimen V 11812.3, described by Wu et al. in 2000, remains an exception because it has an additional secondary extra ridge between the anterotropid and metalophid. For all specimens of m1, the anterolophid is slightly concave mesially, labial end slightly curved distally and free-ended; its lingual end slightly curved distally too, and gradually merges into the metaconid lingually. The metalophid is lingually connected to the metaconid and extends slightly distolabially, with its labial end turning abruptly mesially to form a hook-like protoconid that is not connected to the anterolophid. The centrolophid is long and extends labially near the mesoconid but does not reach to the labial border of the tooth. Lingually the centrolophid is either separated from or connected with the metaconid. The mesolophid is slightly convex distally and extends mesiolabially where, like the metalophid, it turns abruptly mesially and forms a hook-like mesoconid that is separated from the protoconid mesially and from the hypoconid distally. The posterolophid joins the mesolophid lingually at the entoconid. An endolophid is absent.

The m3 This tooth is mesially much wider than distally. The anterolophid is slightly convex mesially. Except for the four extra ridges seen in m1, there are two more secondary extra ridges: one mesial and the other distal to the posterotropid, respectively. Furthermore, a very small and weak enamel bulge but not ridge is present between the anterolophid and anterotropid.

All lower cheek teeth have two roots, but the mesial root of m1 (V 11812.3) shows a trend of bifurcation at the end.

Several teeth display distinctive striations of abrasion in mesiolingual-distolabial direction on the occlusal surface (Fig. 3), which we record here. We think this information should be useful for further study of this animal in masticatory movement, dietary, and perhaps taxonomy.

Comparisons and discussions As mentioned above, the Junggar glirid, represented by three specimens at the early time, was first assigned to *Glirulus* (Wu et al., 2000) because it is similar to *Glirulus* in having usually nine ridges on both upper and lower cheek teeth, with

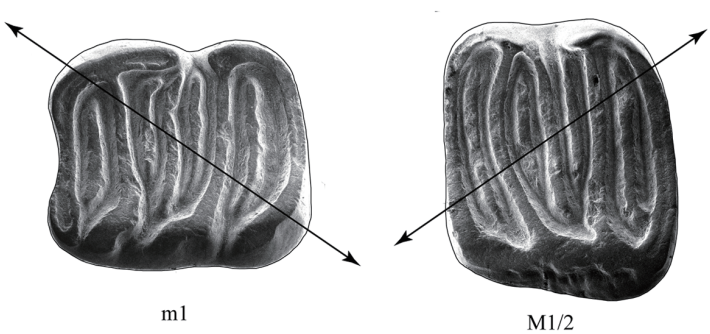

Fig. 3 Occlusal view of the lower and upper cheek teeth of *Gliruloides zhoui*
Arrows indicate the direction of striations caused by wear on the concave crown surface

well-developed anterotrope and posterotrope in upper cheek teeth and the anterotropid and posterotropid in lower cheek teeth. However, additional specimens collected subsequently made us to reconsider the taxonomic assignment of the Junggar glirid. We have listed above several features that differ the Junggar form from *Glirulus* in the differentiate diagnoses. At the same time, we noted that the Junggar form is quite similar to the Turkish Lower Miocene dormouse, *Vasseuromys duplex*, in both upper and lower molars. Thus, we considered that the Junggar glirid should not be assigned to *Glirulus* and have referred it to *Vasseuromys* in several of our papers (Meng et al., 2001, 2006; Ye et al., 2001a, b; 2003a, b) without explaining the reason until this study.

Vasseuromys was established by Baudelot and de Bonis (1966) based on the type species *V. rugosus* from the Lower Miocene of Laugnac, France. The only material of this species was a mandible with p4-m2. The original generic diagnosis states (translated from French by Daams and de Bruijn, 1995:50): "Medium-sized Gliridae. Cheek teeth with concave occlusal surface. Lower molars characterized by a centrolophid reaching the labial border and by a longitudinal prolongation of the labial cusps that form a nearly continuous ectolophid". Based on additional specimens of upper cheek teeth from the type locality de Bonis (1973:54) emended the diagnosis of the genus as: "*Vasseuromys* characterized by multiplicity of the extra ridges and by the upper molars with a continuous endoloph (translated from French)". The upper cheek teeth referred in the work of de Bonis (1973) consisted of one P4, one M1/2, and two M3. While working on the dormice from Austria and Spain, Daxner-Höck and de Bruijn (1981) and Alvarez Sierra et al. (1990) have independently visited the collections of *Vasseuromys rugosus* housed at the University of Utrecht; all the specimens are from the type locality. The two research teams noticed that there were several upper molars of *V. rugosus* with incomplete endoloph. Alvarez Sierra et al. (1990) wrote: "Although de Bonis (1973) characterizes this species as having a continuous endoloph (on the basis of one worn specimen), several M1,2 without endoloph are present in the collections of the University of Utrecht. The specimens from the Utrecht collections have a long anteroloph whose lingual end descends toward the base of the protocone." Daxner-Höck and de Bruijn (1981) further provided figures of the upper and lower molars of *V. rugosus*, which show the V-shaped or narrow U-shaped trigon and incomplete endoloph in the upper molars (Daxner-Höck and de Bruijn, 1981: fig. 1-h,r,s,t,u; fig. 2-m,n,o,p) (see Fig. 4B).

Up to now ten species have been included in this genus (ref. Daams and de Bruijn, 1995; Ruiz-Sánchez et al., 2012a, b; 2014):

Vasseuromys rugosus Baudelot & de Bonis, 1966; type locality and type level: Laugnac of France, MN2B, Early Miocene.

V. priscus de Bonis, 1973; type locality and type level: Moissac 1 of France, MN1, Early Miocene.

V. pannonicus (Kretzoi, 1978); type locality and type level: Budapest, Freshwater Limestone of the Széchenyi hill; MN10?, Late Miocene (Synonym: *V. thenii* Daxner-Höck &

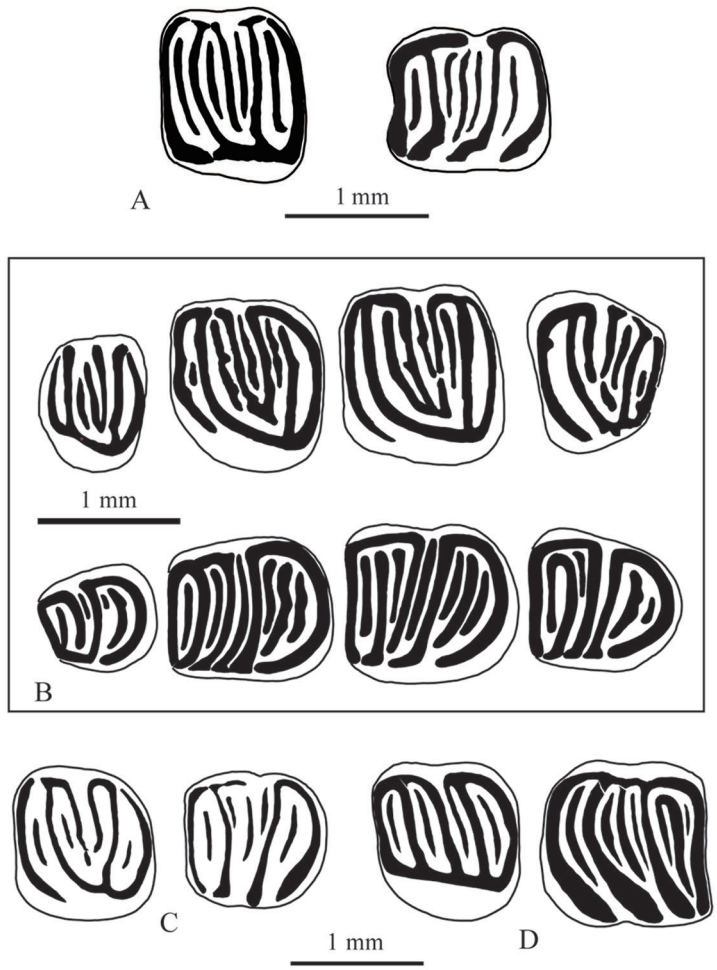

Fig. 4 The comparison of the upper and lower cheek teeth of *Gliruloides zhoui*, *Vasseuromys rugosus*, *Glis guerbuezi*, and *Glirulus japonicus*

A. *Gliruloides zhoui* gen. et sp. nov. from northern Junggar Basin, Late Oligocene (M2 and m2); B. *Vasseuromys rugosus* Baudelot & de Bonis, 1966 from the type locality Laugnac of France, MN2B, Early Miocene (after Daxner-Höck and de Bruijn, 1981) (P4-M3 and p4-m3); C. *Glis guerbuezi* Ünay-Bayraktar, 1989 from Thrace of Turkey (modified from Ünay-Bayraktar, 1989) (M2 and m2); D. *Glirulus japonicus* (Schinz, 1845) from the upper part of Horizon M of Kannondo Cave Site of Japan (modified from Kawamura, 1989) (M1 and m2)

de Bruijn, 1981).

V. autolensis (Cuenca, 1985); type locality and type level: Autol, La Rioja, Spain; MN1, Early Miocene.

V. bacchius (Martínez-Salanova, 1987); type locality and type level: Fuenmayor 2, Autol 1, La Rioja, Spain; MN2B, Early Miocene.

V. elegans Wu, 1993; type locality and type level: Stubersheim 3, Germany, MN3, Early Miocene.

V. duplex Ünay, 1994; type locality and type level: Harami 1, Turkey; MN2, Early Miocene.

V. cristinae Ruiz-Sánchez et al., 2012; type locality and type level: Pico del Fraile 2, Ebro Basin, Spain; MN4/5, Miocene.

V. rambliensis Ruiz-Sánchez et al., 2012; type locality and type level: Pico del Fraile 1, Ebro Basin, Spain; Upper Ramblian, MN3, zone A, Early Miocene

V. bergasensis Ruiz-Sánchez et al., 2014; type locality and type level: Bergasa, Ebro Basin, Spain; MP30, Late Oligocene (ref. Lacomba, 1988).

Apart from the above listed species, *Nievella mayri* Daams, 1976 from the Early Miocene of Cetina de Aragón, the early Late Miocene *Ramys multicresatus* (de Bruijn, 1966) and *Myolidus* may belong to *Vasseuromys*, as so suggested by Agusti et al. (2011).

The taxonomy, phylogeny and biostratigraphy of the known species of *Vasseuromys* are beyond the scope of this study. Our focus is on whether the Junggar form belongs to *Vasseuromys*, a potential assignment we have indicated in our previous studies (Meng et al., 2001, 2006; Ye et al., 2001a, b; 2003a, b).

After intensive survey of the literatures about *Vasseuromys*, we realized that, in general, all European species have features in common with the type species *V. rugosus* and differ from those of the Turkish *V. duplex* and *Vasseuromys* aff. *V. duplex*. We recognize the fundamental difference between them as representing two dental patterns of *Vasseuromys* cheek teeth, primarily reflected in the upper cheek teeth, which are differentiated below:

In European species of *Vasseuromys*, the anterotrope and posterotrope outside the trigon are usually absent; if present, they are short and weak; the ridges are rugose and asymmetrically arranged.

In *V. duplex* and *Vasseuromys* aff. *V. duplex* from Anatolia of Turkey, the anterotrope and posterotrope outside the trigon are always present and long; they extend almost the full length of the corresponding valleys they are in; the ridges are regular and symmetrically arranged.

In fact, Ünay (1994:470) already noted that "The striking features of Turkish *Vasseuromys* are the ever present long extra ridges in the anterior and posterior valleys outside the trigon on the M1/2… different from all European species." We found that the pattern of the anterotrope and posterotrope is present not only on M1/2 but also on P4 and M3 of Turkish *Vasseuromys* (Ünay, 1994). Because of the distinct morphological differences between the Turkish and European *Vasseuromys* species, we think that *V. duplex* should be inevitably assigned to a different genus. The Junggar and Turkish forms are also different from *Glirulus*, as we discussed above.

In addition to the tooth crown structures, we have compared the root number of various species of *Glirulus* (*Paraglirulus* included), *Gliruloides* and *Vasseuromys* (Table 1). All upper cheek teeth of the three genera are triple-rooted except that *Glirulus* (*Paraglirulus*) *werenfelsi* has a double-rooted P4. However, the available data show that the lower cheek teeth of all *Glirulus* species are double-rooted except that p4 of *Glirulus* (*P.*) *agelaki* from Aliveri is

single-rooted and *Glirulus japonicus* has double-rooted p4 and triple-rooted lower molars. *Gliruloides* has also double-rooted lower cheek teeth except that the m3 of *Gliruloides* aff. *G. duplex* is occasionally triple-rooted. Species of *Vasseuromys*, where the root condition is known, however, have a single-rooted p4 and double or triple-rooted lower molars. Table 1 shows that the Junggar form is similar to *G. duplex* not only in their tooth crown structures but also in the root number. However, it should be noted that only the m3 root number (two or three roots) of *Gliruloides* aff. *G. duplex* was provided by Ünay (1994), whereas the root number of m1/2 was not provided. With the survey of the root number distributions among relevant species, we consider the root condition to be of taxonomic information for species of the three genera in question, although more data are needed to verify this consideration.

In short, given that the Junggar and Turkish forms share some distinctive dental features but differ from the *Vasseuromys* and *Glirulus* in various features, we think they should be

Table 1 Comparisons of cheek teeth root number of *Glirulus*, *Gliruloides* and *Vasseuromys*

Genus and species	Root number			
	p4	m1-m3	P4	M1-M3
Glirulus japonicus[1)]	2	3	3	3
G. (*P.*) *schultzi*[2)]	–	2	–	3
G. lissiensis[2)]	2	2	3	3
G. (*P.*) *werenfelsi*[2)]	2	2	2	3
G. diremptus[3)]	2	2 (m1, m2)	3	3
G. conjunctus[3)]	2	2 (m1, m2)	3	3
G. minor[4)]	–	2 (m1)	–	–
G. ekremi[5)]	2	2	3	3
G. (*P.*) *agelakisi*[6)]	1	–	3	–
Gliruloides zhoui	2	2	3	3
Gliruloides duplex[5)]	2	2	3	3
Gliruloides aff. *G. duplex*[5)]	–	2 or 3 (m3)	–	–
Vasseuromys rugosus[7)]	1	–	–	–
V. priscus[7)]	–	–	–	–
V. pannonicus[2)]	1	3	3	3
V. autolensis[8)]	–	–	–	–
V. cristinae[9)]	–	–	–	–
V. bacchius[10)]	–	–	–	–
V. elegans[4)]	1	2	3	3
V. rambliensis[11)]	–	–	–	–
V. bergasensis[12)]	No relavent data are provided			

1) Kawamura, 1989; 2) Daxner-Höck and Höck, 2009; 3) Mayr, 1979; 4) Wu, 1993; 5) Ünay, 1994; 6) Meulen and de Bruijn, 1982; 7) de Bonis, 1973; 8) Cuenca, 1985; 9) Ruiz-Sánchez et al., 2012a; 10) Martinez-Salanova, 1987; 11) Ruiz-Sánchez et al., 2012b; 12) Ruiz-Sánchez et al., 2014.

placed in the same genus; thus we establish the new genus *Gliruloides* to include the Junggar and Turkish forms.

Gliruloides currently includes three species: *G. zhoui, G. duplex* and *Gliruloides* aff. *G. duplex* and tentatively assigned to the subfamily Dryomyinae because of several diagnostic features, such as the concaved surface, basically symmetrical upper molar, and some teeth with nearly complete endoloph.

The Origin of *Gliruloides* The Early Oligocene (ca. MP25) *Glis guerbuezi* from Thrace of Turkey (Ünay-Bayraktar, 1989) is, to our knowledge, the earliest known dormouse that displays considerable resemblance to *Gliruloides* in dental pattern. *G. guerbuezi* has at most nine transverse ridges in either upper or lower molars (see Fig. 4C). On certain M1/2s of *G. guerbuezi*, besides four main ridges, there are precentroloph, postcentroloph and prototrope inside the trigon, and anterotrope and posterotrope outside the trigon. In addition to four main ridges and centrolophid, the anterotropid and posterotropid are developed in m1 and m2, with incipient metatropid and mesotropid present in m2. M1/2 of *G. guerbuezi* also has V-shaped or narrow U-shaped trigon and an incomplete endoloph, and the anterolophid is labially isolated in lower molars. It is probable that *Gliruloides* was derived from a *Glis guerbuezi*-like ancestor, although we are not able to illustrate their detailed evolutionary process because of the limited knowledge available to us. Together with *Gliruloides duplex* and *Gliruloides* aff. *G. duplex*, Ünay (1994) also described two species of *Glirulus*: *G. ekremi* of MN3 (from Keseköy) and *Glirulus* aff. *G. ekremi* of MN2 (from Harami 1, associated with *V. duplex*)) from Anatolia. We have noticed that the Turkish *G. ekremi* has an incomplete endoloph in 27.50% of M1/2 specimens and a precentroloph connected to the endoloph in only 19.2% of M1/2s, and the lower molars of *G. ekremi* are morphologically very similar to those of the Turkish "*Vasseuromys*". Thus, identification of those teeth is not always unquestionable. It is also reasonable to infer that *Glirulus* may also be derived from the same *Glis guerbuezi*-like ancestor so that *Gliruloides* and *Glirulus* share a most recent common ancestor but evolved in different directions as two lineages. The fact that the root number of the most *Glirulus* species is same as that of *Gliruloides*, as shown in Table 1, could be another evidence for their common origin.

Ecology According to Walker (1975: volume 2:979) the living *Glirulus japonicus* inhabits mountain forests from about 400 to 1800 meters in elevation, with the highest recorded elevation being 2900 meters. This animal's diet includes fruits, seeds, insects and bird's eggs. All fossil specimens of *Gliruloides duplex*, *Gliruloides* aff. *G. duplex* and two species of *Glirulus* Ünay (1994) described were from Lower Miocene lignite containing sections (de Bruijn and Saraç, 1991) of Anatolia (from localities Keseköy, Harami 1-3 and Kilçak 0, 0", 3A, 3B). The morphological similarity of teeth in *Gliruloides* and *Glirulus* from Turkey could be attributed to a similar ecological environment (ecotope) and diet. The presence of lignite in the sections probably indicates wet biotopes (de Bruijn and Saraç, 1991; Ünay, 1994). *Gliruloides zhoui* is a member of the Late Oligocene Tieersihababe-I

zone fauna, collected from the same localities (XJ 20004 and XJ 98024) as the giant rhino *Paraceratherium sui* (Ye et al., 2003a) but was discovered from the level immediately above the level where rhinoceros located. Three rhino localities were found in Ulungur River area, which arrange in a west-east extending line with the largest distance of ca. 57 kilometers. *Paraceratherium sui* was discovered from the fluvial sediments at the base of Tieersihabahe Formation. Ye et al. (2012:1530) inferred that the presence of this giant rhino, at the time of ca. 25 Ma, is an implication of a temperature rise in the course of global cooling and aridification that begins from the Early Oligocene, which is coincided with the time of "Late Oligocene warming" (Zachos et al., 2001: fig. 2). *Gliruloides zhoui* might still lived in a relatively wet and warm transitional time somewhat later than *Paraceratherium sui*. We have mentioned above that *Gliruloides* could be derived from the *Glis guerbuezi*-like form. The latter came from the Turkish late Early Oligocene localities situated in the Lignite-Sandstone Formation (Ünay-Bayraktar, 1989:10). The sediments could also indicate that wet and forest environment existed during that period in this regional area.

Acknowledgements We thank Dr. Ruiz-Sánchez from Department of Geology, Division of Paleontology, University of Valencia of Spain for providing us important literatures about spanish *Vasseuromys*. Thanks are also due to the American Museum of Natural History, New York for permission to use the scanning electron microscope. We are grateful to Su Jianfen and Wu Shaoyuan for their hard work in the field and to Yue Qiwan for sorting the miniscule teeth from the concentration of screenwashed samples. We also thank many local peoples who helped us in collecting, transporting and screenwashing dirt samples under the baking sun of the desert. This research has been supported by the Strategic Priority Research Program of Chinese Academy of Sciences (CAS, XDB03020501) and National Basic Research Program of China (2012CB821904).

新疆准噶尔盆地北缘晚渐新世睡鼠再研究

吴文裕[1] 孟 津[1,2] 叶 捷[1] 倪喜军[1] 毕顺东[1,3]

(1 中国科学院古脊椎动物与古人类研究所，中国科学院脊椎动物演化与人类起源重点实验室 北京 100044)

(2 美国自然历史博物馆古生物学部 纽约 10024)

(3 美国宾夕法尼亚州印第安纳大学生物系 印第安纳 PA 15705)

摘要：周氏似日本睡鼠*Gliruloides zhoui*是发现于新疆准噶尔盆地北缘晚渐新世铁尔斯哈巴合哺乳动物组合I带的一个化石新属种。新属似日本睡鼠*Gliruloides*的属征为：中等大小；颊齿咀嚼面凹；上、下颊齿通常具9条主要横脊，有时具次级附脊；上颊齿的前边附脊和后边附脊以及下颊齿的下前边附脊和下后边附脊都很发育，几乎占据了其所在齿谷的整个长度。上颊齿的横脊唇端趋于游离。M1和M2具V形或窄U形三角座，内脊不完整或近

于完整，前中央脊不与内脊相连。下颊齿的下内脊通常不连续；下臼齿的下前边脊在唇端稍向后弯，但不与原尖相连。p4, m1–m3, P4, M1–M3的齿根数分别为2, 2, 3, 3。新属与*Glirulus*在形态上相似，但*Glirulus*的上颊齿的三角座均为宽U型，具有完整的内脊，前中央脊通常与内脊相交，横脊唇端通常不游离。新属与*Vasseuromys*属的最主要形态差异在于上颊齿具有很发育的前边附脊和后边附脊，而后者上颊齿的前边附脊和后边附脊通常缺失或很不发育。归入该属的种还有土耳其早中新世的*Vasseuromys duplex*和*Vasseuromys* aff. *V. duplex*。土耳其Thrace早渐新世的*Glis guerbuezi*很可能是*Gliruloides*和*Glirulus*的共同祖先类型。*Gliruloides*可能生活于温湿的生态环境。

关键词：准噶尔盆地北缘，晚渐新世，铁尔斯哈巴合哺乳动物组合I带，睡鼠

中图法分类号：Q915.873　　**文献标识码**：A　　**文章编号**：1000−3118(2016)01−0036−15

References

Agustí J, Pérez-Rivarés F J, Cabrera L et al., 2011. The Ramblian-Aragonian boundry and its significance for the European Neogene continental chronology. Contributions from the Ebro Basin record (NE Spain). Geobios, 44(2-3): 121−134

Alvarez-Sierra M A, Daams R, Lacomba J I et al., 1990. Paleontology and biostratigraphy (micromammals) of the continental Oligocene-Miocene deposits of the North-Central Ebro Basin (Huesca, Spain). Scripta Geol, 94: 1−77

Baudelot S, Bonis L de, 1966. Nouveaux Gliridés (Rodentia) de l'Aquitanien du basin d'Aquitaine. C R Soc Géol France, 8: 303−304

Bonis L de, 1973. Contribution a l'etude des mammifères de l'Aquitanien de l'Agenais: Rongeurs-Carnivores-Perissodactyles. Mém Mus Natl Hist Nat, Ser C, 28: 1−192

Bruijn H de, 1966. On the mammalian fauna of the *Hipparion*-beds in the Calatayud-Teruel Basin (Prov. Zaragoza, Spain). The Gliridae. Proc K Ned Akad Wet, Ser B, 69(3): 367−387

Bruijn H de, Saraç G, 1991. Early Miocene rodent faunas from the eastern Mediterranean area, Part I. The genus *Eumyarion*. Proc K Ned Akad Wet, Ser B, 94(1): 1−36

Cuenca G, 1985. Los Roedores (Mammalia) del Mioceno Inferior de Autol (La Rioja). Cienc Tierra, 2: 1−96

Daams R, 1976. Miocene rodents (Mammalia) from Cetína de Aragon (Prov. Zaragoza) and Buñol (Prov. Valencia), Spain. Proc K Ned Akad Wet, Ser B, 79(3): 152−182

Daams R, Bruijn H de, 1995. A classification of the Gliridae (Rodentia) on the basis of dental morphology. Histryx, 6(1-2): 3−50

Daxner-Höck G, Bruijn H de, 1981. Gliridae (Rodentia, Mammalia) des Eichkogels bei Mödleng (Niederösterreich). Paläont Z, 55(2): 157−172

Daxner-Höck G, Höck E, 2009. New data on Eomyidae and Gliridae (Rodentia, Mammalia) from Late Miocene of Austria. Ann Naturhist Mus Wien, 111A: 375−444

Freudenthal M, 2004. Gliridae (Rodentia, Mammalia) from the Eocene and Oligocene of the Sierra Palomera (Teruel, Spain). Treb Mus Geol Barcelona, 12: 97−173

Kawamura Y, 1989. Quaternary rodent faunas in the Japanese Islands (part 2). Mem Fac Sci, Kyoto Univ, Ser Geol Mineral, 54(1-2): 125−157

Kretzoi M, 1978. Wichtigere Streufunde in der Wirbeltierpaläontologischen Sammlung der Ungarischen Geologischen Anstalt. Áll Földt Int Évi Jel, 1978: 348−358

Lacomba J I, 1988. Estudio de las faunas de micromamiferos del Oligoceno superior y mioceno inferior en las cuencas de

Loranca, Ebro riojano y Ebro aragonés. Aspectos paleoecológicos. Doctoral thesis. Madrid: Madrid Universidad Complu tense de Madrid. 1−389

Martínez-Salanova J, 1987. Estudio paleontológico de los Micromamiferos del Mioceno inferior de Fuenmayor (La Rioja). Cienc Tierra, 10: 1−99

Mayr H, 1979. Gebissmorphologische Urtersuchungen an miozaenen Gliridae (Mammalia, Rodentia) Süddeutshlands. Inaugural Dissertation. München: Ludwig-Maximilians-Universität. 1−380

Meng J, Ye J, Wu W Y et al., 2001. Two petrosals of gliriform mammals from Late Oligocene of Tieersihabahe, Xinjiang Uygur Autonomous Region, China. Vert PalAsiat, 39(1): 43−53

Meng J, Ye J, Wu W Y et al., 2006. A recommended boundary stratotype section for Xiejia Stage from northern Junggar Basin: implications to related bio-chronostratigraphy and environmental changes. Vert PalAsiat, 44(3): 205−236

Meulen A J van der, Bruijn H de, 1982. The mammal from the Lower Miocene of Aliveri (Island of Evia, Greece). Part 2, The Gliridae. Proc K Ned Akad Wet, Ser B, 85(4): 485−524

Ruiz-Sánchez F J, Murelaga X, Freudenthal M et al., 2012a. A new species of glirid rodent *Vasseuromys* (Gliridae, Rodentia) from the Aragonian (Miocene) of the Ebro Basin (north-eastern Spain). Acta Palaeont Pol, 57(2): 225−239

Ruiz-Sánchez F J, Murelaga X, Freudenthal M et al., 2012b. *Vasseuromys rambliensis* sp. nov. (Gliridae, Mammalia) from the Ramblian (Lower Miocene) of the Tudela Formation (Ebro Basin, Spain). Paleont Electron, 15(1), 4A: 1−16

Ruiz-Sánchez F J, Lacomba-Andueza J I, Freudenthal M et al., 2014. A new species of *Vasseuromys* (Gliridae, Mammalia) from the Upper Oligocene of the Ebro Basin (Spain). Paläont Z, 88(1): 73−84

Ünay E, 1994. Early Miocene rodent faunas from the eastern Mediterranean area. Part IV. The Gliridae. Proc K Ned Akad Wet, Ser B, 97(4): 445−490

Ünay-Bayraktar E, 1989. Rodents from the Middle Oligocene of Turkish Thrace. Utrecht Micropal Bull Spec Publ, 5: 1−119

Walker E P, 1975. Mammals of the World. 3rd ed. Baltimore and London: The Johns Hopkins University Press. 1−1500

Wu W Y, 1993. Neue Gliridae (Rodentia, Mammalia) aus untermiozanen (orleanischen) Spaltenfüllungen Süddeutschlands. Doc Nat, 81: 1−157

Wu W Y, Ye J, Bi S D et al., 2000. The discovery of Late Oligocene dormice from China. Vert PalAsiat, 38(1): 36−42

Ye J, Meng J, Wu W Y, 2003a. Discovery of *Paraceratherium* in the northern Junggar Basin of Xinjiang. Vert PalAsiat, 41(3): 220−229

Ye J, Meng J, Wu W Y, 2003b. Oligocene/Miocene beds and faunas from Tieersihabahe in the northern Junggar Basin of Xinjiang. Bull Am Mus Nat Hist, 279: 568−585

Ye J, Wu W Y, Meng J, 2001a. Tertiary stratigraphy in the Ulungur River Area of the northern Junggar Basin of Xinjiang. J Stratigr, 25(3): 193−200

Ye J, Wu W Y, Meng J, 2001b. The age of Tertiary strata and mammal faunas in Ulungur River Area of Xinjiang. J Stratigr, 25(4): 283−287

Ye J, Wu W Y, Ni X J et al. 2012. The Duolebulejin section of northern Junggar Basin and its stratigraphic and environmental implication. Sci Sin Terrae, 42: 1523−1532

Zachos J, Pagani M, Sloan L et al., 2001. Trends, rhythms and aberrations in global climate 65 Ma to Present. Science, 292: 686−693

第54卷 第1期
2016年1月

古 脊 椎 动 物 学 报
VERTEBRATA PALASIATICA

pp. 51−66
figs. 1−9

Female preference promotes asynchronous sex evolution in Elephantiformes

WANG Shi-Qi[1,2,3] DENG Tao[1,2]

(1 *Key Laboratory of Vertebrate Evolution and Human Origins of Chinese Academy of Sciences*, *Institute of Vertebrate Paleontology and Paleoanthropology*, *Chinese Academy of Sciences* Beijing 100044 wangshiqi@ivpp.ac.cn)
(2 *CAS Center for Excellence in Tibetan Plateau Earth Sciences* Beijing 100101)
(3 *Key Laboratory of Economic Stratigraphy and Palaeogeography*, *Chinese Academy of Sciences* (*Nanjing Institute of Geology and Palaeontology*) Nanjing 210008)

Abstract Sexually dimorphic characters are usually thought to enhance copulatory success by intraspecific competition; for example, larger body size and stronger tusks are sexually dimorphic characters in fossil and extant male proboscideans. Here, we show that some sexually dimorphic characters in fossil Elephantiformes, the largest group of proboscideans, are strongly correlated with the evolution of this group rather than direct sexual competition. In Miocene *Platybelodon grangeri* and *Gomphotherium angustidens*, males tended to initially possess evolutionarily more derived characters than females, and females then evolved similar variation. This phenomenon may have occurred as a result of female preference. During the early evolutionary stage (thriving stage) of Elephantiformes, sexual selection pressure promoted development of more prominent derived characters in males than females. However, during their late evolutionary stage (declining stage), sexual selection pressure seems to have weakened; thus, the asynchrony between the two sexes diminished. This new discovery may help explain a common mechanism of large ungulate evolution and extinction, because substantial sexual dimorphism is often displayed in thriving groups, such as Cervidae and Bovidae, in contrast to little sexual dimorphism in declining groups, such as extant taxa of Equidae, Rhinoceridae, and Giraffidae.

Key words Elephantiformes, sexual dimorphism, female preference, evolution

Citation Wang S Q, Deng T, 2016. Female preference promotes asynchronous sex evolution in Elephantiformes. Vertebrata PalAsiatica, 54(1): 51−66

1 Introduction

Since Darwin, sexual selection has been considered the key factor that influences secondary sexually dimorphic character development within a species (Darwin, 1874; Fisher, 1930; Andersson, 1994). As a result, these characters are thought to improve male copulatory success by intraspecific competition. However, the relationship between sexual dimorphism

国家重点基础研究发展计划项目(编号：2012CB821900)、中国科学院战略性科技先导专项(编号：XDB03020104)、国家自然科学基金(批准号：41372001, 41430102, 41202017)和中国科学院资源地层学与古地理学重点实验室(中国科学院南京地质古生物研究所)资助。

收稿日期：2015-06-30

and evolution is not fully understood. For example, in Elephantiformes Tassy, 1988, sexual dimorphism has been observed in Oligocene *Phiomia*, Miocene *Platybelodon grangeri*, *Gomphotherium angustidens*, ?*Stegotetrabelodon* sp. (Matsumoto, 1924; Osborn and Granger, 1932; Lambert, 1992; Tassy, 1996, 2013; Bibi et al., 2012; Wang et al., 2013), and extant elephants (Nowak, 1999; Roth and Shoshani, 1988; Kurt et al., 1995; Douglas-Hamilton et al., 2006; Lee and Poole, 2011). In *G. angustidens* there is sexual dimorphism not only of body size and tusk characteristics but also of other characters that have not been fully understood (Tassy, 1996, 2013). Furthermore, in large ungulates, substantial sexual dimorphism is often exhibited in early evolutionary stage (thriving) groups, such as Cervidae and Bovidae; however, little sexual dimorphism in late evolutionary stage (declining) groups, such as extant taxa of Equidae, Rhinoceridae, and Giraffidae. Therefore, the mechanism underlying sexual dimorphism and evolution in this group should be studied further.

Recently, a population of fossil *P. grangeri* was discovered from the Middle Miocene Zengjia locality, Guanghe County, Gansu Province, China (Fig. 1). This population included a large number of crania and mandibles (Wang et al., 2013), and therefore provided a good model to study sexual dimorphism in Miocene Elephantiformes and evaluate the relationship between elephantiforme sexual dimorphism and evolution.

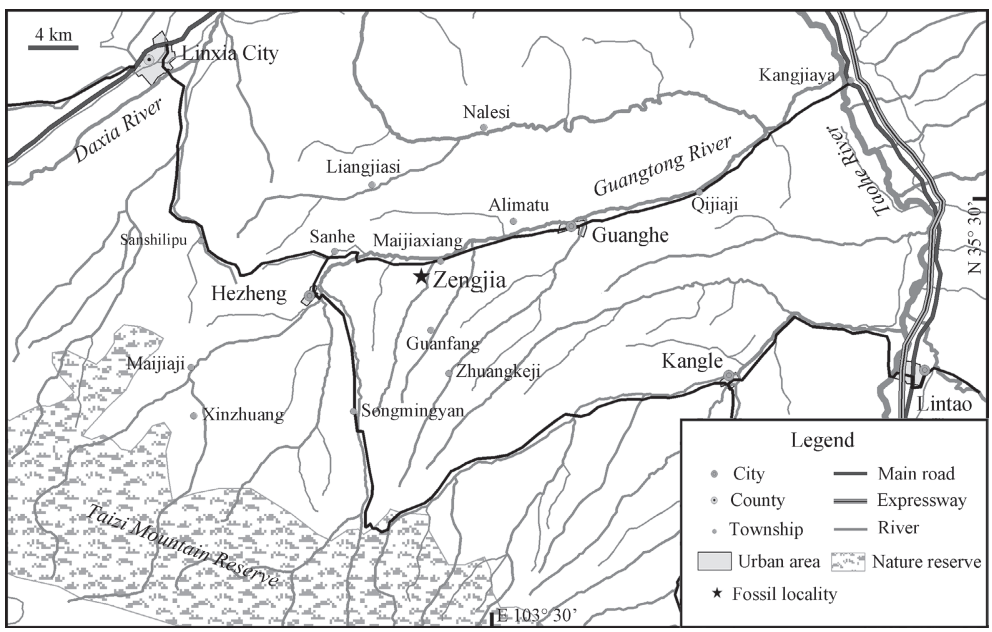

Fig. 1 Map showing the Zengjia locality (N 35°26'23.1", E 103°26'37.6", H 2150 m) yielding the population of *Platybelodon grangeri*

Institutional abbreviations AMNH, American Museum of Natural History, New York, USA; BPV, Beijing Natural History Museum, Beijing, China; HMV, Paleozoological Museum, Hezheng, Gansu, China; MNHN, Muséum National d'Histoire Naturelle, Paris, France.

2 Materials and methods

Specimens All of the *Platybelodon grangeri* specimens from the Zengjia locality are housed in HMV, and a total of 32 specimens were analyzed: HMV 0014–0020, 0022–0039, 0042, 0043, 0939, 0940, 1836, 1841, and 1842. The ontogenetic ages of the specimens range from Dental Age XVIII to XXI (Tassy, 2013), which means all of the specimens were adults (as determined based on functioning m3 and/or M3) with similar ontogenetic ages. *P. grangeri* from Tunggur are AMNH 26408, 26460, 26462, 26469, 26472, and 26490 (Dental Ages from XVIII to XX). These specimens are from the *Platybelodon* Quarry and Wolf Camp localities because they were found in the same horizon (Wang et al., 2003). *Loxodonta africana* specimens are four adult females (AMNH 32732, 42469, 51949, and 88404) and four adult males (AMNH 32734, 39083, 51939, and 113819). Two *Gomphotherium angustidens* crania are MNHN Si37 (male, Dental Age XIX) and MNHN SEP185 (female, Dental Age XXI). An adult skull with an associated mandible (probably a male) of *Platybelodon danovi* is BPV 2000 (Dental Age XX). All of the specimens belong to the museum collections and are open to scientific research.

Locality and age All of the *P. grangeri* specimens that were considered part of the same population were collected from the Zengjia locality (N 35°26′23.1″, E 103°26′37.6″, H 2150 m, No. LX200002, Fig. 1) of the Linxia Basin, Gansu Province, China. The fossil bearing strata belong to the Middle Miocene Hujialiang Formation, which consists of grayish-yellow fine conglomerates and sandstone rocks, which indicate fluvial strata (Deng et al., 2013). The fauna is also composed of a typical Middle Miocene mammalian community, including *Castor* sp., *Alloptox* sp., *Pseudaelurus* sp., *Gomphotherium* cf. *G. subtapiroideum*, *G. wimani*, *Zygolophodon* cf. *Z. gobiensis*, *Chalicotherium* sp., *Anchitherium gobiensis*, *Hispanotherium matritense*, *Listriodon* sp., *Kubanochoerus* sp., and Cervidae indet. (Deng et al., 2013).

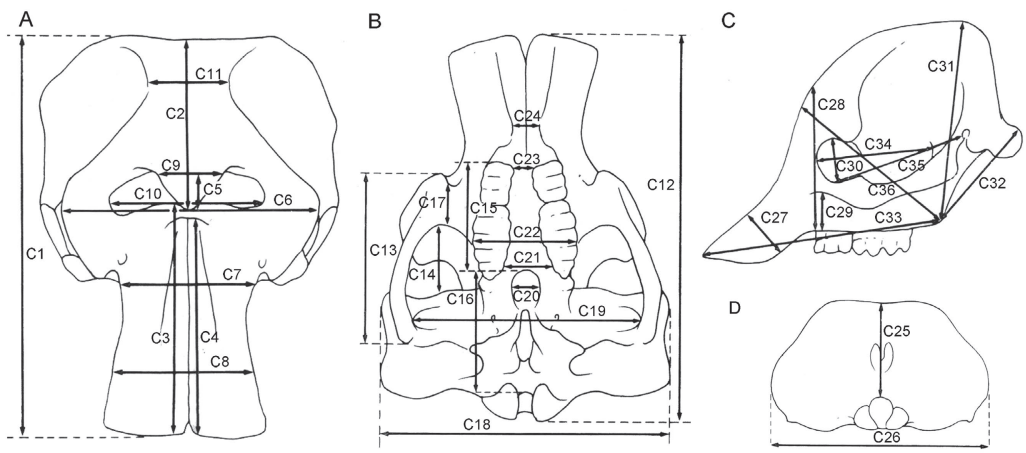

Fig. 2 The cranial measurements of Elephantiformes, after Tassy (1996: fig. 11.1, slightly revised), not scaled
A. dorsal view; B. ventral view; C. lateral view; D. posterior view

Measurements Cranial and mandibular measurements of elephantiforme specimens were based on those described by Tassy (2013); a total of 36 cranial measurements (Fig. 2, indicated by "C") and 24 mandibular measurements (Fig. 3, indicated by "M") were taken. There was one minor change to the measurement protocol: M1 was taken from the anterior border of the incisive alveolus instead of from the lower tusk, which we did not analyze in the present article, to the mandibular condyles.

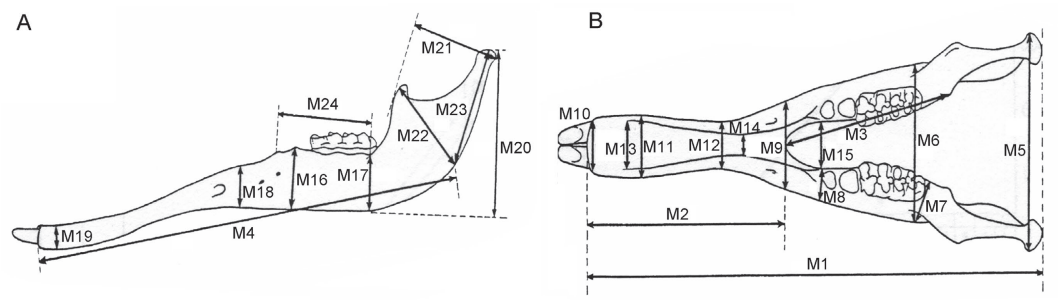

Fig. 3 The mandibular measurements of Elephantiformes in lateral (A) and dorsal (B) views
After Tassy (1996: fig. 11.1, slightly revised), not scaled

Measurement inclusion In multivariate sex assessment, measurements that reflect little sexual dimorphism and have substantial variation may affect the results. Therefore, the only measurements used in analysis are those for which the coefficient of variation is less than 15. The included measurements consist of a total of 21 cranial measurements, C1–4, 6–8, 10–12, 14, 15, 18, 19, 22, 30, 31, and 33–36, and 18 mandibular measurements, M1–10, 12, 13, 17, 20–24.

Data prediction and modification In the multivariate sex assessment analysis, a complete data set is ideal but not available because of the incompleteness of specimens. Therefore, we used a linear regression method (Wang and Deng, 2010) to predict the missing measurements.

For the analyzed material, some measurements were questionable because of substantial deformation or unreliable restoration. In these cases, the questionable data were considered missing. Then, the data were weighted based on the mean of the raw data and the predicted data. The weighted measurement values were calculated as follows:

$$w = \exp(-|p - m|/0.0098p), \quad \text{eq. (1)}$$

where w is the weight, p is the predicted datum, and m is the original measured value ($1 - w$ is assigned as the weight for predicted data). Complete pseudo data sets were constructed using this procedure.

Data normalization We estimated the total length, or size factor (SF), of each specimen based on the C1 and M1 values. In the complete pseudo data set, data were divided by each SF to produce a size-normalized pseudo (SNP) data set to obtain shape information. Then, the SNP data set was logarithmically transformed, because each measurement was of equal importance for morphological discrimination and should be analyzed on the same scale. The following formula was used:

$$X_i = \ln(M_i/\langle M\rangle), \qquad \text{eq. (2)}$$

where M_i was an SNP value of a certain measurement of specimen i and $\langle M\rangle$ was the mean of the SNP values for all specimens. This new data set was defined as the size-normalized logarithmic pseudo (SNLP) data set for multivariate analyses.

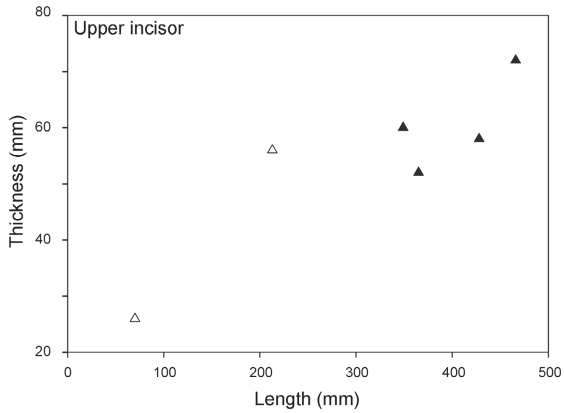

Fig. 4 Bivariate scatter plot of upper tusks in male and female *Platybelodon grangeri*
Solid triangles, male; open triangles, female

Sex assessment Before sex assessment, only the length of upper incisor could be directly used for sexual discrimination (< *ca*. 300 mm for females and > *ca*. 300 mm for males, Fig. 4). These typical adult crania were first selected to form the SNLP data sets (males and females were considered two different groups) and examined by principal component analysis (PCA). The resulting principal components (PCs), of which the cumulative variance contribution rate exceeded 95%, were selected as new variables for Fisher's discriminant function analysis (DFA), and the first discriminant function (DF1) was calculated. Then, the remaining crania of uncertain sex were examined using the DF1 (Appendix 1) and we preliminarily determined the sex for each cranium. Then, these crania were divided into two groups based on inferred sex, and two more SNLP data sets were constructed then re-examined in a new PCA–DFA cycle. If a cranium clustered into the opposite sex group in DFA, we changed the cranium's sex assignment and began another PCA–DFA cycle. Cycles did not stop until the data clustered appropriately based on sex assignment. After several PCA–DFA cycles, an optimal sex assessment was obtained for each cranium.

No sex assignment was proposed based on mandibular characters or measurements. The specimens with long symphyses were considered male, because some were associated with male crania (HMV 0939 and 0940). Consequently, those mandibles with short symphyses were considered female. The same PCA–DFA cycles were performed on the mandibles as on the crania until all of the mandibles had optimal sex assessments.

Univariate analyses Univariate analyses were carried out on individual characters in both sexes. Only the originally measured or modified values were used in analyses, and those specimens missing original measurements were not included. For each measurement (including M3 and m3 measurements), the mean, standard deviation (s.d.), coefficient of variation (c.v.), and maximal and minimal values were calculated. Two-tailed Student's t-tests were performed between the two sexes, and p-values less than 0.05 were considered significant.

Bivariate scatter plots and histograms DF1 from the last PCA–DFA cycle and normalized length from crania and mandibles, length and width from M3 and m3, and length and maximal width of mandibular symphyses were depicted in bivariate scatter plots; the 95% confidential eclipses for both sexes were calculated and also included in the plots. C2/C1, C34/

C31, and M11/M2 measurements of each specimen were calculated and their statistics were performed. The mean + s.d. of the results were shown in histograms. Two-tailed Student's t-tests were performed between the two groups, and p-values less than 0.2 were considered significant.

Simpson's ratio diagrams The formula for Simpson's ratio is as follows:

$$r = \ln(m/s), \qquad \text{eq. (3)}$$

where m is a measured value in an object group, s is the corresponding value in the standard group, and r is the resultant Simpson's ratio. Both m and s are available from individual specimens and the mean of the specimens. Simpson's ratio diagrams were used to compare both sexes of *Platybelodon grangeri*, *Gomphotherium angustidens*, and *Loxodonta africana*.

3 Results

The results show that there is significant sexual dimorphism in the population of fossil *P. grangeri* (Figs. 5A, B, and Appendix 1). In addition to larger and more robust upper tusks, which are beneficial for direct combat, other craniomandibular sexually dimorphic characters in males include: 1) a higher-arched but shorter temporal fossa (C34/C31); 2) more posteriorly positioned nasal bones, which indicates a more developed trunk (C2/C1) (Figs. 6A, B, and I); and 3) a longer mandibular symphysis (M11/M2) (Figs. 6C, D, I, and Fig. 7). The p-values of C34/C31 (0.1775) and C2/C1 (0.1233) indicate that these ratios are significant because they are under the significance level of 0.2. This relatively high significance level is acceptable for two reasons. First, male and female individuals are in the same population of the same species. Therefore, the measurement ratios should not substantially differ. Second, the sample size is relatively small. However, the p-value of M11/M2 (0.0058) is under the significance level of 0.05 (as in the univariate analysis); this is important because we used symphysis length to initially determine sex.

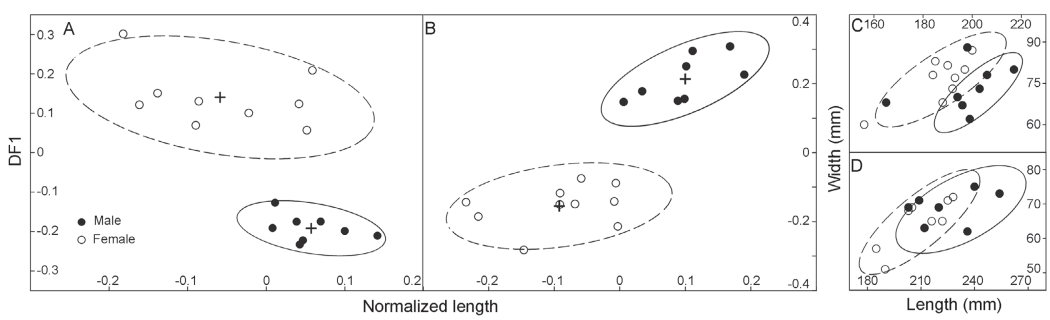

Fig. 5 Bivariate scatter plots showing sexual dimorphism in *Platybelodon grangeri* from the Zengjia locality
Cranium (A) and mandible (B) are examined in PCA–DFA cycles for sex-assessment and the final results are shown in normalized length–DF1 plane. As a result of sex-assessment, measurements from M3 (C) and m3 (D) are also shown on length–width plane. Two sexes are represented by solid (male) and open cycles (female), respectively, with 95% confidential ellipses denoting their distributions (solid-lined ellipses for male and dash-lined ellipses for female)

In addition to the above craniomandibular sexually dimorphic characters, males also possess narrower and longer M3 and m3. Note that the molar measurements, which were not used for sex assessment, are independent variables; thus, this is an independent verification of our sex assessment (Figs. 5C and D). In the Simpson's ratio diagrams, the slopes of C1 & C2, C31 & C34, and M2 & M11 differ between male and female *P. grangeri*, which also indicates sexual dimorphism in these characters (Fig. 8). However, Student's t-tests for single measurements primarily produce large, non-significant p-values (Tables 1 and 2), which indicates a relatively large amount of overlap in variation of these characters between the two sexes. These sexually dimorphic characters are often obscured by difficulty in sex determination and the incompleteness of specimens unless more elaborate methods are used, such as the one presented in this article.

The above sexually dimorphic characters were also observed in *P. grangeri* from

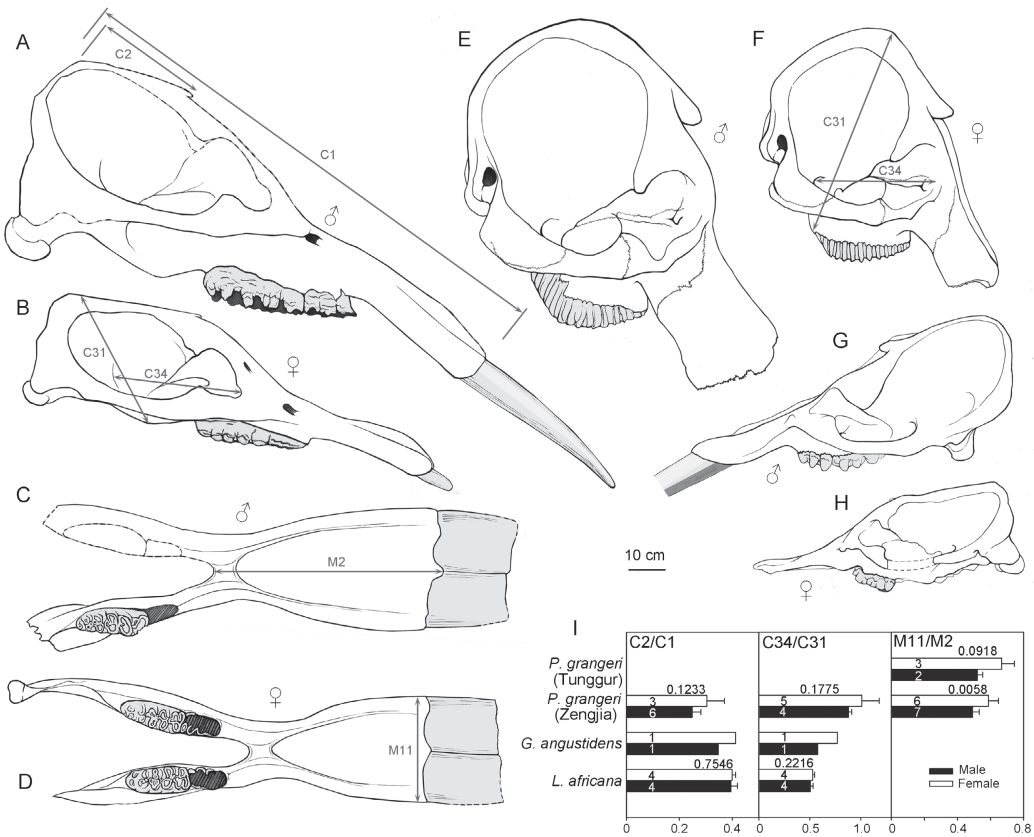

Fig. 6 Sketches showing sexual dimorphism in crania (A, B, E–H) and mandibles (C, D) of *Platybelodon grangeri* (A–D), *Loxodonta africana* (E, F), and *Gomphotherium angustidens* (G, H)

A. HMV 0940; B. HMV 0023; C. HMV 0031; D. HMV 0042; E. AMNH 51939; F. AMNH 88404; G. MNHN Si37; H. MNHN SEP185; I. histograms show sexual dimorphism in three evolutionary significant characters (C2/C1, C34/C31, M11/M2) with the form mean + s.d. ♂, male; ♀, female

Measurements are illustrated on the sketches. The number in each bar represents the sample size n and the number near each pair of bars represents the p-value of the t-test

Tunggur. In a female cranium (AMNH 26462), the upper border of the nostril aperture is located in line with postorbital processes (Osborn and Granger, 1932). In contrast, a possible male (AMNH 26480) has more posteriorly positioned nostril aperture, although the incisors

Table 1 Univariate analyses between male and female crania in *Platybelodon grangeri* (mm)

measurements	sex	n	max	min	mean	s.d.	c.v.	p-value
C1	male	8	1107	968	1018.5	46.8	4.6	0.045
	female	7	1060	800	933.3	97.2	10.4	
C2	male	8	288	227	258.4	25.4	9.8	0.081
	female	7	334	255	287.7	34.6	12.0	
C3	male	6	877	689	766.8	70.1	9.1	0.491
	female	3	778	695	734.3	41.7	5.7	
C4	male	8	829	635	721.4	62.3	8.6	0.021
	female	8	725	560	637.9	66.4	10.4	
C6	male	6	494	452	476.0	14.3	3.0	0.347
	female	9	568	378	446.3	72.7	16.3	
C7	male	7	297	207	246.7	36.5	14.8	0.321
	female	8	266	194	230.9	22.1	9.6	
C8	male	8	210	173	190.4	12.5	6.6	0.107
	female	8	215	135	173.5	24.8	14.3	
C10	male	8	345	225	282.6	38.1	13.5	0.949
	female	8	362	232	284.0	46.5	16.4	
C11	male	7	266	205	237.0	22.7	9.6	0.217
	female	9	272	157	216.0	37.9	17.5	
C12	male	8	1136	952	1049.0	69.2	6.6	0.323
	female	5	1105	858	1002.0	95.2	9.5	
C14	male	6	317	253	285.0	27.0	9.5	0.456
	female	5	304	220	270.8	33.6	12.4	
C15	male	7	363	236	303.4	41.2	13.6	0.112
	female	6	373	313	335.8	21.5	6.4	
C18	male	8	591	442	524.5	50.7	9.7	0.235
	female	5	544	450	490.8	39.8	8.1	
C19	male	6	466	404	440.0	24.6	5.6	0.402
	female	4	464	362	419.0	51.0	12.2	
C22	male	8	272	212	244.5	21.5	8.8	0.425
	female	9	270	212	236.6	18.5	7.8	
C30	male	6	120	67	100.8	18.8	18.6	0.118
	female	6	135	100	116.7	12.7	10.9	
C31	male	6	456	388	424.8	22.5	5.3	0.277
	female	7	455	334	400.1	48.3	12.1	
C33	male	8	805	645	723.1	52.6	7.3	0.092
	female	8	750	570	670.3	63.9	9.5	
C34	male	8	450	344	393.9	39.0	9.9	0.904
	female	6	417	358	391.7	22.5	5.8	
C35	male	8	418	382	403.5	11.6	2.9	0.762
	female	7	469	343	398.4	44.8	11.3	
C36	male	6	427	320	370.2	40.4	10.9	0.420
	female	5	443	360	390.4	38.4	9.8	
length of M3	male	8	217	165	197.3	14.9	7.56	0.156
	female	9	200	156	187.2	12.8	6.84	
width of M3	male	8	88	62	73.3	8.36	11.4	0.450
	female	9	87	60	76.4	8.28	10.8	

Note: Measurements see Fig. 2.

Table 2 Univariate analyses between male and female mandibles in *Platybelodon grangeri* (mm)

measurements	sex	n	max	min	mean	s.d.	c.v.	p-value
M1	male	7	1630	1356	1489.9	98.2	6.6	0.003
	female	5	1344	1066	1256.0	113.1	9.0	
M2	male	8	853	598	722.1	81.3	11.3	0.036
	female	6	688	490	623.2	71.9	11.5	
M3	male	8	530	452	496.3	26.4	5.3	0.005
	female	8	470	355	439.3	41.0	9.3	
M4	male	8	1494	1206	1378.9	98.1	7.1	0.001
	female	7	1287	944	1128.7	130.1	11.5	
M5	male	5	455	343	406.6	43.2	10.6	0.919
	female	5	464	352	409.6	47.2	11.5	
M6	male	8	403	299	355.5	41.3	11.6	0.546
	female	10	401	301	344.9	31.6	9.2	
M7	male	7	106	81	95.6	9.5	9.9	0.883
	female	10	117	78	96.5	14.4	14.9	
M8	male	7	75	51	65.9	8.9	13.5	0.482
	female	10	73	61	68.1	3.7	5.4	
M9	male	8	200	155	180.0	15.5	8.6	0.847
	female	10	205	152	181.5	16.7	9.2	
M11	male	7	364	329	343.1	11.5	3.4	0.255
	female	6	415	286	364.3	45.3	12.4	
M12	male	8	176	153	166.9	9.5	5.7	0.696
	female	9	191	151	164.8	11.9	7.2	
M13	male	8	375	250	302.6	47.1	15.6	0.833
	female	6	366	243	307.8	41.4	13.5	
M17	male	8	144	106	131.9	13.0	9.8	0.323
	female	8	156	92	123.0	20.8	16.9	
M20	male	4	374	320	346.8	22.5	6.5	0.236
	female	5	374	250	312.8	47.9	15.3	
M21	male	5	288	247	273.2	16.8	6.2	0.090
	female	5	264	185	241.6	32.5	13.5	
M22	male	5	289	201	259.2	34.4	13.3	0.445
	female	5	284	210	242.2	32.5	13.4	
M23	male	5	300	259	280.0	15.9	5.7	0.126
	female	6	311	181	244.3	44.6	18.3	
M24	male	8	397	260	327.1	46.3	14.2	0.279
	female	9	347	264	306.9	26.5	8.6	
length of m3	male	7	254	203	224.86	18.8	8.36	0.107
	female	8	228	185	209.25	16.14	7.71	
width of m3	male	7	75	62	68.857	4.845	7.04	0.228
	female	8	72	51	64.75	7.265	11.2	

Note: Measurements see Fig. 3.

were broken. There are also two types of mandibular symphyses, short and long, which may represent females and males, respectively (Fig. 7). However, juvenile individuals exhibit width/length ratios that are intermediate between adult males and females (Fig. 7). Furthermore, these sexually dimorphic characters were also observed in Middle Miocene *G. angustidens*. In male crania, the temporal fossa is higher but short, and the nasal bones are more posteriorly positioned (Figs. 6G, H, I, and Fig. 8; Tassy, 1996: fig. 11.4).

Sexual dimorphism in ancestral *Phiomia serridens* and derived *Loxodonta africana* has also been studied (Matsumoto, 1924; Roth and Shoshani, 1988; Lee and Poole, 2011).

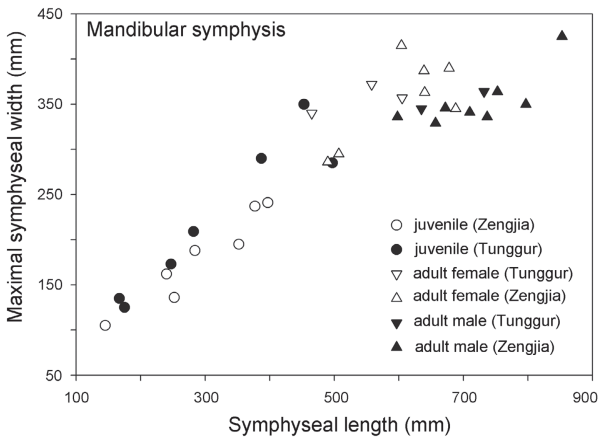

Fig. 7 Bivariate scatter plot of length vs. maximal width of mandibular symphysis in *Platybelodon grangeri*
♂, male; ♀, female

In *P. serridens*, there appears to have sexual dimorphism with regard to size but only have slight sexual dimorphism with regard to symphyseal morphology. For instance, *P.* "*osborni*" Matsumoto, 1922 differs from *P.* "*wintoni*" (Andrews, 1905) in more posteriorly positioned proximal edge of mandibular symphysis (Matsumoto, 1924). However, these two species now have been considered junior synonyms of *P. serridens* (Shoshani and Tassy, 1996: appendix C2). However, in extant *L. africana*, although size difference is still prominent (Roth and Shoshani, 1988; Lee and Poole, 2011), the high-arched cranium, extremely posteriorly positioned nostril aperture, and stout mandibles are highly homomorphic in both sexes (Figs. 6E, F). In the Simpson's ratio diagram, the shapes of polylines that represent the two sexes of *L. africana* are almost identical, which means that individuals of the two sexes display highly similar cranial shapes (Fig. 8).

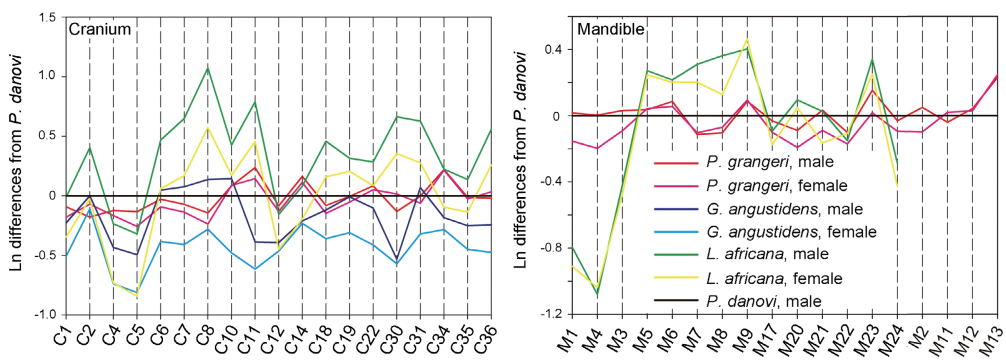

Fig. 8 Simpson's ratio diagrams showing the cranial and madibular sexual dimorphsim between two sexes in Elephantiformes
A skull of *Platybelodon danovi* (BPV 2000) is shown as the standard (the black lines)
Measurements see Figs. 2 and 3

4 Discussion

We analyzed sexual dimorphism in four different elephantiforme taxa covering its entire known evolutionary range (Oligocene *Phiomia*, Miocene *Gomphotherium*, *Platybelodon*, and extant *Loxodonta*). These taxa are closely related and represent key nodes in the evolution of Elephantiformes. Previous phylogenetic analyses revealed that *Phiomia* is the sister group

of all other taxa of Elephantiformes, except the contemporary *Palaeomastodon* (Shoshani and Tassy, 2005; Gheerbrant and Tassy, 2009). Therefore, *Phiomia* is an ideal primitive elephantiforme model. *Gomphotherium* is considered the most important representative of the group trilophodont gomphotheres s. s., which is derived from *Phiomia* and sister to Elephantoidea; thus, *Gomphotherium* represents an intermediate stage between primitive *Phiomia* and derived elephants. *Platybelodon* (a member of Amebelodontinae), which is also derived from *Phiomia*, is a close relative of trilophodont gomphotheres s. s. and includes the group trilophodont gomphotheres s. l.. Moreover, as one of the two representatives of extant elephant genera, *Loxodonta* is representative of elephantiforme terminal taxa.

Many sexually dimorphic characters differ among these taxa. However, larger and stronger upper tusks in males were observed in all taxa. These sexually dimorphic characters are clearly associated with male social behavior, such as combat. However, it is difficult to interpret the role of other sexually dimorphic characters in sexual competition, such as C34/C31, C2/C1, M11/M2, and length/width of M3 and m3 in *Platybelodon* and the sexually dimorphic characters C34/C31 and C2/C1 in *Gomphotherium*. Nevertheless, these characters have strong evolutionary significance in Elephantiformes (Andrews, 1906; Maglio, 1972). The nostril aperture is anterior to the orbit in *Phiomia*, the same level as the orbit in *Gomphotherium* and *Platybelodon*, and posterior to the orbit in *Loxodonta*, which indicates gradual elongation of the trunk in the evolutionary history of Elephantiformes. The brain case is flat and anteroposteriorly elongated in *Phiomia*, slightly arched and shortened in *Gomphotherium* and *Platybelodon*, and strongly arched and shortened in *Loxodonta*; this represents gradual vertical orientation of m. temporalis, which indicates that masticatory function shifted from grinding shearing to horizontal shearing (Maglio, 1972). Therefore, an arched brain case and posteriorly positioned nostril aperture are derived characters in Elephantiformes. Furthermore, the mandibular symphysis is short in *Phiomia* but long in *Platybelodon*, and m3 and M3 are wide in *Phiomia* but narrow in *Platybelodon* (narrowness of m3 and M3 is a diagnostic feature in Amebelodontinae; Tassy, 1986). Therefore, at least in Amebelodontinae, a long symphysis and narrow m3 and M3 are derived characters.

Based on the sexual dimorphism analysis, we can draw two conclusions. First, four evolutionarily significant characters were sexually dimorphic in Miocene *Gomphotherium* or *Platybelodon* and perhaps other members of the trilophodont gomphotheres s. l. group, but were not sexually dimorphic in the primitive taxon *Phiomia* and terminal taxon *Loxodonta*. Second, in *Gomphotherium*, *Platybelodon*, and perhaps other members of the trilophodont gomphotheres s. l. group, if a character was sexually dimorphic, males always possessed evolutionary more derived character states than females. This issue is of interest with regard to elephantiforme evolutionary history, because the two sexes show asynchronous evolution. This asynchrony might have evolved in primitive *Phiomia*, become exaggerated in the Miocene trilophodont gomphotheres, and ceased in extant elephants. It appears as though character variation in males slightly preceded similar variation in females, and eventually the females evolved similar character variation (Fig. 9). However, at present, it is not entirely clear why

this phenomenon occurred.

It is difficult to determine the mechanism underlying the production of the sexually asynchronous morphological variations in the evolution of Elephantiformes at genetic and ontogenetic levels. We hypothesize that this asynchrony may reflect female preference; that is, in the evolution of a sex-related character in a group, female choice plays a key role (Fisher, 1930; Anderson, 1994). For example, in a population of *Gomphotherium* or *Platybelodon*, genetic variation (possibly sex-linked gene(s)) produces variation in a sexually dimorphic character, such as trunk length variation in males. The individuals with a longer-than-average trunk, which was determined when there was a more posteriorly positioned nostril aperture (values less than C2/C1), were more attractive to females; this could be because a longer trunk enhances survival of both the males and their offsprings. Similar cases could also be made for the characters C34/C31 and M11/M2 . Therefore, this sexual selection pressure may have promoted the prevalence of the sex-linked allele or alleles that code for a longer trunk in the population and produced the sexual dimorphism we observed in *Gomphotherium* and *Platybelodon*.

This "runaway selection" process (Fisher, 1930) represents the first step of the asynchronous sex evolution; the derived male character variation slightly preceded similar variation in females. Because the newly developed character in males was also advantageous in females, the longer trunk allele(s) were gradually fixed as non-sex-linked gene(s). Finally, as determined by similar C2/C1 values for both sexes, extant female Elephantiformes also have longer trunks, as can be observed in extant *Loxodonta*. Moreover, sexual selection pressure also weakened, and it was not necessary for males to have longer trunks than females. This process represents the second step of the asynchronous sex evolution: the females evolved similar traits to those of the males. This two-step hypothesis is plausible for explaining the sexual asynchrony observed in elephantiforme evolution and describing the development of this newly derived character within Elephantiformes.

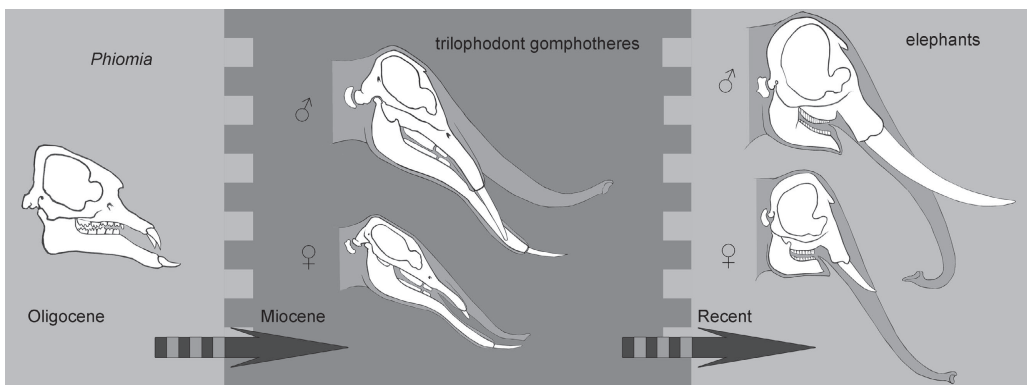

Fig. 9 Schematics showing asynchronous evolution between two sexes in Elephantiformes
The gray scales in the background represent relatively greater (relatively darker) or smaller (relatively lighter) sexual-dimorphism, not to scale. ♂, male; ♀, female. Sketches of *Phiomia* after Andrews (1906)

This asynchronous sex evolution in Elephantiformes appears to be correlated with thriving and declining groups. Miocene *Gomphotherium* and *Platybelodon* show more prominent sexual dimorphism than primitive *Phiomia* and terminal *Loxodonta*. The Miocene is a thriving period for Elephantiformes, who had a broad geological distribution and diverse taxa; in contrast, there are only three extant species of elephants, which are confined to tropical areas in Asia and Africa (Shoshani and Tassy, 1996). One possible reason for this correlation with asynchronous sex evolution is that females became less selective of these traits in males and sexual selection pressure consequently decreased, which led to extant elephantiforme females and males possessing similar derived characters. For example, females seem very picky in copulation and often refuse to mate with males they dislike (Douglas-Hamilton et al., 2006). Furthermore, relationships between sexual dimorphism and evolution were also observed in other groups of large ungulates. For example, thriving groups, such as Cervidae and Bovidae, often exhibit substantial sexual dimorphism, whereas declining groups, such as extant members of Equidae, Rhinoceridae, and Giraffidae (Janis, 1982), often exhibit little sexual dimorphism. However, some extinct taxa of Equidae and Rhinoceridae, such as *Hyracotherium* and *Chilotherium*, have strong sexual dimorphism during their thriving period (Gingerich, 1981; Chen et al., 2010).

The patterns observed in this study may be related to the relationship between male competition and female preference. As Darwin (1874) and Fisher (1930) have discussed, both factors contribute to animals' mating behaviors. In most cases (especially in the thriving groups), the two factors do not contradict each other. A male elephant does compete and defeat competitors to gain copulatory priority, because female elephants are often attracted to and want to mate with the winner. However, in some cases (appears more frequently being in declining groups), even the winner in male competitions may not successfully attract females. A previous study showed that female elephants may refuse males' mating attempts (Douglas-Hamilton et al., 2006). As in humans, males can attract females by various direct or indirect competitions with other males, but the ultimate decision is often up to the female.

The second issue is that the variation in males is less than that in females. The 95% confidential eclipses of females take up a larger area in Fig. 5A, B, and most standard deviations from female measurements are greater than those of male measurements (Tables 1 and 2). This phenomenon has also been noticed in other larger ungulates, such as extant *Equus hemionus* and fossil *Chilotherium wimani* (Chen et al., 2010; Wang, 2010), and even observed in some birds, reptiles, anurans, and invertebrates (Johnston, 1966; Stamps and Gon III, 1983). This phenomenon could occur if males are opportunists and would be willing to mate with a wide range of females, however females are picky because of their greater sexual investment in fewer gametes (Fisher, 1930; Anderson, 1994). This mechanism may also have been involved in the observed asynchronous sex evolution and would be helpful for preserving potential variation in the genomes of the species to maintain evolutionary potential, which facilitates rapid response to dramatic environmental changes.

5 Conclusions

In this paper, we studied sexual dimorphism in a fossil population of *Platybelodon grangeri* from the Middle Miocene Zengjia locality in China. In this population, males possess larger and stronger upper tusks than females. However, several other morphological characters also slightly differ between the sexes, and males have: 1) slightly more arched brain cases, 2) slightly more posteriorly positioned nostril apertures; 3) longer mandibular symphyses; and 4) narrower m3 and M3. The slightly more arched brain cases and slightly more posteriorly positioned nostril apertures are also observed in Miocene *Gomphotherium* but not in primitive *Phiomia* and terminal *Loxodonta*. By comparing these data with previously determined elephantiforme evolutionary data, we observed asynchronous evolution between males and females. In the thriving period of Elephantiformes, males possessed more derived characters than females; however, in the declining period, females and males possessed similar derived characters. This type of asynchronous sex evolution should be studied further because it might also have occurred in other large ungulates.

Acknowledgments We thank P. Tassy, U. Göhlich, M. Pickford, Z. X. Qiu, J. Ye, Y. G. Zhang, Q. Q. Shi, S. K. Chen, S. K. Hou, H. B. Lü and Y. N. Zhang for discussions and advice on this work; and W. He, S. Q. Chen, P. Tassy, J. Meng, J. Galkin, E. Westwig, Y. G. Zhang, and Z. H. Zeng for preparing the specimens.

雌性偏好促进象型类的性别异时进化

王世骐[1,2,3] 邓 涛[1,2]

(1 中国科学院古脊椎动物与古人类研究所，中国科学院脊椎动物演化与人类起源重点实验室 北京 100044)

(2 中国科学院青藏高原地球科学卓越创新中心 北京 100101)

(3 中国科学院资源地层学与古地理学重点实验室(中国科学院南京地质古生物研究所) 南京 210008)

摘要：性双型的特征通常被认为产生于种内争夺交配优先权的斗争。例如，现生和化石的雄性长鼻类动物具有较大的体型和较粗壮的上门齿。本研究阐释了如下现象：化石象型类动物(Elephantiformes, 长鼻类的主要类群)一些性双型特征与其进化历史具有相关性，而与性别竞争并非直接相关。在中新世的葛氏铲齿象(*Platybelodon grangeri*)和狭齿嵌齿象(*Gomphotherium angustidens*)中，雄性比雌性倾向于具有进化中更进步的特征，如同雄性在进化中领先雌性一步。这种现象可能与雌性偏好的机制相耦合。在象型类动物进化的早期(繁荣期)，性别选择压促使雄性比雌性产生更加显著的进步特征；然而，在它们进化的晚期(衰退期)，性别选择压似乎减弱，性别的异时进化也减少。这种新的发现或许在大型有蹄类的演化过程中有一定的普遍意义，因为那些繁荣的类群中通常性双型显著，如鹿科和牛科；而衰落的类群中通常性双型不显著。

关键词：长鼻类，性双型，雌性偏好，进化

中图法分类号：Q915.878 **文献标识码**：A **文章编号**：1000-3118(2016)01−0051−16

References

Andersson M, 1994. Sexual Selection. Princeton: Princeton University Press. 1–599

Andrews C W, 1906. A Descriptive Catalogue of the Tertiary Vertebrata of the Fayûm, Egypt. London: British Museum (Natural History). 1–324

Bibi F, Kraatz B, Craig N et al., 2012. Early evidence for complex social structure in Proboscidea from a Late Miocene trackway site in the United Arab Emirates. Biol Lett, 8(4): 670–673

Chen S K, Deng T, Hou S K et al., 2010. Sexual dimorphism in perissodactyl rhinocerotid *Chilotherium wimani* from the Late Miocene of the Linxia Basin (Gansu, China). Acta Palaeont Pol, 55: 587–597

Darwin C, 1874. The Descent of Man, and Selection in Relation to Sex. New ed. Revised and Augmented. Philadelphia: David McKay. 1–705

Deng T, Qiu Z X, Wang X M et al., 2013. Late Cenozoic biostratigraphy of the Linxia Basin, northwestern China. In: Wang X M, Flynn L J, Fortelius M eds. Fossil Mammals of Asia: Neogene Biostratigraphy and Chronology of Asia. New York: Columbia University Press. 243–273

Douglas-Hamilton I, Barnes R, Shoshani H et al., 2006. Elephants. In: MacDonald D W ed. The Encyclopedia of Mammals. New York: Facts On File, Inc. 90–101

Fisher R A, 1930. The Genetical Theory of Natural Selection. Oxford: Clarendon Press. 1–272

Gheerbrant E, Tassy P, 2009. L'origine et l'évolution des éléphants. C R Palevol, 8: 281–294

Gingerich P D, 1981. Variation, sexual dimorphism, and social structure in the Early Eocene horse *Hyracotherium* (Mammalia, Perissodactyla). Paleobiology, 7: 443–455

Janis C, 1982. Evolution of horns in ungulates: ecology and paleoecology. Biol Rev, 57: 261–318

Johnston R F, 1966. The adaptive basis of geographic variation in color of the purple martin. Condor, 68: 219–228

Kurt F, Hartl G B, Tiedemann R, 1995. Tuskless bulls in Asian elephant *Elephas maximus*. History and population genetics of a man-made phenomenon. Acta Theriol, Suppl 3: 125–143

Lambert W D, 1992. The feeding habits of the shovel-tusked gomphotheres: evidence from tusk wear patterns. Paleobiology, 18: 132–147

Lee P C, Poole J H, 2011. Reproductive strategies and social relationships. In: Moss C J, Croze H, Lee P C eds. The Amboseli Elephants, a Long-term Perspective on a Long-lived Mammal. Chicago: The University of Chicago Press. 184–286

Maglio V J, 1972. Evolution of mastication in the Elephantidae. Evolution, 26: 638–658

Matsumoto H, 1924. A revision of *Palaeomastodon* dividing it into two genera, and with descriptions of two new species. Bull Am Mus Nat Hist, 50: 1–58

Nowak R M, 1999. Walker's Mammals of the World. 6th ed. Baltimore: The Johns Hopkins University Press. 1–1936

Osborn H F, Granger W, 1932. *Platybelodon grangeri*, three growth stages, and a new serridentine from Mongolia. Am Mus Novit, 537: 1–13

Roth V L, Shoshani J, 1988. Dental identification and age determination in *Elephas maximus*. J Zool Lond, 214(4): 567–588

Shoshani J, Tassy P, 1996. The Proboscidea: Evolution and Palaeoecology of Elephants and Their Relatives. Oxford: Oxford University Press. 1–472

Shoshani J, Tassy P, 2005. Advances in proboscidean taxonomy & classification, anatomy & physiology, and ecology & behavior. Quat Int, 126-128: 5–20

Stamps J A, Gon III S M, 1983. Sex-biased pattern variation in the prey of birds. Annu Rev Ecol Syst, 14: 231–253

Tassy P, 1986. Nouveaux Elephantoidea (Mammalia) dans le Miocène du Kenya: Essai de Réévaluation Systématique. Paris: E'ditions du Centre National de la Recherche Scientifique. 1–135

Tassy P, 1988. The classification of Proboscidea: how many cladistic classifications? Cladistics, 4: 43–57

Tassy P, 1996. Growth and sexual dimorphism among Miocene elephantiformes: the example of *Gomphotherium angustidens*. In: Shoshani J, Tassy P eds. The Proboscidea: Evolution and Palaeoecology of Elephants and Their Relatives. Oxford: Oxford University Press. 92–100

Tassy P, 2013. L'anatomie cranio-mandibulaire de *Gomphotherium angustidens* (Cuvier, 1817) (Proboscidea, Mammalia): données issues du gisement d'En Péjouan (Miocène moyen du Gers, France). Geodiversitas, 35(2): 377–445

Wang S Q, 2010. The variations of limb bones in the male and the female *Equus hemionus*. In: Dong W ed. Proceedings of the Twelfth Annual Meeting of the Chinese Society of Vertebrate Paleontology. Beijing: China Ocean Press. 77–84

Wang S Q, Deng T, 2010. Recovering the missing data of defective fossil samples using linear regression method. Vert PalAsiat, 48: 161–168

Wang S Q, He W, Chen S Q, 2013. Gomphotheriid mammal *Platybelodon* from the Middle Miocene of Linxia Basin, Gansu, China. Acta Palaeont Pol, 58(2): 221–240

Wang X M, Qiu Z D, Opdyke N D, 2003. Litho-, bio-, and magneto-stratigraphy and paleoenvironment of Tunggur Formation (Middle Miocene) in central Inner Mongolia, China. Am Mus Novit, 3411: 1–31

Appendix 1 The weighs of cranial and mandibular measurements in final DFA

Cranium			Mandible		
measurements	values for normalization	weighs in DFA	measurements	values for normalization	weighs in DFA
C1	961.104	0.015	M1	1347.978	0.183
C2	0.288	0.379	M2	0.486	−0.263
C3	0.739	−0.013	M3	0.345	−0.116
C4	0.700	−0.050	M4	0.911	0.330
C6	0.478	0.259	M5	0.296	−0.448
C7	0.250	−0.180	M6	0.262	0.102
C8	0.190	−0.117	M7	0.073	0.114
C10	0.296	0.468	M8	0.050	−0.102
C11	0.236	−0.290	M9	0.136	−0.252
C12	1.026	0.050	M11	0.263	−0.404
C14	0.290	−0.030	M12	0.123	−0.155
C15	0.343	0.410	M13	0.224	−0.184
C18	0.516	−0.236	M17	0.094	0.226
C19	0.439	0.010	M20	0.242	−0.307
C22	0.252	−0.062	M21	0.187	−0.071
C30	0.120	0.251	M22	0.183	−0.111
C31	0.431	−0.295	M23	0.192	0.048
C33	0.722	0.032	M24	0.234	−0.301
C34	0.407	0.015			
C35	0.412	0.036			
C36	0.399	0.232			
threshold = −0.089 male < −0.089; female > −0.089			threshold = 0.021 male > 0.021; female > −0.021		

Note: Here we demonstrate the procedure for determining the sex of a specimen based on the table. Note that the table is only suitable for *Platybelodon grangeri* from the Zengjia locality. Firstly, the missing and questionable data should be predicted or modified as shown in Materials and methods section, forming a pseudo data vector for all the measurements of the specimen. Secondly, each pseudo datum is divided by measurement C1 (for cranium) or M1 (for mandible), except C1 or M1 itself, forming SNP data; and each SNP datum is again divided by the corresponding value for normalization listed in the column two (for cranium) or column five (for mandible), taking the natural logarithm, and forming the SNLP data. Thirdly, each SNLP datum is multiplied by the corresponding weights listed in the column three (for cranium) or column six (for mandible), and then sum them up. Finally, compare the sum to the thresholds in the bottom of the table for determination of the sex for the specimen.

第54卷 第1期
2016年1月

古 脊 椎 动 物 学 报
VERTEBRATA PALASIATICA

pp. 67−78
figs. 1−2

A new hadrosauroid dinosaur from the Late Cretaceous of Tianzhen, Shanxi Province, China

XU Shi-Chao[1] YOU Hai-Lu[2*] WANG Jia-Wei[3] WANG Suo-Zhu[1] YI Jian[1] JIA Lei[1,2]

(1 *Shanxi Museum of Geology* Taiyuan 030024, China)
(2 *Key Laboratory of Vertebrate Evolution and Human Origins of Chinese Academy of Sciences*, *Institute of Vertebrate Paleontology and Paleoanthropology*, *Chinese Academy of Sciences* Beijing 100044, China * Corresponding author: youhailu@ivpp.ac.cn)
(3 *Faculty of Geology*, *Lomonosov Moscow State University* Moscow 119991, Russian Federation)

Abstract A new non-hadrosaurid hadrosauroid dinosaur (*Datonglong tianzhenensis* gen. et sp. nov.) is reported. The new taxon is recovered from the Upper Cretaceous Huiquanpu Formation of Tianzhen County, Shanxi Province in northern China, and represented by an almost complete right dentary with dentition. Different from all other hadrosauroids, *Datonglong* possesses two functional teeth in each alveolus, and the pattern of ridge development on the lingual surface of its dentary crown shows a unique combination of character states (for example: distally offset primary ridge; well-developed secondary ridge; no additional ridge(s); slightly distally curved apical half of primary ridge). Comparative studies indicate advanced non-hadrosaurid hadrosauroids experienced a complex pattern in the evolution of their dentary, especially dentary dentition. Derived hadrosaurid features occurred frequently in these taxa, such as high height/width ratio of tooth crown in *Bactrosaurus*, one primary and one faint ridges in *Gilmoreosaurus*, median placed primary ridge in *Zhanghenglong*, rostrally inclined coronoid process in *Nanningosaurus*, and two functional teeth in each alveolus in *Datonglong*. This implies incredible diversities and attempts close to the origin of Hadrosauridae and difficulties to elucidate their phylogenetic relationships.

Key words Tianzhen, Shanxi; Late Cretaceous; dinosaur, hadrosauroid

Citation Xu S C, You H L, Wang J W et al., 2016. A new hadrosauroid dinosaur from the Late Cretaceous of Tianzhen, Shanxi Province, China. Vertebrata PalAsiatica, 54(1): 67−78

1 Introduction

The Huiquanpu Formation was established by the Regional Geological Survey Team of

中国科学院百人计划、国家自然科学基金(批准号：41472020)和山西省国土资源厅资助。
收稿日期：2015-04-13

Hebei Province in 1959. It refers to the over 200 meter thick terrestrial deposits bounded by the pre-Cambrian rocks and the Miocene basalts, and is distributed in an area of about 150 km^2 around the boundary of Tianzhen County of Shanxi Province and Yangyuan County of Hebei Province in northern China, with an age assignment of Eocene. Liu (1983) and Chen et al. (1983) reassigned its age to Late Cretaceous based on discoveries of dinosaurs, especially Hadrosauridae dinosaurs. In 1989 and 1991−1994, Shijiazhuang Economic University of Hebei Province excavated over 2300 dinosaur specimens mainly in the Kangdailiang Quarry of Tianzhen County, Shanxi Province (Pang et al., 1996), and two new dinosaurs have been established, namely an ankylosaur *Tianzhenosaurus* youngi Pang & Cheng, 1998, and a sauropod *Huabeisaurus allocotus* Pang & Cheng, 2000. In 1998, another ankylosaur *Shanxia tianzhenensis* Barrett et al., 1998 was also reported from the Wujiashan Quarry of Tianzhen County, about 7 km northeast of the previous Kangdailiang Quarry. These two ankylosaurs may be distinct from each other (Upchurch and Barrett, 2000; Thompson et al., 2012), or represent the same taxon (Sullivan, 2000); while *Tianzhenosaurus* may be synonymous with *Saichania* (Sullivan, 1999). Recent restudy of *Huabeisaurus allocotus* shows this taxon is probably a member of the Cretaceous East Asian endemic clade of Euhelopodidae (D'Emic et al., 2013).

Pang et al. (1996) and Pang and Chen (2000, 2001) also mentioned the existence of theropod cf. *Szechuanosaurus campi* Young, 1942 and hadrosaurid cf. *Shantungosaurus* sp. in the Huiquanpu Formation. The former has been regarded as a nomen dubium (Carrano et al., 2012); while the assignment of fragmentary material to cf. *Shantungosaurus* sp. is based on observation of their tibia similarity (Pang and Cheng, 2000, 2001).

Here we report a new hadrosauroid specimen recovered from the Kangdailiang Quarry by the Shanxi Museum of Geological and Mineral Science and Technology (now Shanxi Museum of Geology, SXMG) in 2008 (Fig. 1). Although the specimen is represented only by

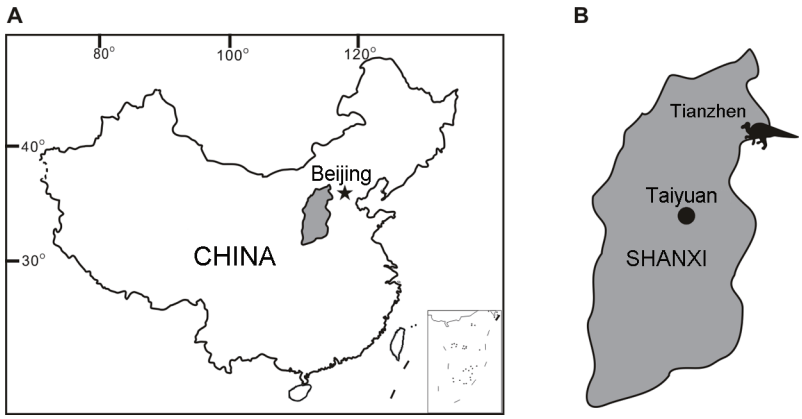

Fig. 1 Locality of *Datonglong tianzhenensis* gen. et sp. nov. (SXMG V 00005)
A. Shanxi Province in China; B. Tianzhen County in Shanxi Province

a right dentary with dentition, it provides numerous important anatomical features to depict its taxonomic status and systematic relationship. Based on our anatomical observation and taxonomic comparison, the new specimen is distinct from all previous known hadrosauroid dinosaurs, represents a new taxon (*Datonglong tianzhenensis* gen. et sp. nov.), and belongs to an advanced non-hadrosaurid hadrosauroid.

Institutional abbreviations AMNH, American Museum of Natural History (New York City, New York); LPM, Liaoning Paleontological Museum (Beipiao, Liaoning); NHMG, Natural History Museum of Guangxi Zhuang Autonomous Region (Nanning, Guangxi); SBDE, Sino-Belgium Dinosaur Expedition, Inner Mongolia Museum (Hohhot, Nei Mongol Autonomous Region); SXMG, Shanxi Museum of Geology (Taiyuan, Shanxi); XMDFEC, Xixia Museum of Dinosaur Fossil Eggs of China (Xixia, Henan).

2 Systematic paleontology

Dinosauria Owen, 1842
Ornithischia Seeley, 1887
Ornithopoda Marsh, 1881
Iguanodontia Dollo, 1888 sensu Sereno, 2005
Ankylopollexia Sereno, 1986 sensu Sereno, 2005
Styracosterna Sereno, 1986 sensu Sereno, 2005
Hadrosauriformes Sereno, 1997 sensu Sereno, 1998
Hadrosauroidea Sereno, 1986 sensu Sereno, 2005
***Datonglong* gen. nov.**
***Datonglong tianzhenensis* sp. nov.**

Holotype SXMG V 00005, almost complete right dentary with dentition.

Etymology The generic name “Datong” is after “Datong City”, and Tianzhen is a county belonging to it; “long” means “dragon” in Chinese. The specific name “Tianzhen” is after “Tianzhen County”, where the current material is discovered.

Locality and horizon Kangdailiang Quarry, Tianzhen County, Datong City, Shanxi Province, China. Huiquanpu Formation, Upper Cretaceous.

Differential diagnosis (for genus and species by monotypy) Advanced non-hadrosaurid hadrosauroid with one autapomorphy (two functional teeth in each alveolus along at least the mid- and caudal dentary occlusal plane) and the following unique combination of character states in the pattern of ridge development on the enameled lingual surface of dentary tooth crown: 1) distally offset primary ridge, 2) well-developed secondary ridge, 3) no additional ridge(s), 4) slightly distally curved apical half of primary ridge.

Description An almost complete 34 cm long right dentary is preserved, missing its rostral end including the rostral end of the tooth row (Fig. 2). The preserved ramus of the

dentary is rectangular in lateral view, with roughly parallel dorsal and ventral margins, 14 cm high at the mid portion with the occlusal plane or 10.5 cm high without it (Fig. 2A). The tooth row (28 cm long) ends caudally right medial to the caudal margin of the coronoid process (Fig. 2B). The 8 cm high coronoid process is almost perpendicular and slightly caudodorsally-directed to the ramus, and the dentary height along it is 17 cm. Although the tip of the coronoid process is not preserved, its dorsal portion is expanded at least rostrally as evidenced by its broken contour, and its craniocaudal width at base is 4.8 cm. Its lateral surface bulges slightly, while the medial one is flat, bearing a faint vertical ridge limiting its caudal two fifths with further ridges on it. In dorsal view, the caudal half of the ramus curves laterally, with caudally increasing distance between the tooth row and the lateral surface of the ramus, ending in an about 3 cm wide horizontal shelf separating the coronoid process and the caudal end of the tooth row (Fig. 2C). In caudal view, a triangular fossa is bounded by the coronoid process (Fig. 2D). The fossa extends ventrally to the mandibular adductor fossa. Rostral to the adductor fossa, the Meckelian groove is deep and long, and progressively decreases its dimensions toward the preserved rostral end.

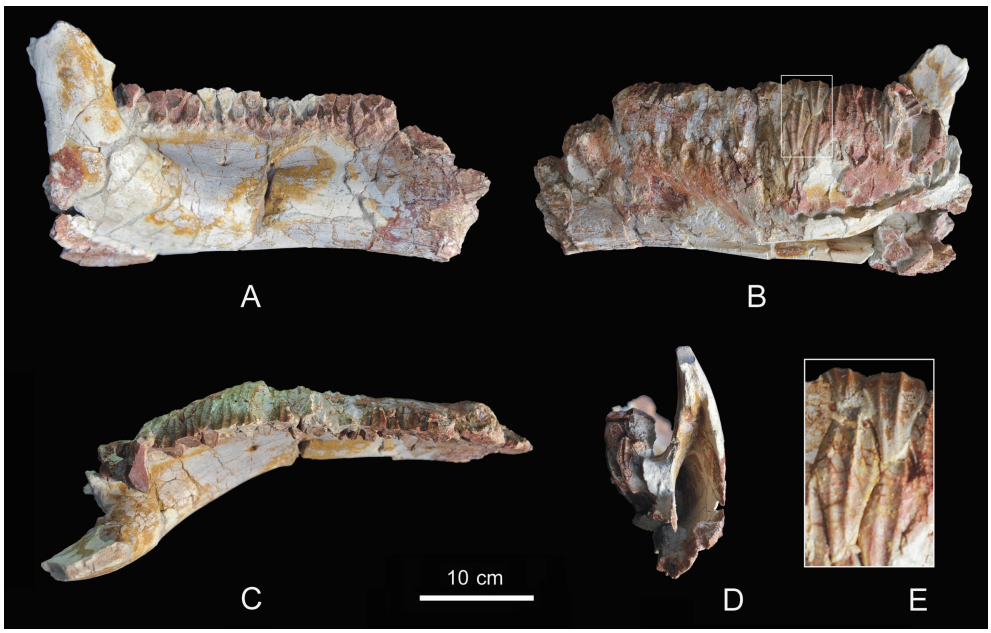

Fig. 2 Photos of right dentary of *Datonglong tianzhenensis* gen. et sp. nov. (SXMG V 00005)
A. lateral view; B: medial view. C: dorsal view; D. caudal view;
E. close-up of partial dentition in B; E is not in scale

The tooth row is largely preserved, with 17 alveoli full of teeth plus five successive most caudal alveoli bearing several scattered teeth. At least another five alveoli exist rostral to the above 22 alveoli judging by the preserved length and the existence of two broken teeth in this portion. Therefore, a total of at least 27 alveoli are expected for this animal; and the

actual number is probably less than 30 based on the general alveolar contour, which reduces its depth rapidly rostrodorsally. In medial view, a row of neurovascular foramina slightly extends caudodorsally along the mid-caudal portion of the ramus, and in this portion about three quarters of the dorsoventral depth of the dentary ramus is occupied by the alveoli. The partial septum dividing the fourth and fifth most caudal alveoli is exposed, and it is straight and relatively thick (2 mm).

The teeth are best exposed in the mid-caudal portion of the tooth row. In medial view, two or three teeth are vertically aligned in each alveolus (Fig. 2B). In lateral view, each alveolus bears two functional teeth, of which the upper one is large and obviously the same as the uppermost one seen medially, while the lower one should be the remaining worn facet of the earlier functional tooth (Fig. 2A). Therefore, three or four teeth are held in each alveolus. Both worn surfaces in each alveolus are slightly concave, and in some alveoli the upper one is not continuous with the lower one, with the latter placed more medially.

The teeth are large, and their morphology can be best shown in the tenth functional and eleventh replacement positions counting from the caudal (Fig. 2E). A distally offset primary ridge exists on the enameled lingual side in teeth, and is accompanied by a well-developed secondary ridge in the mesial half of the crown. These two roughly parallel ridges divide the lingual crown surface into three zones, without evidence of any subsidiary ridges on it. The ventral halves of these two ridges are vertical, while the dorsal halves curve slightly caudodorsally. The unerupted tooth is diamond-shaped, with the height of 5.5 cm and maximum width of 2.0 cm, a ratio of 2.75. One scattered tooth attached to the third last alveolus exposes its mesial margin, where small mammillated papillae occur apically.

Comparison In the evolution from non-hadrosaurid hadrosauroids to hadrosaurids, their dentaries acquired several key innovations. In all hadrosaurids, the tooth row ends caudally to the caudal margin of the coronoid process (Xing et al., 2014: character 56) and the coronoid process inclines rostrally (Xing et al., 2014: character 48). In addition, the dentary dental battery bears more than 30 alveoli (Xing et al., 2014: character 1), and the unworn crown in the mid-tooth row is elongate lanceolate with a height/width ratio greater than 3.1 (Sues and Averianov, 2009). All these features are not present in *Datonglong*. Therefore, *Datonglong* does not belong to Hadrosauridae, and our comparison will focus on non-hadrosaurid hadrosauroids, especially those from the Late Cretaceous of China. Based on Wang et al. (2013), Xing et al. (2014), and Tsogtbaatar et al. (2014), 15 Late Cretaceous non-hadrosaurid hadrosauroid genera have been reported, with eight from China (*Tanius* Wiman, 1929; *Bactrosaurus* Gilmore, 1933; *Gilmoreosaurus* Brett-Surman, 1979; *Nanyangosaurus* Xu et al., 2000; *Shuangmiaosaurus* You et al., 2003; *Nanningosaurus* Mo et al., 2007; *Yunganglong* Wang et al., 2013; *Zhanghenglong* Xing et al., 2014), three from North America (*Claosaurus* Marsh, 1890 ; *Eolambia* Kirkland, 1998; *Protohadros* Head, 1998), two from Europe (*Telmatosaurus* Nopcsa, 1903; *Tethyshadros* Dalla Vecchia, 2009), one from Central Asia (*Levnesovia* Sues & Averianov, 2009), and one from Mongolia (*Plesiohadros*

Tsogtbaatar et al., 2014). Among these eight Chinese taxa, three (*Tanius*, *Nanyangosaurus*, and *Yunganglong*) do not preserve comparable parts with *Datonglong*.

Nanningosaurus, recovered from the Upper Cretaceous red beds of Guangxi in southern China, was originally reported as a lambeosaurine hadrosaurid (Mo et al., 2007). Recently, it was recovered as a non-hadrosaurid hadrosauroid (Xing et al., 2014). A left dentary and an isolated dentary tooth are included in the holotype (NHMG 8142). It has a high coronoid process that inclines slightly rostrally and ends slightly caudal to the coronoid process, definitely derived features typical for hadrosaurids and different from the conditions in *Datonglong*. However, two ridges are present on the lingual crown of dentary tooth as in *Datonglong*. The primary ridge is sinuous as seen in *Tsintaosaurus*.

An isolated left dentary (LPM 0166) is referred to *Shuangmiaosaurus gilmorei* (You et al., 2003a). In *Shuangmiaosaurus*, the coronoid process inclines caudodorsally and the tooth row ends in a position medial to the middle of the coronoid process. Moreover, the dorsal edge of the dentary ramus slightly bows dorsally and the 27 alveoli clearly incline caudodorsally. All these features are not present in similar-sized *Datonglong*.

Bactrosaurus was originally studied by Gilmore (1933) based on material from a bonebed in Quarry 141 (Johnson's Quarry) collected by Central Asiatic Expeditions of the American Museum of Natural History. AMNH 6553 is designated as the holotype, and it contains more than one individual including left and right dentaries. Based on Gilmore (1933), 12 dentaries have been collected in this bonebed, and more than half of them pertain to juveniles. However, Gilmore's description of dentary seems to be based on AMNH 6353 (a right dentary), with a drawing of its medial and dorsal views. The length of adult dentary is 222 mm, and the length of the longest tooth row is 152 mm with 23 alveoli. Each alveolus holds one replacement tooth, and at most two functional teeth. A large unworn tooth crown has a ratio of 3.3 (33/10 mm).

Prieto-Marquez (2011) studied the ontogeny of *Bactrosaurus*. He notices that in the adult dentary (AMNH 6553: 23 cm long) there are as many as three teeth per alveolus arranged dorsoventrally at mid-length of the dental battery with two functional teeth. The tooth crowns have a height/width ratio of 3.1–3.2 as in juvenile specimens; in contrast to 2.75 in *Datonglong* (55/20 mm). The position of the primary ridge is slightly or modestly offset from the midline.

Godefroit et al. (1998) studied *Bactrosaurus* from another bonebed excavated by SBDE in 1995, within 1 km to AMNH Quarry 141. It contains several hundred bones of at least four hadrosaur individuals, including a left dentary (SBDE 95E5/12). Godefroit also demonstrated that all hadrosauroids in Quarry 141 belong to *Bactrosaurus* as Gilmore originally suggested. SBDE 95E5/12 is about the same size as the holotype dentary (AMNH 6553), and bears 20 alveoli. In contrast, around 30 alveoli have been estimated for *Datonglong*; however, the length of dentary in *Datonglong* is about 1.5 times as that in adult *Bactrosaurus*. Godefroit et al. (1998) described that each alveolus is composed of one functional tooth and at least two

replacement teeth. However, based on the illustration, two or three teeth can be seen medially, and two functional teeth are visible laterally in the preserved mid- and caudal portion of the tooth row. Here, based on our observation in *Datonglong*, the lower functional tooth should be from the earlier worn facet, but not from any tooth can be seen medially. Therefore, in both *Bactrosaurus* and *Datonglong*, at most two replacement and two functional teeth are present in one alveolus. However, two functional teeth seem to persist along the entire tooth tow in *Datonglong*, but not in the rostral portion of the tooth row in *Bactrosaurus* as shown in AMNH 6553. As in *Datonglong*, *Bactrosaurus* also has two ridges, one primary and one relatively well developed secondary ridge on the lingual tooth crown; however in *Bactrosaurus* there are evidence of other faint ridges in the adults, and a third caudal ridge appears in caudal most teeth. The primary ridges may curve slightly caudally in *Bactrosaurus* as in *Datonglong*.

Therefore, the crown ratio, the number of alveoli, and the condition of functional teeth in rostral portion of tooth row are different between *Bactrosaurus* and *Datonglong*. The details of ridge development pattern in the dentary tooth crown are also different.

Prieto-Marquez and Norell (2010) redescribed the second hadrosauroid *Gilmoreosaurus mongoliensis* from the Iren Dabasu Formation in Irenhot. This species is represented by at least four individuals from quarries 145 and 149. Among the material, only a partial right dentary (AMNH FARB 30654) and an isolated dentary tooth (AMNH FARB 30661) are preserved. The dentary mainly consists of the rostral and middle portion without the coronoid process and dentition (295 mm long and 71 mm high), and it is hard to tell definite diagnostic differences between it and *Datonglong*, although the latter seems to be more robust. In contrast, the worn half crown of an isolated dentary tooth possesses only one ridge that lies off center, different from the condition in *Datonglong*, which has two ridges. *Gilmoreosaurus* probably possesses one primary and one faint ridges on its dentary tooth crown (personal communication with Xing Hai).

Zhanghenglong is a recently described hadrosauroid from the Santonian Majiacun Formation of Xixia Basin, Henan Province in central China (Xing et al., 2014). Its holotype (XMDFEC V0013) preserves an incomplete, disarticulated cranium, including a right dentary with dentition. In *Zhanghenglong*, the tooth row bows dorsally and its long axis is nearly parallel to the lateral side of the dentary ramus, unlike the horizontal and diverged condition in *Datonglong*. The 26 alveoli bear one functional tooth at the rostral and caudal portions, two in the midsection, and even three in the 17th tooth alveolus; while in *Datonglong*, two functional teeth seem to persist along the entire tooth row. In *Zhanghenglong*, the primary ridge is situated median (about 40%) or distally offset on the lingual crown of the dentary, a clear secondary ridge is on the mesial half, and additional faint ridge(s) may appear close to the mesial edge; in contrast in *Datonglong*, all primary ridges are placed in the distal halves, and no additional ridge(s) are evident besides the secondary one. The dentary tooth crown has an approximate height/width ratio of 2.36 in *Zhanghenglong*, and less than 2.75 as in

Datonglong.

The latest reported non-hadrosaurid hadrosauroid is *Plesiohadros djadokhtaensis* from the Campanian of Mongolia (Tsogtbaatar et al., 2014). *Plesiohadros* preserves a left dentary with dentition. The dentary is relatively slender with a straight ramus in occlusal view, while that of *Datonglong* is relatively robust with a laterally curved ramus. Besides the primary and mesial secondary ridges, a distal secondary ridge occurs in some teeth in *Plesiohadros*, while only two ridges exist in *Datonglong*.

3 Discussion

Several dentition features show that *Datonglong* is an advanced taxon among non-hadrosaurid hadrosauroids. The dentary teeth became miniaturized in the evolution of hadrosauroids. In relatively primitive ones, such as *Jinzhousaurus* Wang & Xu, 2001, *Equijubus* You et al., 2003, *Xuwulong* You et al., 2011, *Probactrosaurus* Rozhdestvensky, 1966, *Eolambia* Kirkland, 1998, *Protohadros* Head, 1998, and *Levnesovia* Sues & Averianov, 2009, the dentary teeth are large and shield-shaped relative to the alveolar trough (Norman, 2015: character 65). In contrary, in *Datonglong*, as well as in *Bactrosaurus*, *Gilmoreosaurus*, *Nanningosaurus*, *Zhanghenglong*, *Tethyshadros*, *Telmatosaurus*, and hadrosaurids, the dentary teeth are miniaturized, and the lateral alveolar walls of tooth grooves became narrow and parallel-sided, rather than shaped by successional dentary crowns (Norman, 2015: character 66). *Probactrosaurus* and *Levnesovia* possess both large and shield-shaped teeth and narrow and parallel-sided lateral alveolar walls. *Bactrosaurus* is unique in having a height/width ratio greater than 3.1 as in hadrosaurids, defining the dentary tooth crown in the mid-tooth row as an elongate lanceolate rather than diamond-shaped contour (Gilmore, 1933; Sues and Averianov, 2009; Prieto-Marquez, 2011).

The developments of ridges on the enameled lingual surface of the dentary tooth crown show various complex patterns and are characteristic for different taxa among hadrosauroids. The pattern in *Datonglong* shows a unique combination of character states. Generally, the positon of the primary ridge shifted from distal to median on the crown, and the number of ridges reduced from five or more to only one primary ridge. In all hadrosaurids, the primary ridge is median placed; in *Zhanghenglong*, the primary ridge is either median or slightly distally offset; while in *Datonglong* and all other known hadrosauroids, the primary ridge is distally offset (Xing et al., 2014: character 7). Therefore, *Datonglong* is probably more basal than *Zhanghenglong* based on the placement of the primary ridge.

One the other hand, *Datonglong* possesses two ridges as in *Telmatosaurus*, while many others including *Protohadros*, *Levnesovia*, *Bactrosaurus*, and *Tethyshadros* have three or more (Xing et al., 2014: character 6), and *Gilmoreosaurus*, *Eolambia* and *Claosaurus* have only one

ridge (the primary ridge). Although both possess secondary ridge, it is strongly developed in *Datonglong*, in contrary to the faint one in *Telmatosaurus*. Therefore, *Datonglong* is probably more basal than *Gilmoreosaurus* but more advanced than *Bactrosaurus* based on the number of ridges on the dentary tooth crown.

The inclination of the coronoid process shifted from caudally-, vertically-, to rostrally inclined along the course of hadrosauroid evolution. In *Shuangmiaosaurus* it is caudally inclined, in *Datonglong* it is basically vertical, while in *Nanningosaurus* it is rostrally inclined. Therefore, *Datonglong* is probably more advanced than *Shuangmiaosaurus*, but less so than *Nanningosaurus* based on the nature of the coronoid process. It is possible that as a non-hadrosaurid hadrosauroid, *Nanningosaurus* convergently achieved a rostrally inclined coronoid process as in hadrosaurids.

Datonglong is unique in possessing two functional teeth in each alveolus at least along the mid- and caudal portion and probably along the entire occlusal plane. In primitive hadrosauroids, such as *Jinzhousaurus*, only one functional tooth exists in each alveolus. In more advanced non-hadrosaurid hadrosauroids, such as *Equijubus*, *Xuwulong*, *Probactrosaurus*, *Eolambia*, *Bactrosaurus*, *Gilmoreosaurus*, and *Tethyshadros*, a second functional tooth may occur in some alveoli in the middle portion of the dentary tooth row, in *Zhanghenglong* one mid-alveolus possesses a third functional tooth although its rostral and caudal portions still having one, while in *Telmatosaurus* (Norman, 2015: character 54) and hadrosaurids, a third functional tooth adds on at least in some alveoli (Xing et al., 2014: character 4). Therefore, *Datonglong* seems to represent an advanced non-hadrosaurid hadrosauroid based on the development and pattern of functional teeth.

The above discussion shows a complex pattern in the evolution of dentary, especially dentary dentition among advanced non-hadrosaurid hadrosauroids. Derived hadrosaurid features occurred earlier frequently in non-hadrosaurids, such as high height/width ratio of tooth crown in *Bactrosaurus*, one primary and one faint ridges in *Gilmoreosaurus*, median placed primary ridge in *Zhanghenglong*, rostrally inclined coronoid process in *Nanningosaurus*, and two functional teeth per alveolus along at least mid- and caudal portion of the tooth row in *Datonglong*. This implies incredible diversities and attempts close to the origin of Hadrosauridae and how difficult to elucidate their phylogenetic relationships.

Acknowledgments We are grateful to Mr. Tang Zhi-Lu for arranging this study; to the crew of the Shanxi Museum of Geology for discovering, excavating, and preparing the specimen; to reviewers for reviewing the ms. Funding was provided by the Hundred Talents Project of the Chinese Academy of Sciences, the National Natural Science Foundation of China (41472020), and the Department of Land and Resources of Shanxi Province.

山西天镇晚白垩世一新鸭嘴龙超科恐龙

续世朝[1] 尤海鲁[2*] 王嘉玮[3] 王锁柱[1] 伊 剑[1] 贾 磊[1, 2]

(1 山西地质博物馆 太原 030024)

(2 中国科学院脊椎动物演化与人类起源重点实验室，中国科学院古脊椎动物与古人类研究所 北京 100044
*通讯作者)

(3 俄罗斯罗蒙诺索夫莫斯科国立大学地质系 莫斯科 119991)

摘要：记述了山西天镇晚白垩世灰泉堡组发现的一鸭嘴龙超科恐龙新属种：天镇大同龙*Datonglong tianzhenensis* gen. et sp. nov.。标本为一保存较完好的右侧齿骨并带牙齿。与其他鸭嘴龙超科恐龙不同，大同龙每个齿槽有两个功能齿，而且舌面齿冠上嵴的发育也具有独特的特征组合(主嵴向远中方向偏移；次嵴发育；无其他附嵴；主嵴上半段略后弯)。对比研究发现，在较进步的非鸭嘴龙科鸭嘴龙超科类群中齿骨和牙齿的演化过程复杂，许多鸭嘴龙科的特征在这些类群中时而出现，如：巴克龙*Bactrosaurus*齿冠具有较大的高/宽比；吉尔摩龙*Gilmoreosaurus*齿冠上只有一个主嵴和纤弱的附嵴；张衡龙*Zhanghenglong*齿冠上主嵴中置；南宁龙*Nanningosaurus*下颌冠状突前倾；大同龙*Datonglong*每个齿槽有两个功能齿。这表明为了获得更有效的牙齿咀嚼方式，在鸭嘴龙科起源前它的姐妹群们曾进行过多种尝试；这也告诫我们，受大量趋同演化的影响，要厘清这些类群间的关系并非易事。

关键词：山西天镇，晚白垩世，恐龙，鸭嘴龙超科

中图法分类号：Q915.864 **文献标识码**：A **文章编号**：1000−3118(2016)01−0067−12

References

Barrett P M, You H L, Upchurch P et al., 1998. A new ankylosaurian dinosaur (Ornithischia: Ankylosauria) from the Upper Cretaceous of Shanxi Province, People's Republic of China. J Vert Paleont, 18: 376−384

Brett-Surman M K, 1979. Phylogeny and palaeobiogeography of hadrosaurian dinosaurs. Nature, 277: 560−562

Carrano M T, Benson R B J, Sampson S D, 2012. The phylogeny of Tetanurae (Dinosauria: Theropoda). J Syst Palaeont, 10: 211−300

Chen Y G, Feng Z C, Fan Z Z, 1983. The age of the Huiquanbao Formation in the area of Yangyuan and Yuxian, Hebei. Region Geol China, 7: 39−45

Dalla Vecchia F M, 2009. *Tethyshadros insularis*, a new hadrosauroid dinosaur (Ornithischia) from the Upper Cretaceous of Italy. J Vert Paleont, 29: 1100−1116

D'Emic M D, Mannion P D, Upchurch P et al., 2013. Osteology of *Huabeisaurus allocotus* (Sauropoda: Titanosauriformes) from the Upper Cretaceous of China. PLoS ONE, 8: e69375

Dollo L, 1888. Iguanodontidae et Camptonotidae. C R Acad Paris, 106: 775−777

Gilmore C W, 1933. On the dinosaurian fauna of the Iren Dabasu Formation. Bull Am Mus Nat Hist, 67: 23−78

Godefroit P, Dong Z M, Bultynck P et al., 1998. Sino-Belgian Cooperation Program: 'Cretaceous dinosaurs and mammals

from Inner Mongolia' 1. New *Bactrosaurus* (Dinosauria: Hadrosauroidea) material from Iren Dabasu (Inner Mongolia, P. R. China). Bull Inst R Sci Nat Belg, 68: 3−70

Head J J, 1998. A new species of basal hadrosaurid (Dinosauria, Ornithischia) from the Cenomanian of Texas. J Vert Paleont, 18: 718−734

Kirkland J I, 1998. A new hadrosaurid from the Upper Cedar Mountain Formation (Albian−Cenomanian: Cretaceous) of eastern Utah − the oldest known hadrosaurid (Lambeosaurine?). In: Lucas S G, Kirkland J I, Estep J W eds. Lower and Middle Cretaceous Terrestrial Ecosystems,Vol. 14. New Mexico Museum of Natural History and Science Bulletin. Albuquerque: New Mexico Museum of Natural History and Science. 283−295

Liu X Q, 1983. A new dinosaur locality in Tianzhen County, Shanxi Province. Vert PalAsiat, 21(3): 272

Marsh O C, 1881. Principal characters of American Jurassic dinosaurs. Part V. Am J Sci, Ser 3, 21: 417−423

Marsh O C, 1890. New Cretaceous dinosaurs. Am J Sci, 39: 422−425

Mo J Y, Zhao Z R, Wang W et al., 2007. The first hadrosaurid dinosaur from southern China. Acta Geol Sin-Engl Ed, 81: 550−554

Norman D B, 2015. On the history, osteology, and systematic position of the Wealden (Hastings group) dinosaur *Hypselospinus fittoni* (Iguanodontia: Styracosterna). Zool J Linn Soc, 173(1): 92−189

Nopcsa F B, 1903. *Telmatosaurus*, new name for the dinosaur *Limnosaurus*. Geol Mag, 410: 94−95

Owen R, 1842. Report on British fossil reptiles. Rep Br Assoc Adv Sci, 9: 60−204

Pang Q Q, Cheng Z W, 1998. A new ankylosaur of Late Cretaceous from Tianzhen, Shanxi. Prog Nat Sci, 8(3): 326−334

Pang Q Q, Cheng Z W, 2000. A new family of sauropod dinosaur from the Upper Cretaceous of Tianzhen, Shanxi Province, China. Acta Geol Sin-Engl Ed, 74: 117−125

Pang Q Q, Cheng Z W, 2001. The Late Cretaceous dinosaur fauna and strata from Tianzhen, Shanxi and Yangyuan, Hebei, China. In: Deng T, Wang Y Q eds. Proceedings of the Eighth Annual Meeting of the Chinese Society of Vertebrate Paleontology. Beijing: China Ocean Press. 75−82

Pang Q Q, Cheng Z W, Yang J P et al., 1996. The preliminary report on Late Cretaceous dinosaur fauna expeditions in Tianzhen, Shanxi. J Hebei Coll Geol, 19(3-4): 227−235

Prieto-Marquez A, 2011. Cranial and appendicular ontogeny of *Bactrosaurus johnsoni*, a hadrosauroid dinosaur from the Late Cretaceous of northern China. Palaeontology, 54: 773−792

Prieto-Marquez A, Norell M A, 2010. Anatomy and relationships of *Gilmoreosaurus mongoliensis* (Dinosauria: Hadrosauroidea) from the Late Cretaceous of Central Asia. Am Mus Novit, 3694: 1−49

Rozhdestvensky A K, 1966. New iguanodonts from Central Asia. Int Geol Rev, 9: 556−566

Seeley H G, 1887. On the classification of the fossil animals commonly named Dinosauria. Proc R Soc London, 43: 165−171

Sereno P C, 1986. Phylogeny of the bird-hipped dinosaurs (Order Ornithischia). Natl Geogr Res, 2: 234−256

Sereno P C, 1997. The origin and evolution of dinosaurs. Annu Rev Earth Planet Sci, 25: 435−489

Sereno P C, 1998. A rationale for phylogenetic definitions, with application to the higher-level taxonomy of Dinosauria. Neues Jahrb Geol Paläont Abh, 210: 41−83

Sereno P C, 2005. Stem Archosauria Version 1.0. TaxonSearch. Available at http://wwwtaxonsearchorg/Archive/stem-archosauria-10php, Accessed January 15, 2015

Sues H D, Averianov A, 2009. A new basal hadrosauroid dinosaur from the Late Cretaceous of Uzbekistan and the early radiation of duck-billed dinosaurs. Proc R Soc B-Biol Sci, 276: 2549−2555

Sullivan R M, 1999. *Nodocephalosaurus kirtlandensis*, gen. et sp. nov., a new ankylosaurid dinosaur (Ornithischia: Ankylosauria) from the Upper Cretaceous Kirtland Formation (Upper Campanian), San Juan Basin, New Mexico. J Vert Paleont, 19: 126−139

Sullivan R M, 2000. The taxonomic status of *Shanxia tianzhenensis* (Ornithischia, Ankylosauridae): a response to Sullivan (1999) − Reply. J Vert Paleont, 20: 218−219

Thompson R S, Parish J C, Maidment S C R et al., 2012. Phylogeny of the ankylosaurian dinosaurs (Ornithischia: Thyreophora). J Syst Palaeont, 10: 301−312

Tsogtbaatar K, Weishampel D B, Evans D C et al., 2014. A new hadrosauroid (*Plesiohadros djadokhtaensis*) from the Late Cretaceous Djadokhtan Fauna of southern Mongolia. In: Eberth D A, Evans D C eds. Hadrosaurs. Bloomington & Indianapolis: Indiana University Press. 108−135

Upchurch P, Barrett P M, 2000. The taxonomic status of *Shanxia tianzhenensis* (Ornithischia, Ankylosauridae): a response to Sullivan (1999). J Vert Paleont, 20: 216−217

Wang R F, You H L, Xu S C et al., 2013. A new hadrosauroid dinosaur from the early Late Cretaceous of Shanxi Province, China. PLoS ONE, 8(10): e77058

Wang X L, Xu X, 2001. A new iguanodontid (*Jinzhousaurus yangi* gen. et sp. nov.) from the Yixian Formation of western Liaoning, China. Chin Sci Bull, 46(19): 1669−1672

Wiman C, 1929. Die Kriede-dinosaurier aus Shantung. Palaeont Sin, Ser C, 6: 1−67

Xing H, Wang D Y, Han F L et al., 2014. A new basal hadrosauroid dinosaur (Dinosauria: Ornithopoda) with transitional features from the Late Cretaceous of Henan Province, China. PLoS ONE, 9(6): e98821

Xu X, Zhao X J, Lü J C et al., 2000. A new iguanodontian from Sangping Formation of Neixiang, Henan and its stratigraphical implication. Vert PalAsiat, 38: 185−191

You H L, Ji Q, Li J L et al., 2003a. A new hadrosauroid dinosaur from the mid-Cretaceous of Liaoning, China. Acta Geol Sin-Engl Ed, 77: 148−154

You H L, Luo Z X, Shubin N H et al., 2003b. The earliest-known duck-billed dinosaur from deposits of late Early Cretaceous age in Northwest China and hadrosaur evolution. Cretaceous Res, 24(3): 347−355

You H L, Li D Q, Liu W C, 2011. A new hadrosauriform dinosaur from the Early Cretaceous of Gansu Province, China. Acta Geol Sin-Engl Ed, 85: 51−57

第54卷 第1期
2016年1月

古 脊 椎 动 物 学 报
VERTEBRATA PALASIATICA

pp. 79−88
figs. 1−2

A new type of dinosaur eggs from Early Cretaceous of Gansu Province, China

XIE Jun-Fang[1] ZHANG Shu-Kang[2*] JIN Xing-Sheng[1] LI Da-Qing[3] ZHOU Ling-Qi[3]

(1 *Zhejiang Museum of Natural History* Hangzhou 310014)
(2 *Key Laboratory of Vertebrate Evolution and Human Origins of Chinese Academy of Sciences*, *Institute of Vertebrate Paleontology and Paleoanthropology*, *Chinese Academy of Sciences* Beijing 100044 * Corresponding author: zhangshukang@ivpp.ac.cn)
(3 *Gansu Geological Museum* Lanzhou 730030)

Abstract The Early Cretaceous outcrops in Gansu Province, northern China, have yielded numerous dinosaur skeleton remains and tracks; however, fossil eggs have not been reported in literatures. Here, we describe a new type of dinosaur eggs from the Lower Cretaceous Hekou Group in the Lanzhou-Minhe Basin, representing a new oogenus and a new oospecies, attributed to a new oofamily. The new specimen can be distinguished from other known dinosaur eggs by the combination of the following eggshell micro-features: branched eggshell units lacking a compact layer near the outer surface; interlocking or isolated multi-angular eggshell units, as viewed in tangential sections; and irregular pore canals. Dinosaur eggs from China largely come from the Late Cretaceous deposits, with occasional reports from the Early Cretaceous in Liaoning Province, northeastern China. The new discovery expands the geological and geographical distribution of the fossil record of dinosaur eggs in China and may reveal the origin of eggshell microstructures of spheroolithid eggs.

Key words Lanzhou-Minhe Basin, Gansu; Early Cretaceous; Polyclonoolithidae; dinosaur egg

Citation Xie J F, Zhang S K, Jin X S et al., 2016. A new type of dinosaur eggs from Early Cretaceous of Gansu Province, China. Vertebrata PalAsiatica, 54(1): 79−88

1 Introduction

Compared to those from Upper Cretaceous deposits, fossil eggs from the Lower Cretaceous worldwide are relatively rare. They have been recovered from China, Mongolia, Thailand, Korea, Japan, Spain, and North and South America, including elongatoolithids, macroelongatoolithids, prismatoolithids, spheroolithids, faveoloolithids, dendroolithids,

国家自然科学基金(批准号：41172027)资助。
收稿日期：2015-07-17

reptilian eggs belonging to turtle and crocodile, as well as eggs whose parataxonomic positions are still unknown (Nessov and Kaznachkin, 1986; Kurzanov and Mikhailov, 1989; Kohring, 1990; Bray, 1998; Zelenitsky et al., 2000; Azuma, 2003; Buffetaut et al., 2005; Buscalioni et al., 2008; Kim et al., 2009; Canudo et al., 2010; Grellet-Tinner et al., 2012; Moreno-Azanza et al., 2009, 2014a, b). In China, fossil eggs from the Lower Cretaceous were only reported in Liaoning Province, assigned to the oofamily Elongatoolithidae (Zhao and Zhao, 1999). Most of the ootaxa mentioned above were also recovered from Upper Cretaceous deposits.

The Lower Cretaceous Hekou Group in the Lanzhou-Minhe Basin of Gansu Province is very rich in dinosaur bones and tracks (Qi and Yu, 1999; Zhang et al., 2006; You et al., 2005, 2006, 2008), whereas discoveries of dinosaur eggs are rare. In 2009, the Chinese Academy of Geological Sciences discovered some fossil eggshell fragments in Zhongpu, a town in Lanzhou Basin. However, this discovery remains unpublished, possibly because of uncertainty about the locality and formation that yields the fossil material. In November of 2012, fossil eggshells were again discovered in the Lanzhou-Minhe Basin. Here, we provide a detailed description of the new discovery of dinosaur egg and associated eggshell fragments from Gansu Province. Based on the unique microstructure of the eggshell, we established a new oogenus and oospecies, within a new oofamily. The new discovery has important implications for understanding the diversity and the geological and geographical distribution of Early Cretaceous dinosaur eggs in China, as well as the evolution of dinosaur eggshell structure.

2 Material and methods

The incomplete egg (ZMNH M1849) was collected from the Lanzhou-Minhe Basin, by a work team from Gansu Geological Museum (GGM), Institute of Vertebrate Paleontology and Paleoanthropology, Chinese Academy of Sciences (IVPP) and Institute of Geology, Chinese Academy of Geological Sciences (IGCAGS) during the field investigation. Laboratory preparation included removal of sediment from the eggshell with small hand tools. The poorly preserved egg exhibits varying degrees of weathering. Therefore, the least weathered fragments were selected for examination, using a Nikon SMZ1000 stereomicroscope to view the outer surfaces. The eggshell fragments were prepared as standard radial and tangential petrographic thin sections (0.03 mm thick) and studied under a Nikon Eclipse polarized light microscopy (Nikon eclipse LV100POL, PLM). Additional eggshells were coated in gold (10 nm), mounted on aluminum stubs, and imaged by a Hitachi S-3700N Scanning Electron Microscopy (SEM) at 20 kV. Structural attributes (eggshell thickness, eggshell unit width) were measured and analyzed with Java image processing software and a digital caliper. The eggshell fragments and the eggshell thin sections are catalogued at the Zhejiang Museum of Natural History (ZMNH).

3 Locality and geological setting

The specimen occurred in outcrops near the border of Yongjing and Lintao counties (Yang et al., 2013: fig. 1), in the central region of the Lower Cretaceous Lanzhou-Minhe Basin. The Lanzhou-Minhe Basin is located on the border of Gansu and Qinghai provinces, and represents a typical Mesozoic-Cenozoic intracontinental rift basin in western China. Within the basin, the Lower Cretaceous Hekou Group is well exposed (Ye, 1980; Song, 1993; Meng, 1994; Ji, 1995; Cai et al., 2001). It unconformably overlies Ordovician beds or contacts with the Middle and Upper Jurassic by faults. The Hekou Group has a thickness of 4000 m and is composed of sandstone, mudstone, and conglomerate (Editorial Committee of Chinese Stratigraphic Standard, 2000). The Hekou Group is formally divided into Lower and Upper formations and eight informal lithostratigraphic units (Li et al., 2002). The rich dinosaur fauna of the Lanzhou-Minhe Basin includes diverse assemblages of dinosaurs, pterosaurs, and bird tracks (Zhang et al., 2006), three basal titanosauriform sauropod dinosaurs (You et al., 2005, 2006; Li et al., 2014), advanced iguanodontid *Lanzhousaurus magnidens* (You et al., 2005) and Polacanthinae (Yang et al., 2013). The fossil egg comes from the first layer of siltstone from the top of the section measured by Yang et al. (2013) of the Hekou Group (Yang et al., 2013: fig. 2), which indicates a late Early Cretaceous age. This unit records offshore-shallow lacustrine deposits comprised of red brown mudstone with interbedded sage green silty mudstone. The fossil egg was discovered in the same locality with the nodosaurid dinosaur, *Taohelong jinchengensis* (Yang et al., 2013).

4 Systematic paleontology

Polyclonoolithidae oofam. nov.

Etymology From the type oogenus *Polyclonoolithus*.

Type oogenus *Polyclonoolithus* oogen. nov.

Included oogenera The type and only oogenus *Polyclonoolithus*.

Distribution and age As for the type and only oogenus.

Diagnosis As for the type and only oogenus.

***Polyclonoolithus* oogen. nov.**

Etymology *Polyclon-*, in Greek, means “numerous small branches”, in reference to the branched eggshell units; *oo*, in Greek, from the combining form for ova, meaning egg; *lithos*, in Greek, means stone.

Type oospecies *Polyclonoolithus yangjiagouensis* oosp. nov.

Diagnosis As for the type and only oospecies.

***Polyclonoolithus yangjiagouensis* oosp. nov.**

(Figs. 1, 2)

Etymology Yangjiagou, locality of the fossil egg in Gansu Province.

Holotype An incomplete and highly fragmented egg (ZMNH M1849), housed in ZMNH.

Locality and horizon Yangjiagou Town, border region of Lintao and Yongjing counties, Gansu Province, China; Lower Cretaceous Hekou Group.

Diagnosis 1.9 mm thick on average, branched eggshell units and obvious horizontal accretion lines. Eggshell units typically fused towards the outer surface, but lacking a compact layer. Multi-angular eggshell units are interlocked or isolated in tangential sections. Pore canals irregular in shape with large cavities near the inner surface of the eggshell.

Description The eggshell fragments are surrounded by calcareous sandstone and partly cemented to the matrix, whereas in other areas the eggshells separated easily from sandstone (Fig. 1A). The poor condition provides little information about the egg shape other than it may be less than 10 cm in diameter. Because of extensive weathering, the outer surface of ZMNH M1849 is strongly sculptured, which facilitates identification of eggshell units and the pore openings in hand sample (Fig. 1B).

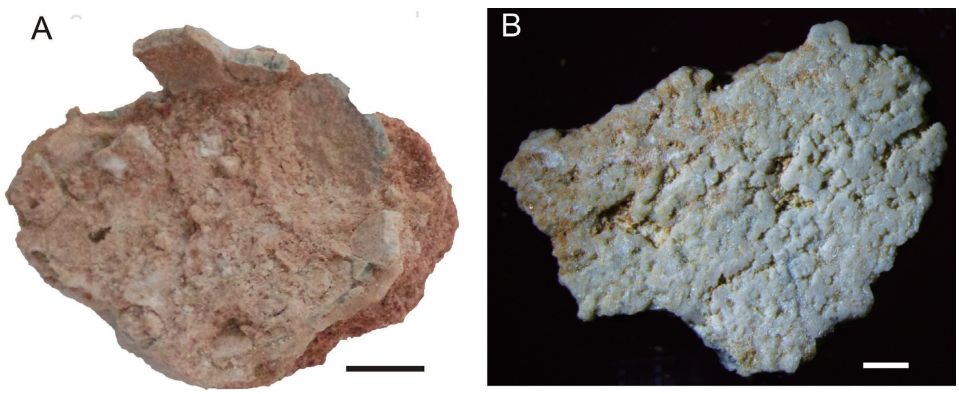

Fig. 1 Photograph of the eggshells, ZMNH M1849
A. The largest eggshell fragment, an incomplete egg, scale bar equals 1 cm;
B. Eggshell fragment showing highly weathered surface, scale bar equals 1 mm

The eggshell thickness ranges between 1.84 and 2.05 mm, with an average of 1.9 mm (Fig. 2A). The closely arranged cones at the inner surface of the eggshell show radiating structure under PLM and SEM (Fig. 2A-B). The height of the cones is about 1/7 of the eggshell thickness. The highly recrystallized portion of the eggshell above the cones represents about 1/4 of the eggshell thickness. The margins of the eggshell units are rather vague in this area. However, the upper 3/5 of the eggshell is well preserved. Eggshell units branch 2-4 times, displaying a sweeping extinction under cross-polarized light. Each eggshell unit typically has more than five branches. The parallel horizontal accretion lines

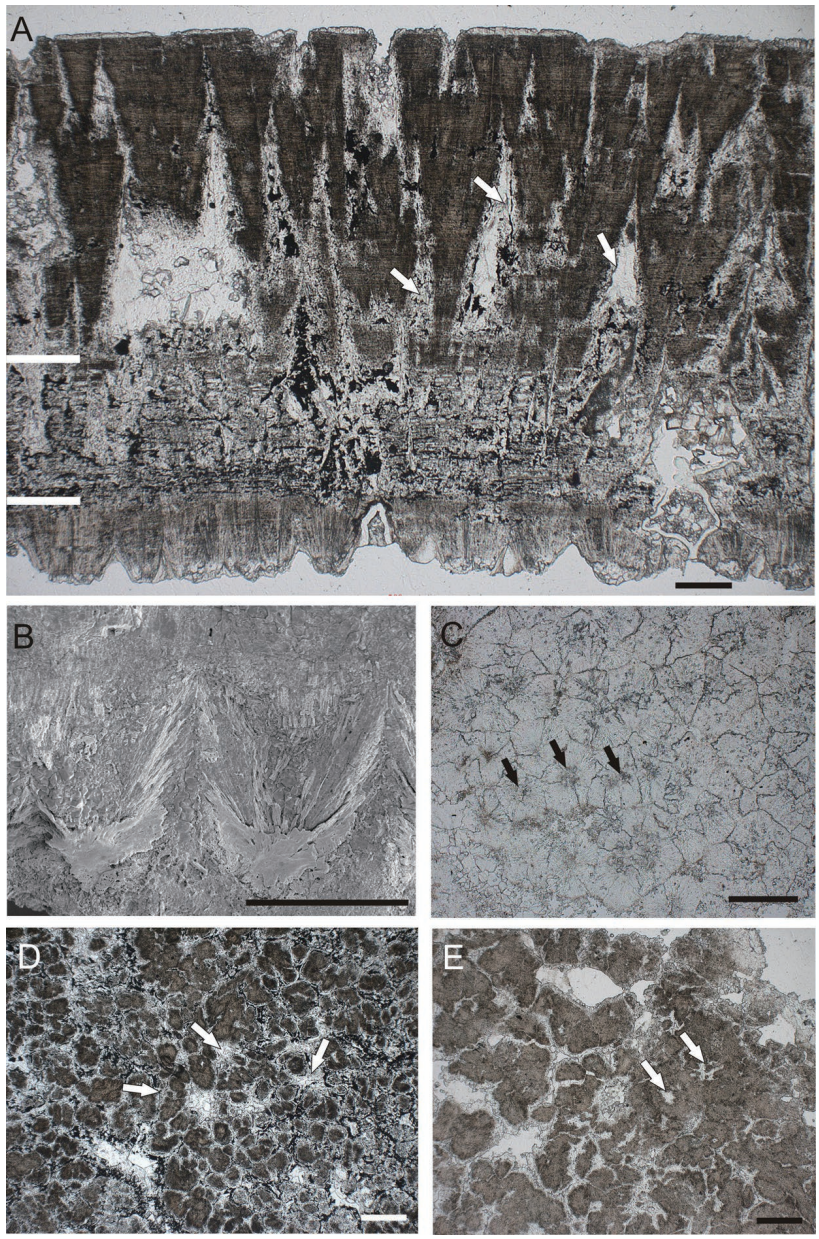

Fig. 2 *Polyclonoolithus yangjiagouensis* eggshell, ZMNH M1849

A. Radial section of eggshell under PLM, showing branched eggshell units and irregular pore canals; the lower white bar marks the boundary between the cones and the upper portion of the eggshell; the upper white bar marks upper 3/5 well preserved eggshell; white arrows point to pore canals; B. Enlargement of cones under SEM; C. Tangential section near the inner surface of eggshell, showing tightly arranged cones; black arrows point to growing centers of cones; D. Tangential section through the middle part of eggshell, showing the isolated eggshell units; white arrows point to pore canals; E. Tangential section through the upper part of eggshell, showing the eggshell units that have fused together; white arrows point to pore canals; scale bars equal 200 μm for A, B, C, and 300 μm for D, E

are distributed evenly throughout the eggshell units. Pore canals between eggshell units or the branches of eggshell units are irregular in shape, gradually narrowing towards the outer eggshell surface. The branches of eggshell units are smaller and more closely spaced near the outer surface of the eggshell (Fig. 2A). Tangential sections of the inner surface show multi-angular eggshell units that are tightly packed together (Fig. 2C). There are about 45 cones per square millimeter. In the middle portion of the eggshell, multi-angular eggshell units are separated by large rimiform pore canals, whereas most branches of eggshell units are fused near the outer surface of the eggshell (Fig. 2D-E).

Comparison With the exception of the oofamilies Dendroolithidae Zhao & Li, 1988, Dictyoolithidae Zhao, 1994 and Similifaveoloolithidae Wang et al., 2011, ZMNH M1849 can be easily distinguished from all other oofamilies by the presence of branched eggshell units.

Compared with eggs of the Dendroolithidae, the eggshell units of ZMNH M1849 are not totally fused together near the outer surface of the eggshell; however, we cannot exclude the possibility that this is a result of weathering. A significant difference between ZMNH M1849 and dendroolithid eggs is that the branches of the eggshell units of *Polyclonoolithus yangjiagouensis* are gradually narrowing towards the inner surface of eggshell, probably indicating that these branches are independent eggshell units. Perhaps because of recrystallization, radially arranged calcite crystals are absent in the upper portion of the eggshell under SEM. In contrast to ZMNH M1849, the diameters of branches of the eggshell units are relatively constant in radial sections of dendroolithid eggs. On the other hand, dendroolithid eggs' eggshell units are round or worm-like in tangential sections (Zhao and Li, 1988; Zhao and Zhao, 1998), differing from the multi-angular eggshell units of ZMNH M1849.

Eggs of the Dictyoolithidae are remarkable for their superimposed branched eggshell units (Zhao, 1994; Wang et al., 2013). But the arrangement of the eggshell units is very irregular, forming a reticulate structure, which is not seen in ZMNH M1849. In tangential sections, the shapes of eggshell units of dictyoolithid eggs are similar to those of dendroolithid eggs, which can be easily distinguished from those of ZMNH M1849.

Eggshell microstructure of similifaveoloolithid eggs in radial sections resembles that of dendroolithid eggs. The diameters of branches of eggshell units are also constant in radial sections. Tangential sections show numerous, evenly distributed pores with irregular shapes. Adjacent eggshell units fuse together to form the walls of pore canals (Wang et al., 2011). Both radial and tangential eggshell microstructures differ from those of ZMNH M1849. According to these comparisons, we erect a new oofamily Polyclonoolithidae based on the features of ZMNH M1849.

5 Discussion

In China, abundant dinosaur eggs from the Upper Cretaceous have been divided into

several dinosaur egg faunas, showing a general process of evolution of dinosaur eggs. The dinosaur egg fauna from the Tiantai Basin, Zhejiang Province, mainly consists of faveoloolithid, dictyoolithid and macroelongatoolithid eggs, which represents a group that retains primitive structural attributes. The age of this dinosaur egg fauna is 98-91 Ma, corresponding to the early Late Cretaceous (Cenomanian-Turonian) (Wang et al., 2012). Another primitive dinosaur egg fauna is reported from the Xixia Basin, Henan Province, which primarily includes dendroolithid and macroelongatoolithid eggs. Although the absolute age of these dinosaur eggs is unknown, they are believed to come from Late Cretaceous strata based on the studies of other fossils (Wang et al., 2012).

According to the comparison above, ZMNH M1849 likely shares a close relationship to the oofamilies Dendroolithidae, Dictyoolithidae and Similifaveoloolithidae. Considering the horizon of ZMNH M1849 (Lower Cretaceous), it may represents a more basic type of dinosaur egg than aforementioned oofamilies, which had been extinct in Late Cretaceous. The discovery of this new oofamily possibly indicates there is an unknown dinosaur egg fauna preserved in the Early Cretaceous strata of China.

According to the branched eggshell units and irregular pore canals, ZMNH M1849 should have the same eggshell formation mechanism as dendroolithid, dictyoolithid and faveoloolithid eggs (Zhao, 1993). Interestingly, the multi-angular eggshell units are somewhat similar to the eggshell units in the tangential sections near the inner surface of eggshells of spheroolithid eggs (*Spheroolithus spheroides*, *S. chiangchiungtingensis* and *S. megadermus*) (Zhao and Jiang, 1974; Liu et al., 2013), possibly suggesting that this new type of dinosaur egg has some relationships with spheroolithid eggs. If the hypothesis is true, the eggshell formation mechanism of spheroolithid eggs may be the same as that of ZMNH M1849. The “columnar layer” of spheroolithid eggs which is composed of superimposed eggshell units probably was evolved from the branches of eggshell units of the new oofamily Polyclonoolithidae, otherwise may indicates that the branches of eggshell units are actually superimposed eggshell units.

6 Conclusions

The fossil egg ZMNH M1849 from Gansu, China is referable to a new oofamily Polyclonoolithidae based on following diagnosis: branched eggshell units without a compact layer near the outer surface, interlocked or isolated multi-angular eggshell units in tangential sections and irregular pore canals. The discovery of the new material expands the diversity and distribution of Early Cretaceous dinosaur eggs in China. The new oofamily Polyclonoolithidae should represents a very basic ootaxon among known oofamilies. Furthermore, ZMNH M1849 has the same eggshell formation mechanism as that of dendroolithid, dictyoolithid and faveoloolithid eggs, and shows some relationships with spheroolithid eggs. It may reveal the origin of eggshell microstructures of spheroolithid eggs.

Acknowledgements The authors would like to thank Ji Shu-An from IGCAGS, You Hai-Lu from IVPP and Yang Jing-Tao from China University of Geosciences (Beijing) for field work and explain the stratigraphic information of Lanzhou-Minhe Basin. We thank Frankie D. Jackson from Montana State University for improving the English text.

甘肃早白垩世恐龙蛋化石新类型

谢俊芳[1] 张蜀康[2*] 金幸生[1] 李大庆[3] 周伶琦[3]

(1 浙江自然博物馆 杭州 310014)

(2 中国科学院脊椎动物演化与人类起源重点实验室，中国科学院古脊椎动物与古人类研究所 北京 100044 *通讯作者)

(3 甘肃地质博物馆 兰州 730030)

摘要：甘肃省早白垩世地层中，出土了大量恐龙骨骼以及恐龙足迹化石，但是至今未有蛋化石的报道。根据发现于兰州—民和盆地下白垩统河口组的蛋壳化石，建立一恐龙蛋新蛋属、蛋种，并将其归于一新蛋科：Polyclonoolithidae （多小枝蛋科）。新发现的蛋化石标本不同于所有已知的恐龙蛋类型，具有独特的显微特征组合：分叉的蛋壳单元向外延伸至蛋壳外表面，并未在靠近蛋壳外表面处融合成层；弦切面上具相互链接或独立的多角形的蛋壳单元；以及不规则的气孔道。中国的恐龙蛋化石大多出自晚白垩世地层，仅在辽宁有早白垩世恐龙蛋的报道。新发现扩展了中国恐龙蛋化石的地质和地理分布，也有可能为圆形蛋科蛋壳结构的起源提供新的认识。

关键词：甘肃兰州—民和盆地，早白垩世，多小枝蛋科，恐龙蛋

中图法分类号：Q915. 21 **文献标识码**：A **文章编号**：1000-3118(2016)01-0079-10

References

Azuma Y, 2003. Early Cretaceous vertebrate remains from Katsuyama City, Fukui Prefecture, Japan. Mem Fukui Pref Dinosaur Mus, 2: 17-21

Bray S, 1998. Dinosaur eggshell *Boletuoolithus carlylensis*, oogenus nov. from the Lower Cretaceous Cedar Mountain Formation of Utah. In: Lucas S G, Kirkland J I, Estep J W eds. Lower and Middle Cretaceous Terrestrial Ecosystems. New Mexico Mus Nat Hist Sci Bull, 14: 221-228

Buffetaut E, Grellet-Tinner G, Suteethorn V et al., 2005. Minute theropod eggs and embryo from the Lower Cretaceous of Thailand and the dinosaur-bird transition. Naturwissenschaften, 92: 477-482

Buscalioni A D, Fregenal M A, Bravo A et al., 2008. The vertebrate assemblage of Buenache de la Sierra (Upper Barremian of Serrania de Cuenca, Spain) with insights into its taphonomy and palaeoecology. Cretaceous Res, 29: 687-710

Cai X F, Li C A, Zhan C S, 2001. Characteristics of dinosaur footprint fossils in the Lanzhou-Minhe Basin and their

relation to the environment and tectonism. Region Geol China, 20: 62−66

Canudo J I, Gasca J M, Aurell M et al., 2010. La Cantalera: an exceptional window onto the vertebrate biodiversity of the Hauterivian-Barremian transition in the Iberian Peninsula. J Iber Geol, 36: 205−224

Chinese Academy of Geological Sciences, 2009. The Annual Report of Chinese Academy of Geological Sciences. Beijing: Geological Publishing House. 1−144

Editorial Committee of Chinese Stratigraphic Standard: Cretaceous, 2000. Chinese Stratigraphic Standard: Cretaceous. Beijing: Geological Publishing House. 1−124

Grellet-Tinner G, Fiorelli L E, Salvador R B, 2012. Water vapor conductance of the Lower Cretaceous dinosaurian eggs from Sanagasta, La Rioja, Argentina: paleobiological and paleoecological implications for South American faveoloolithid and megaloolithid eggs. Palaios, 27: 35−47

Ji L M, 1995. Sporo-pollen assemblages from late phase of Early Cretaceous in Minhe Basin. Acta Bot Sin, 37: 566−573

Kim S B, Kim Y G, Jo H R et al., 2009. Depositional facies, architecture and environments of the Sihwa Formation (Lower Cretaceous), mid-west Korea with special reference to dinosaur eggs. Cretaceous Res, 30: 100−126

Kohring R, 1990. Fossil reptile egg shells (Chelonia, Crocodilia, Dinosauria) from the Lower Barremian of Galve (Province of Teruel, SE Spain). Palaeont Z, 64: 329−344

Kurzanov S M, Mikhailov K E, 1989. Dinosaur eggshells from the Lower Cretaceous of Mongolia In: Gillette D D, Lockley M G eds. Dinosaurs Tracks and Traces. New York: Cambridge University Press. 109−113

Li L G, Li D Q, You H L et al., 2014. A new titanosaurian sauropod from the Hekou Group (Lower Cretaceous) of the Lanzhou-Minhe Basin, Gansu Province, China. PLoS ONE, 9: e85979

Li Q L, Xie G Q, Zhou L Q et al., 2002. Sequence stratigraphic framework of the Hekou Group and evolution of the Lanzhou-Minhe Basin. Sediment Geol Tethyan Geol, 22: 73−78

Liu J Y, Wang Q, Zhao Z K et al., 2013. A parataxonomic revision of spheroolithid eggs from the Upper Cretaceous Quantou Formation in Changtu, Liaoning. Vert PalAsiat, 51: 278−288

Meng Z F, 1994. Magnetostratigraphy of Lower Cretaceous (Hekou Group) near Lanzhou. Acta Geophys Sin, 37 (Supp 2): 342−347

Moreno-Azanza M, Canudo J I, Gasca J M, 2009. Megaloolithidae eggshell fragments from the Lower Cretaceous of Zaragoza Province (Villanueva de Huerva Formation, Zaragoza, Spain). In: Huerta Hurtado P, Torcida Fernández-Baldor F eds. Actas de las IV Jornadas Internacionales sobre Paleontología de Dinosaurios y su Entorno, Salas de los Infantes, Burgos. 253−262

Moreno-Azanza M, Canudo J I, Gasca J M, 2014a. Unusual theropod eggshells from the Early Cretaceous Blesa Formation of the Iberian Range, Spain. Acta Palaeont Pol, 59: 843–854

Moreno-Azanza M, Canudo J I, Gasca J M, 2014b. Spheroolithid eggshells in the Lower Cretaceous of Europe: implications for eggshell evolution in ornithischian dinosaurs. Cretaceous Res, 51: 75−87

Nessov L A, Kaznachkin M N, 1986. Discovery of a site in the USSR with remains of eggs of Early and Late Cretaceous dinosaurs. Biol Sci, Zool, 9: 35−49

Qi H R G, Yu Q W, 1999. The first Cretaceous dinosaur footprints from Minhe Basin, Lanzhou. Region Geol China, 18: 223

Song J J, 1993. Cretaceous System in Gansu. Acta Geol Gansu, 2: 1−48

Wang Q, Zhao Z K, Wang X L et al., 2011. New ootypes of dinosaur eggs from the Late Cretaceous in Tiantai Basin, Zhejiang Province, China. Vert PalAsiat, 49: 446−449

Wang Q, Zhao Z K, Wang X L et al., 2013. New forms of dictyoolithids from the Tiantai Basin, Zhejiang Province of China and a parataxonomic revision of the dictyoolithids. Vert PalAsiat, 51: 43−54

Wang X L, Wang Q, Jiang S X et al., 2012. Dinosaur egg faunas of the Upper Cretaceous terrestrial red beds of China and their stratigraphical significance. J Stratigr, 36: 400−416

Yang J T, You H L, Li D Q et al., 2013. First discovery of polacanthine ankylosaur dinosaur in Asia. Vert PalAsiat, 51: 265−277

Ye L S, 1980. Hekou Group in the Minhe Basin across the Gansu and Qinghai provinces. J Stratigr, 4: 96−105

You H L, Ji Q, Li D Q, 2005. *Lanzhousaurus magnidens* gen. et sp. nov. from Gansu Province, China: the largest-toothed herbivorous dinosaur in the world. Geol Bull China, 24: 785−794

You H L, Li D Q, Zhou L Q et al., 2006. *Huanghetitan liujiaxiaensis*, a new sauropod dinosaur from the Lower Cretaceous Hekou Group of Lanzhou Basin, Gansu Province, China. Geol Rev, 52: 668−674

You H L, Li D Q, Zhou L Q et al., 2008. *Daxiatitan binglingi*: a giant sauropod dinosaur from the Early Cretaceous of China. Gansu Geol, 17: 1−10

Zelenitsky D K, Carpenter K, Currie P J, 2000. First record of elongatoolithid theropod eggshell from North America: the Asian oogenus *Macroelongatoolithus* from the Lower Cretaceous of Utah. J Vert Paleont, 20: 130–138

Zhang J P, Li D Q, Li M L et al., 2006. Diverse dinosaur-, pterosaur-, and bird-track assemblages from the Hekou Formation, Lower Cretaceous of Gansu Province, Northwest China. Cretaceous Res, 27: 44−55

Zhao H, Zhao Z K, 1998. Dinosaur eggs from Xichuan Basin, Henan Province. Vert PalAsiat, 36: 282−296

Zhao H, Zhao Z K, 1999. A new form of elongatoolithid dinosaur eggs from the Lower Cretaceous Shahai Formation of Heishan, Liaoning Province. Vert PalAsiat, 37: 278−284

Zhao Z K, 1993. Structure, formation and evolutionary trends of dinosaur eggshells. In: Kobayashi I, Mutvei H, Sahni A eds. Structure, Formation and Evolution of Fossil Hard Tissues. Tokyo: Tokai University Press. 195−212

Zhao Z K, 1994. The dinosaur eggs in China: on the structure and evolution of eggshells. In: Carpenter K., Hirsch K F, Horner J R eds. Dinosaur Eggs and Babies. Cambridge: Cambridge University Press. 184−203

Zhao Z K, Jiang Y K, 1974. Microscopic studies on the dinosaurian eggshells from Laiyang, Shantung Province. Sci Sin, 17: 73−83

Zhao Z K, Li Z C, 1988. A new structural type of the dinosaur eggs from Anlu County, Hubei Province. Vert PalAsiat, 26: 107−115